1.3 Gravimetric survey

1.3.1 Summary of gravimetric survey

Gravimetric survey was carried out to make clear the subsurface structure of the Sierra La Primavera Caldera. A La Coste & Romberg type gravimeter (G-type) was used for the gravimetric survey. Analyses were made on not only the regional Bouguer analysis but also the two-dimensional analysis of the cross section. The results of the analyses are summariezed as follows:

① The Bouguer anomaly within the Sierra La Primavera Caldera is characterized by a low gravity anomaly as a whole. Some high gravity anomaly was observed locally. A two-dimentional analysis reveals that the high anomaly was formed with the uplift of this caldera and exhibits an ellipse or a rectangle having the apse line of NE-SW trend.

② The north and west rims of the Caldera have clear borders showing a steep gravity gradient, whereas the south rim, judged from gravity gradient, is located to the south of caldera wall in geological map. The local low anomaly probably corresponds to a portion of the Tala Tuff and thick lake sediments.

③ The regional Bouguer anomaly map shows that the region occupied by the "basement rocks" and Tertiary system is typified by a dominance of the NW-SE or N-S trending structure. Therefore, this structural trend is inferred to be dominant in the Cordilleran Volcanics and basement rocks beneath the geothermal manifestation area. This trend does not harmonize with the NE-SW trend previously mentioned (①). The NE-SW trend depends upon the shallow rock facies or upon the insurgence and is formed recently (several ten thousands years ago).

1.3.2 Result of gravimetric survey

(1) Measurement of gravity

① Measuring station: Gravity values were measured at a total of 306 stations over 238 km^2 in the Sierra La Primavera Caldera. One hundred fifty eight stations of 306 points were arranged at 400 m intervals in the geothermal manifestation area to analyze the gravity in detail, and the rest were set up at 800 m intervals in and around the manifestation area.

Besides, a regional gravity survey was carried out within the extent of 14,000 km^2 with 156 measuring stations to make clear a regional structure. Measuring stations are shown in Figs. II.1-26 and 35.

② Base value: The base value for the gravity measurement is 977,927.15 mgal at the international gravity base station No. 04669E in the Meteorological Agency, Mexico City. The base station, No. 1000, was established at the Guadalajara office of CFE for the survey work. The gravity value at the base station was set to 978,188.034 mgal.

③ Fixed point observation of gravity: To check the in-day change of gravity, a fixed point observation of gravity was carried out every 30 minutes on the 27th of August

from 6.00 a.m. to 24.00 in Rio Caliente to the west of this area. The gravity values fluctuate from −165 to +85 mgal in the fixed point. On the basis of a curve matching of observed values with a theoretical curve, the value 1.15 was accepted as the tidal correction constant (Fig. II.1-24).

④ Leveling

Elevation was decided from leveling at 291 stations and from measurements by Paulin's precision altimeter at the rest.

(2) Data processing

The data processing began with the m gal-conversion which converts the read-out values of the gravimeter to the gravity unit. Subsequently, the gravity values were calculated by various corrections such as the altitude correction (caused by the difference between measuring and leveling points), the tidal correction, the drift correction, the latitude correction, the free-air reduction, the Bouguer correction and the topographical correction. The topographical correction of this area has been based on the cross section map of site sketch within a radius of 20 m and on the altitude read out of topographical map within a radius of 20 m to 60 km of the measuring point. Moreover, the topographical correction for the regional gravity survey was carried out by the altitude read out using two charts on a area ranging from the measuring point to 36 km.

An example of gravity values after the correction is shown in Table II.1-12.

(3) Density for gravity correction and Bouguer anomaly

The density of rock samples, which were taken in and around the surveyed area, were measured to determine the density for gravity correction. Fig. II.1-25 shows the results of measurements which are divided into 7 geological groups, containing 47 samples of which 12 samples are cores. As shown in this Table, the density increases as the rock becomes older, and a clear density boundary is found between tuff and andesite in the Cordilleran Volcanics. The average density of the Quaternary, which forms the topography of this area, is 2.12 g/cm^3 and that of the lake sediments is lower than 2.12 g/cm^3. Therefore, it had better select out ρ = 2.00 g/cm^3 (the density for gravity correction) to analyze the gravity anomaly among the Bouguer anomaly maps of ρ = 1.90 g/cm^3 (Fig. II.1-26), ρ = 2.00 g/cm^3 (Fig. II.1-27) and ρ = 2.20 g/cm^3 (Fig. II.1-28).

1.3.3 Subsurface structure based on gravity analysis

(1) Bouguer anomaly and its trend surface analysis

Fig. II.1-27 indicates that the Bouguer anomaly values in this area range from −109 mgal to −126 mgal, and the maximum value is located in the northwest end, while the minimum value is located near the station No. 112 at the center. Low gravity area with less than −120 m gal occupies a wide area including the central part of this area. Taking a wide view of points, a large-scale low gravity anomaly of the central part is a circularly or elliptically shaped.

The contours of iso-gravity anomaly are crowded and the Bouguer anomaly values show

a remarkable variation at the northern, western and southern ends of these gravity anomaly. In contrast, the Bouguer anomaly varies gradually at the eastern end.

As described above, the Bouguer anomaly within the Sierra La Primavera Caldera is characterized by low gravity anomaly as a whole. Some high gravity anomaly was observed locally. The inside of the low gravity anomaly has a fairly complicated structure. To remove this local anomaly, the 2nd- and 3rd-order trend surface analyses were made against Fig. II.1-II.1-27. A trend surface and a residual surface were prepared in Figs. II.1-29~32. These figures show that the center of the Caldera is situated in the vicinity of stations No. 87, 89 and 121, and the north and west rims of the Caldera have clear borders showing steep gravity gradient.

(2) Two-dimentional gravity analysis of cross section

A two-dimentional analysis was carried out in cross sections A-A', B-B' and C-C' in Fig. II.1-27 to investigate a cause of local high gravity anomalies. The results are shown in Fig. II.1-33. The calculation was based on the Talwani's equation. The three layered-structures of gravity were assumed in this analysis defined as follows:

The 1st layer	$\rho = 2.20$ g/cm^3	Rhyolite, Tala Tuff the upper Cordilleran Volcanics
The 2nd layer	$\rho = 2.40$ g/cm^3	the lower Cordilleran Volcanics consisting mainly of andesite
The 3rd layer	$\rho = 2.27$ g/cm^3	"basement rocks"

Further, the lake sediments (ρ = 1.60 g/cm^3), Rhyolite (ρ = 2.00 g/cm^3) and the Tala Tuff (μ 2.00 g/cm^3) were partially added to the 1st layer as a local low density part. The control points of the boundary between two layers were settled in PR-2 for line A-A', in PR-9 for line B-B' and in PR-5 for line C-C' respectively. Since the upper boundary of the 3rd layer was only confirmed in PR-9, the control point of that boundary was set at the same depth in three profiles. The results of analysis include a step-like structure (real line) and a fairly smooth structure (broken line). These two structures indicate nearly equal gravity anomalies.

When the throw of the Caldera wall is estimated to be 500 ~ 600 m, the observed values are consistent with the calculated values as shown in Fig. II.1-33. The estimated throw is in general conformed with the collapse-throw which was determined by the geological survey and the well data. The local high gravity anomaly at the central part (Cerritos Colorados) can be interpreted by the uplift of 400 m of a high density layer. Because the 260 m difference is a minimum estimate of uplift of the Caldera on the basis of Mahood (1980)'s estimate, the high gravity anomaly seems to be caused by the Caldera resurgence or insurgence. The shape of the uplift would be rectangular or ellipitical with its apse line of the NE-SW trend as shown in Fig. II.1-27.

Subsequently, a consideration on the local low gravity anomaly is followed by the above mentioned high anomaly. The low gravity anomalies near the stations No. 39, No. 69 and No. 112 coincide with the area of elevated topography and the lake sediments by correspondence of Figs. II.1-27 and 1-33 with the geological map. Fig. II.1-33 indicates that the over-correction occurred in the area of the lake sediments, of which density ρ = 1.60 g/cm^3 is

markedly less than the density of the 1st layer (ρ = 2.20 g/cm^3). Therefore, the low gravity anomaly corresponds to the thick lake sediments.

However, the low anaomaly by No. 286 is located in the area where the lake sediments are not distributed, showing a low elevation. The origin of this anomaly is not clear, but it might be attributed to the thick Tala Tuff (ρ = 2.00 g/cm^3). A structural analysis shown in Fig. II.1-34 can be obtained from the summarizing the above interpretation. The south margin of the caldera wall is characteristically located in more southern position compared with a conventional geological map.

The uplift and its orientation was clarified by the gravimetric survey, offering useful information for geothermal surveys as a result.

(3) Regional Bouguer anomaly distribution

It is difficult to correlate the gravity anomaly with Tertiary formations because the area of Sierra La Primavera is widely covered by the Quaternary. Consequently, the gravimetric survey has been extended as far as the region containing "basement rock" and the Tertiary, followed by a study on the validity of correlation between the geology and the gravity anomaly applied for a two-dimentional analysis.

Fig. II.1-35 shows a regional Bouguer anomaly map with the density for gravity correction of ρ = 2.20 g/cm^3. Higher Bouguer anomalies more than −110 mgal are distributed in the southern and southwestern region of Sierra La Primavera Caldera, extending partially from the north of Ameca to Lake La Vega as shown in Fig. 1-35. It can be found that the Creteceous sedimentary rocks and granitic rocks, which are the oldest rocks in this area, are exposed in the high gravity anomaly area, based on the geological map (1:100,000 in scale) prepared by C.F.E. The Paleogene and the Miocene both consisting of igneous rocks are also confirmed with the local high gravity anomaly. The Pliocene and the Quaternary correspond in general to the low gravity anomaly except for Tequila Volcano and Cerro Grande to the east.

The above results are harmonized with the density classification shown in Fig. II.1-25 and with the layer dividing obtained from the two-dimentional analysis. Futhermore, the shape of gravity anomaly indicates the NW-SE and N-S trending structures. They are coincided with the Tepic-Chapala structural trend (NW-SE) and the Colima structural trend (N-S) respectivily. Thus, the orientation of "basement rocks" and the Tertiary trends NW-SE or N-S, whereas the local high gravity anomaly within the Caldera indicates the NE-SW trending uplift.

The discordance of the upheaval trend against the deep-seated structure is ascribed to the following two reasons:

① The local high gravity anomaly is governed by the rock facies of comparatively shallow depth (ex. rhyolite).

② The insurgence by the magma intrusion took place in the deeper part of the uplift zone having a NE-SW trend.

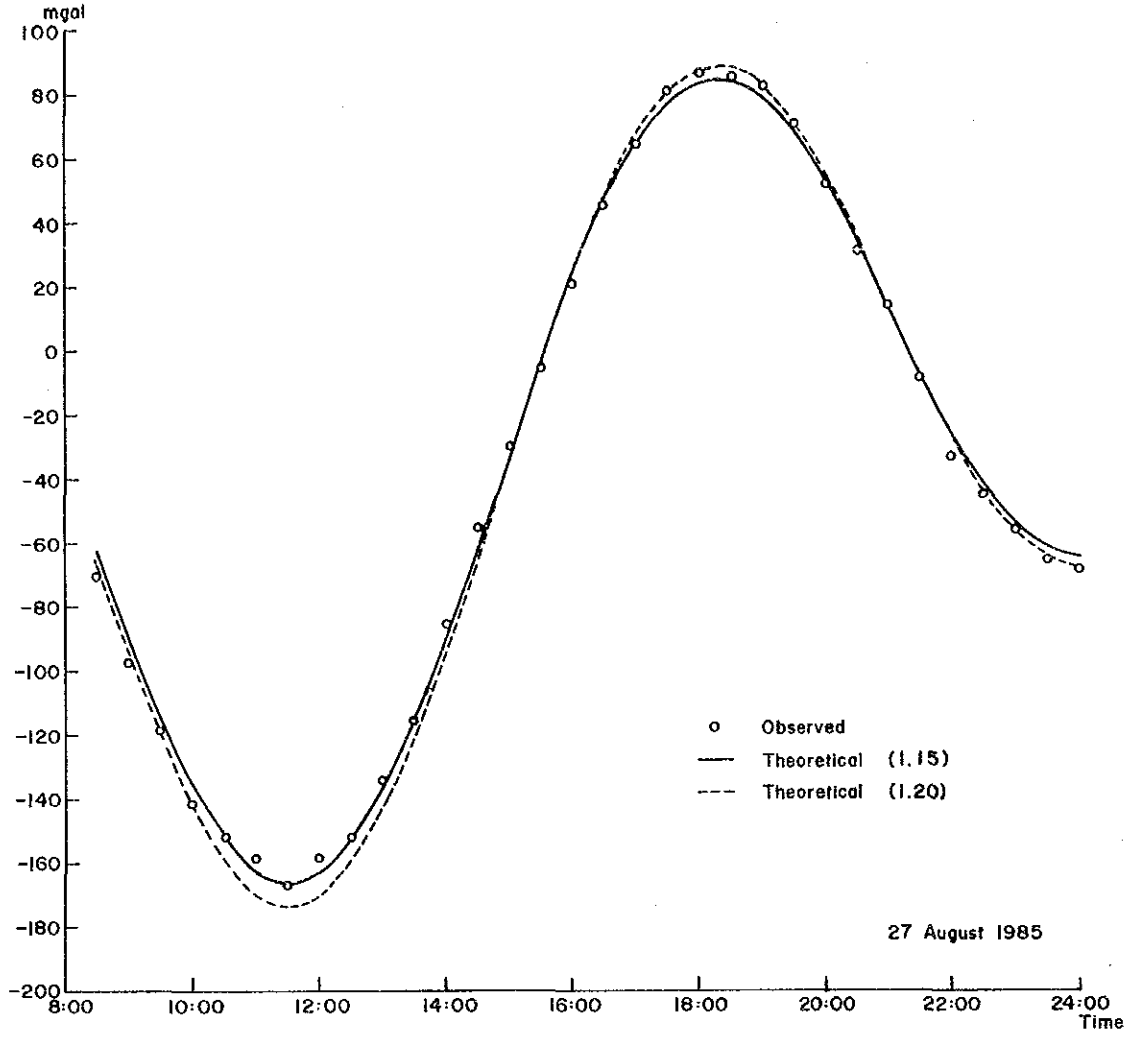

Fig. II. 1-24 Observation of Diurnal Gravity Variation

Geology		Wet Density (g/cm³)	Number of Sample	Mean Density (g/cm³)		
Quaternary	rhyolite (Central Dome)		6	2.21	2.12	2.21
	Welded tuff (Tala tuff)		9	2.06		
Tertiary	rhyolite		10	2.33	2.28	
	tuff		7	2.22		
	andesite		7	2.39		
	basalt		6	2.60		
Cretaceous sedimentary rock			2	2.57		

• Surface Sample ▫ Core Sample

Fig. II. 1-25 Density of Rock Samples in the Sierra La Primavera Area

Table II. 1-12 An Example of List of Gravity Survey

ST. NO.	OBS.	DAY	LATITUDE			LONGITUDE			LEVEL	ABS. G	ETC		*	DENSITY = 2.00 (G/CM ··· 3) TERR. C	F.E.C	B.G.C	NORM. G	ANOM. F	ANOM. B
			D	M	S	D	M	S											
1	85	729	20	43	36.4	103	33	41.2	1603.564	978.204169	L	L	*	.698	494.860	-134.379	978.678885	20.842	-113.536
2	85	729	20	43	40.0	103	33	11.8	1613.990	978.201158	L	L	*	.657	498.077	-135.252	978.678946	20.947	-114.305
3	85	729	20	43	37.2	103	32	42.8	1622.917	978.199354	L	L	*	.438	500.832	-136.000	978.678898	21.725	-114.275
4	85	729	20	43	42.8	103	32	17.2	1621.771	978.200320	L	L	*	.463	500.479	-135.904	978.678992	22.269	-113.635
5	85	729	20	43	43.5	103	31	48.9	1618.128	978.200906	L	L	*	.596	499.354	-135.599	978.679004	21.852	-113.747
6	85	729	20	43	42.3	103	31	21.2	1622.816	978.198519	L	L	*	.624	500.801	-135.992	978.678984	20.960	-115.032
7	85	729	20	43	37.5	103	30	53.7	1627.836	978.197019	L	L	*	.691	502.350	-136.413	978.678905	21.156	-115.257
8	85	729	20	43	28.5	103	30	26.1	1634.000	978.196598	L	L	*	1.055	504.252	-136.929	978.678755	23.150	-113.779
9	85	730	20	43	21.5	103	29	60.0	1645.983	978.194347	L	L	*	.644	507.950	-137.933	978.678638	24.302	-113.631
10	85	730	20	43	14.1	103	29	35.2	1649.806	978.193514	L	L	*	.506	509.130	-138.254	978.678516	24.634	-113.620
11	85	730	20	43	6.4	103	29	9.4	1650.910	978.192914	L	L	*	.447	509.471	-138.346	978.678389	24.443	-113.903
12	85	730	20	42	59.4	103	28	44.2	1649.998	978.192044	L	L	*	.353	509.189	-138.270	978.678272	23.315	-114.955
13	85	730	20	42	50.4	103	28	17.1	1667.535	978.186812	L	L	*	.321	514.601	-139.739	978.678123	23.612	-116.127
14	85	730	20	42	29.7	103	27	57.9	1674.354	978.184716	L	L	*	.287	516.706	-140.311	978.677780	23.928	-116.383
15	85	730	20	42	10.4	103	27	41.6	1673.997	978.183765	L	L	*	.269	516.595	-140.281	978.677460	23.170	-117.111
16	85	730	20	41	48.8	103	27	22.8	1676.045	978.182600	L	L	*	.316	517.227	-140.453	978.677102	23.042	-117.411
17	85	730	20	41	23.4	103	27	20.0	1677.650	978.179948	L	L	*	.336	517.723	-140.587	978.676681	21.326	-119.262
18	85	730	20	40	57.7	103	27	18.9	1682.783	978.177298	L	L	*	.339	519.307	-141.017	978.676255	20.689	-120.328
19	85	730	20	40	31.4	103	27	19.1	1686.919	978.175647	L	L	*	.429	520.583	-141.364	978.675819	20.840	-120.524
20	85	730	20	40	3.9	103	27	6.3	1695.492	978.172975	L	L	*	.478	523.229	-142.082	978.675365	21.316	-120.766
21	85	730	20	39	42.7	103	26	57.6	1681.368	978.175907	L	L	*	.472	518.870	-140.899	978.675014	20.235	-120.663
22	85	730	20	39	19.2	103	26	47.1	1664.113	978.180220	L	L	*	.408	513.545	-139.453	978.674625	19.547	-119.906
23	85	730	20	38	57.0	103	26	38.0	1649.423	978.182950	L	L	*	.331	509.012	-138.222	978.674258	18.035	-120.187
24	85	730	20	38	34.5	103	26	29.0	1646.545	978.183303	L	L	*	.272	508.124	-137.980	978.673886	17.812	-120.168
25	85	730	20	38	12.3	103	26	19.2	1639.129	978.183241	L	L	*	.248	505.835	-137.359	978.673519	15.805	-121.554
26	85	730	20	37	48.5	103	26	9.8	1632.628	978.183981	L	L	*	.241	503.829	-136.814	978.673125	14.926	-121.888
27	85	730	20	37	46.8	103	26	36.4	1640.427	978.181501	L	L	*	.297	506.236	-137.468	978.673097	14.938	-122.530
28	85	730	20	37	45.7	103	27	3.3	1651.555	978.178494	L	L	*	.346	509.670	-138.400	978.673079	15.430	-122.970
29	85	731	20	37	39.4	103	27	28.9	1660.000	978.176318	L	L	*	.445	512.276	-139.108	978.672976	16.063	-123.045
30	85	731	20	37	29.2	103	27	53.5	1678.702	978.171673	L	L	*	.586	518.047	-140.675	978.672807	17.500	-123.176
31	85	731	20	37	18.1	103	28	19.5	1704.044	978.165896	L	L	*	.823	525.868	-142.799	978.672623	19.964	-122.835
32	85	731	20	37	7.6	103	28	45.5	1729.120	978.160554	L	L	*	.849	533.606	-144.900	978.672450	22.560	-122.340
33	85	731	20	36	57.7	103	29	9.4	1760.404	978.154951	L	L	*	.796	543.261	-147.522	978.672287	26.721	-120.801
34	85	731	20	36	44.6	103	29	36.4	1806.031	978.147432	L	L	*	1.128	557.341	-151.345	978.672071	33.830	-117.515
35	85	731	20	37	6.3	103	30	2.4	1877.774	978.130091	L	L	*	1.023	579.481	-157.357	978.672429	38.165	-119.192
36	85	731	20	36	59.4	103	30	30.1	1940.490	978.114946	L	L	*	1.229	598.835	-162.613	978.672315	42.695	-119.918
37	85	731	20	37	6.5	103	30	56.2	1946.705	978.109827	L	L	*	1.054	600.753	-163.134	978.672431	39.203	-123.931
38	85	731	20	37	17.0	103	31	5.8	1946.210	978.110141	L	L	*	1.263	600.600	-163.092	978.672605	39.400	-123.692
39	85	731	20	37	28.6	103	30	57.7	1937.059	978.110544	L	L	*	1.639	597.776	-162.326	978.672797	37.163	-125.163
40	85	731	20	37	42.2	103	30	52.4	1921.340	978.115450	L	L	*	1.735	592.926	-161.008	978.673022	37.088	-123.920
41	85	731	20	37	55.2	103	30	47.5	1908.658	978.119485	L	L	*	1.629	589.012	-159.946	978.673236	36.890	-123.055
42	85	731	20	38	7.5	103	30	44.6	1908.249	978.120367	L	L	*	1.978	588.886	-159.911	978.673439	37.791	-122.120
43	85	731	20	38	17.9	103	30	43.4	1895.733	978.124836	L	L	*	1.979	585.023	-158.862	978.673611	38.227	-120.635
44	85	731	20	38	31.2	103	30	45.7	1919.187	978.120508	L	L	*	1.260	592.261	-160.828	978.673832	40.197	-120.631
45	85	731	20	38	41.4	103	30	52.2	1909.421	978.122995	L	L	*	1.050	589.247	-160.009	978.674000	39.293	-120.717
46	85	731	20	38	47.7	103	31	5.6	1878.609	978.130207	L	L	*	1.390	579.739	-157.427	978.674104	37.232	-120.196
47	85	731	20	38	53.6	103	31	16.9	1877.019	978.130160	L	L	*	1.378	579.248	-157.294	978.674202	36.584	-120.710
48	85	731	20	39	6.4	103	31	24.4	1841.839	978.138992	L	L	*	1.322	568.392	-154.346	978.674413	34.293	-120.053
49	85	731	20	39	11.0	103	31	34.3	1811.461	978.146345	L	L	*	1.724	559.017	-151.800	978.674489	32.597	-119.203
50	85	731	20	39	19.9	103	31	43.9	1799.966	978.148766	L	L	*	1.436	555.470	-150.837	978.674636	31.036	-119.801

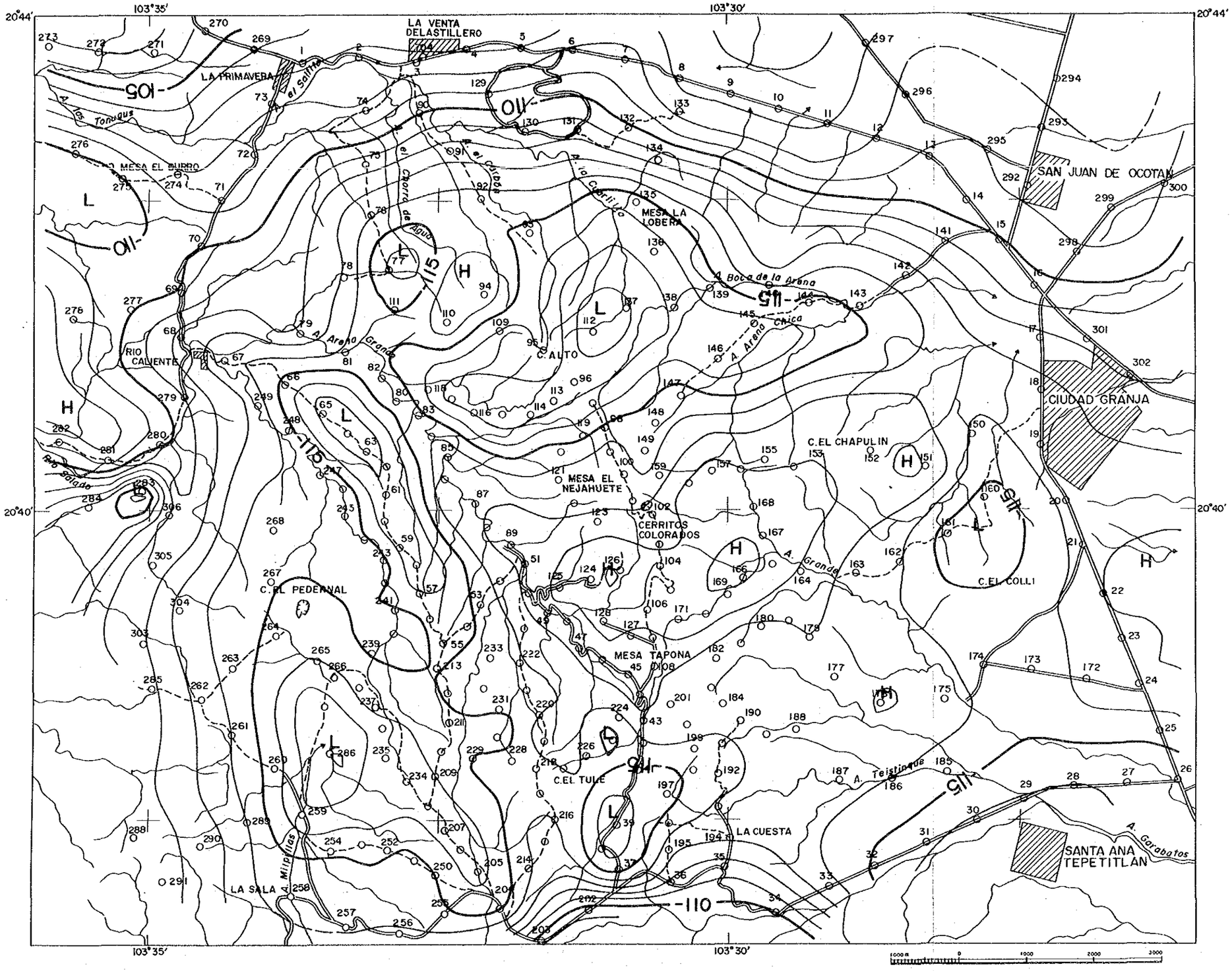

Fig. II. 1-26 Bouguer Anomaly Map (ρ=1.90g/cm³)

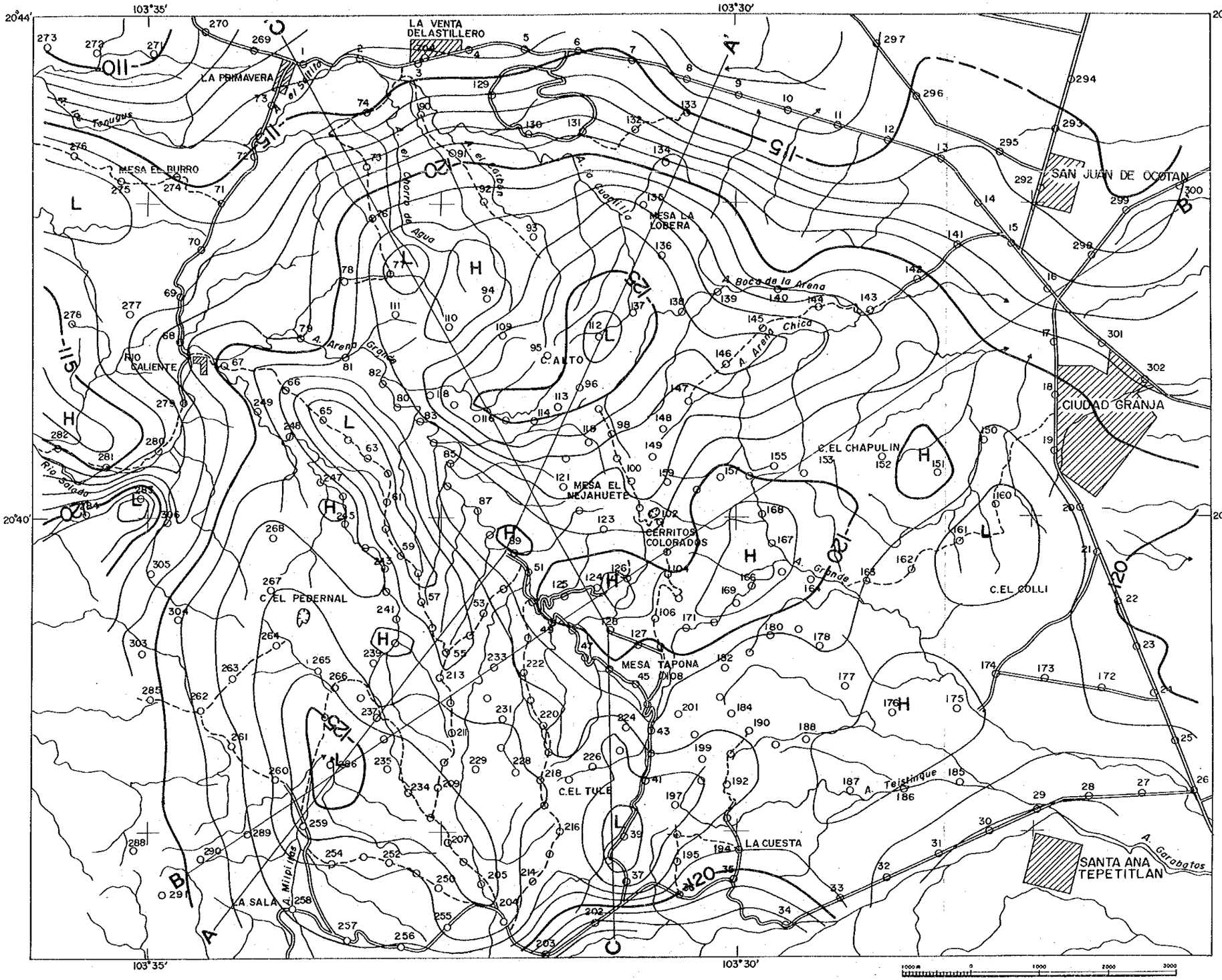

Fig. II. 1-27 Bouguer Anomaly Map (ρ=2.00g/cm³)

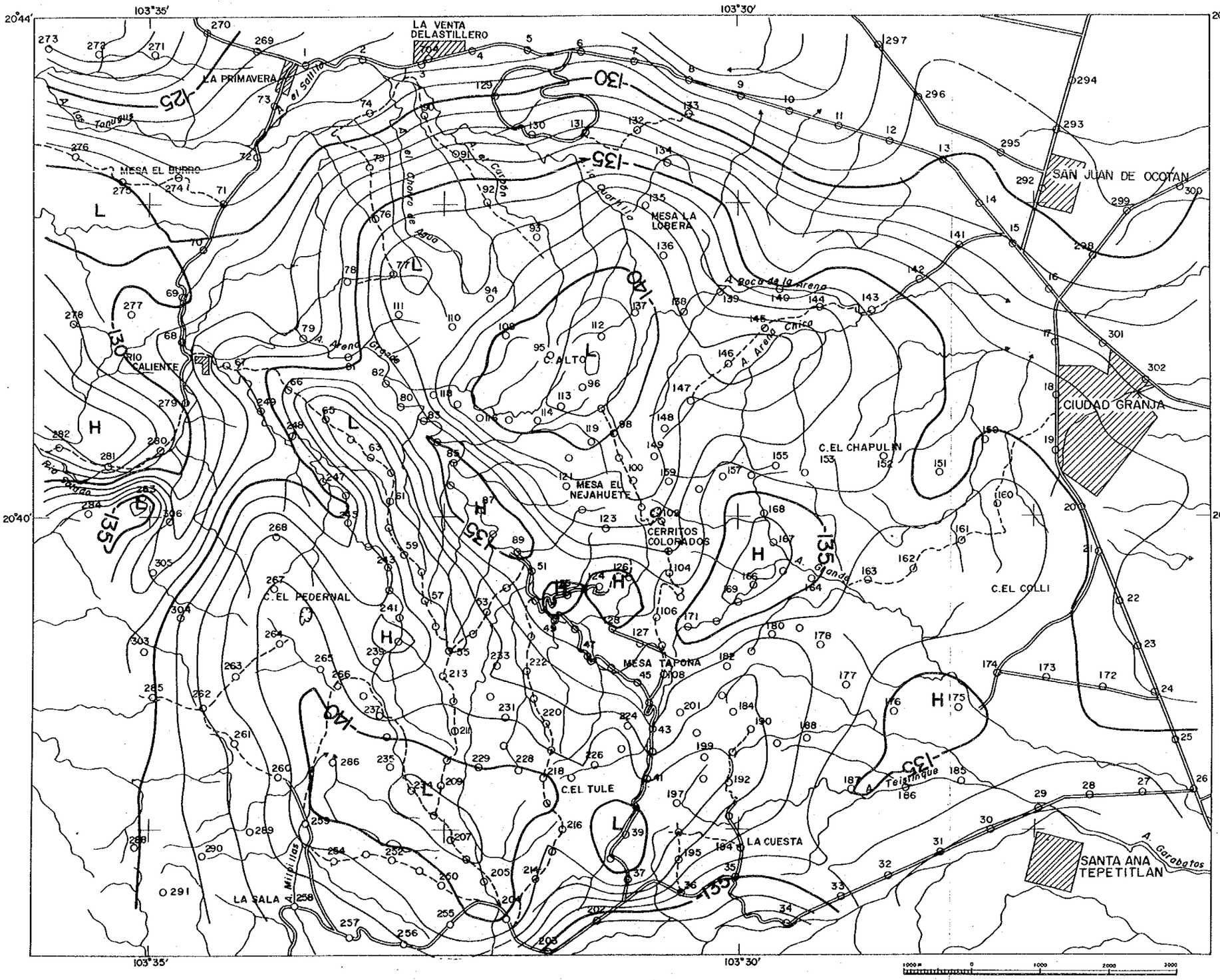

Fig. II. 1-28 Bouguer Anomaly Map (ρ=2.20g/cm³)

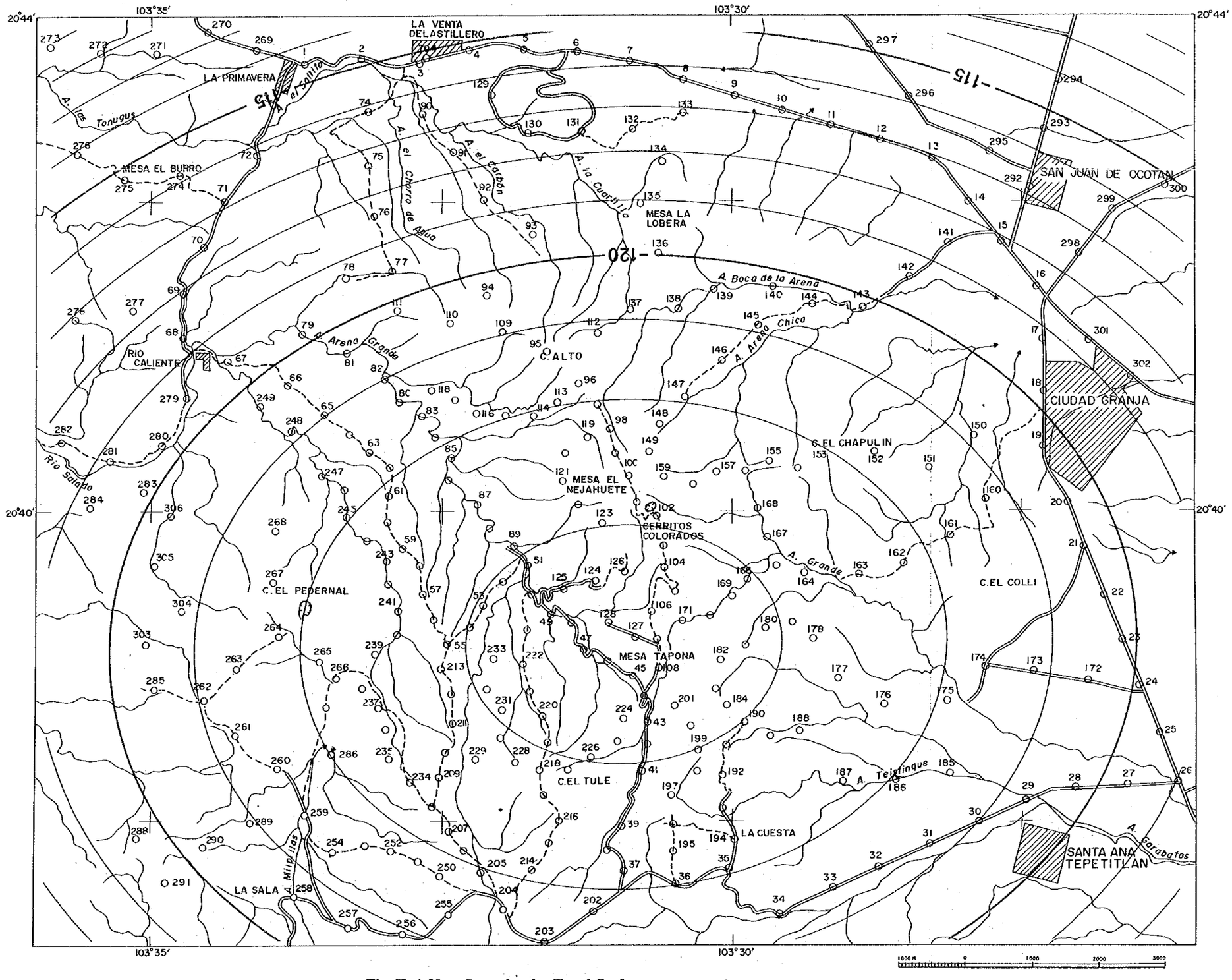

Fig. II. 1-29 Second-order Trend Surface

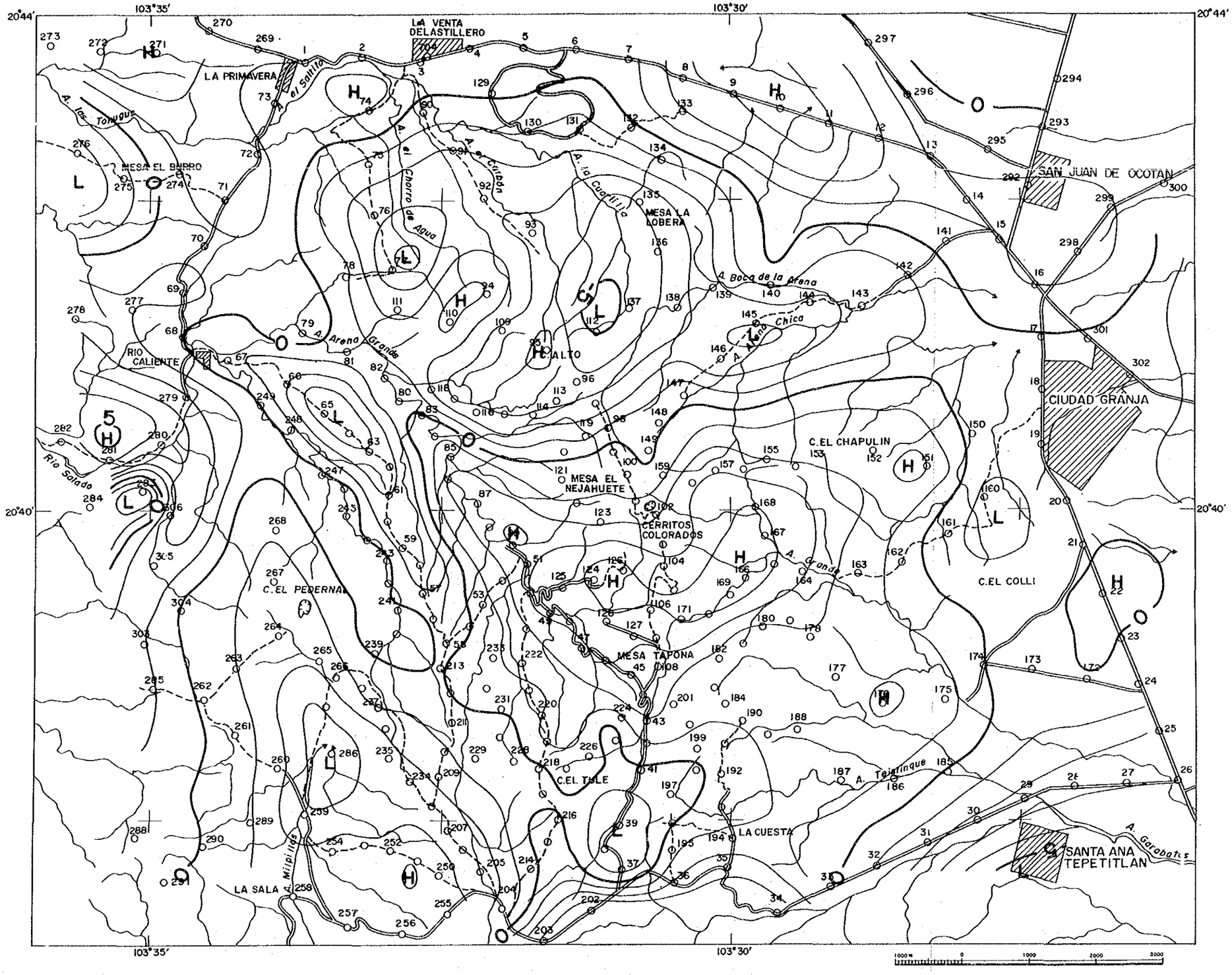

Fig. II. 1-30 Residuals of Third-order Trend Surface

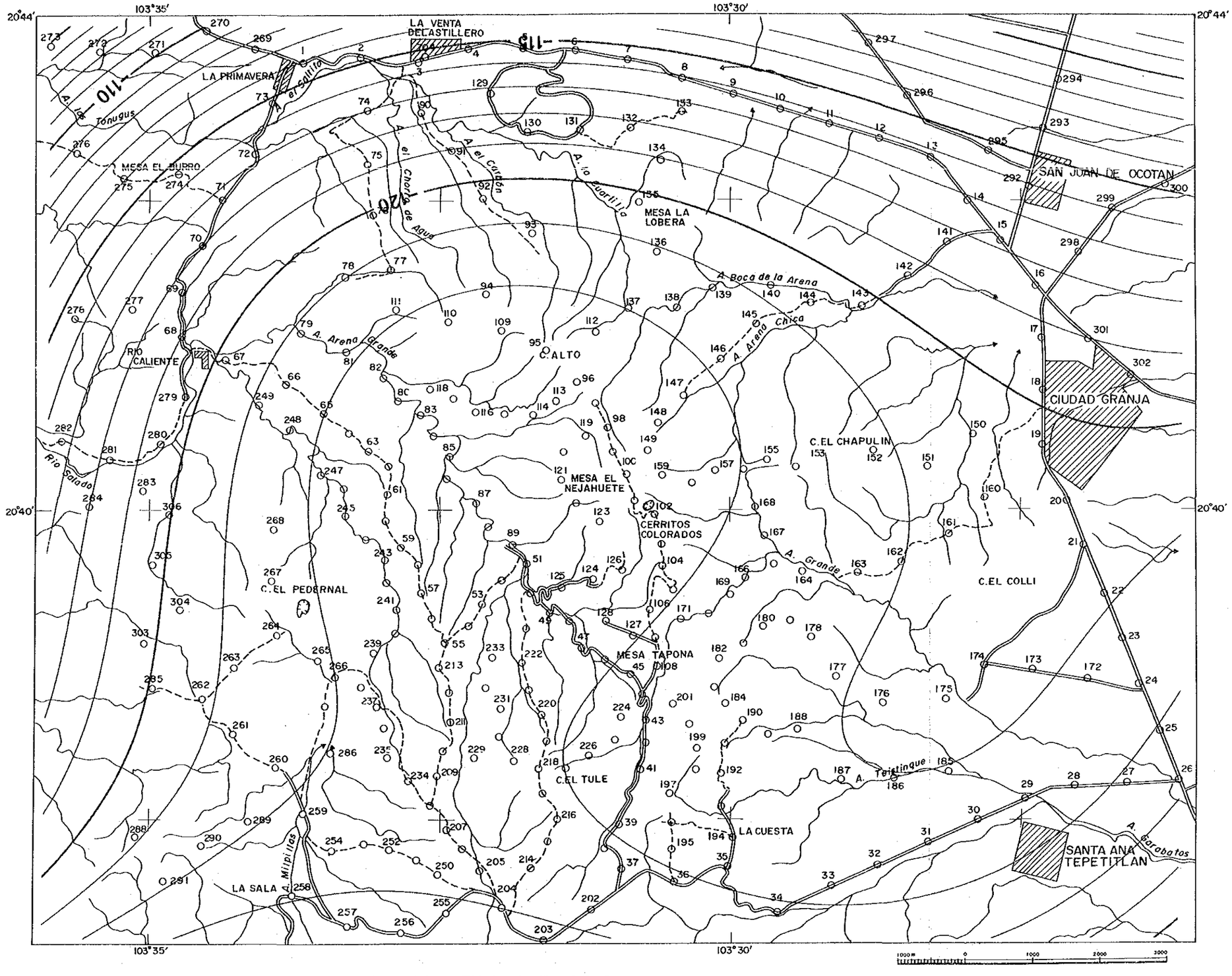

Fig. II. 1-31 Third-order Trend Surface

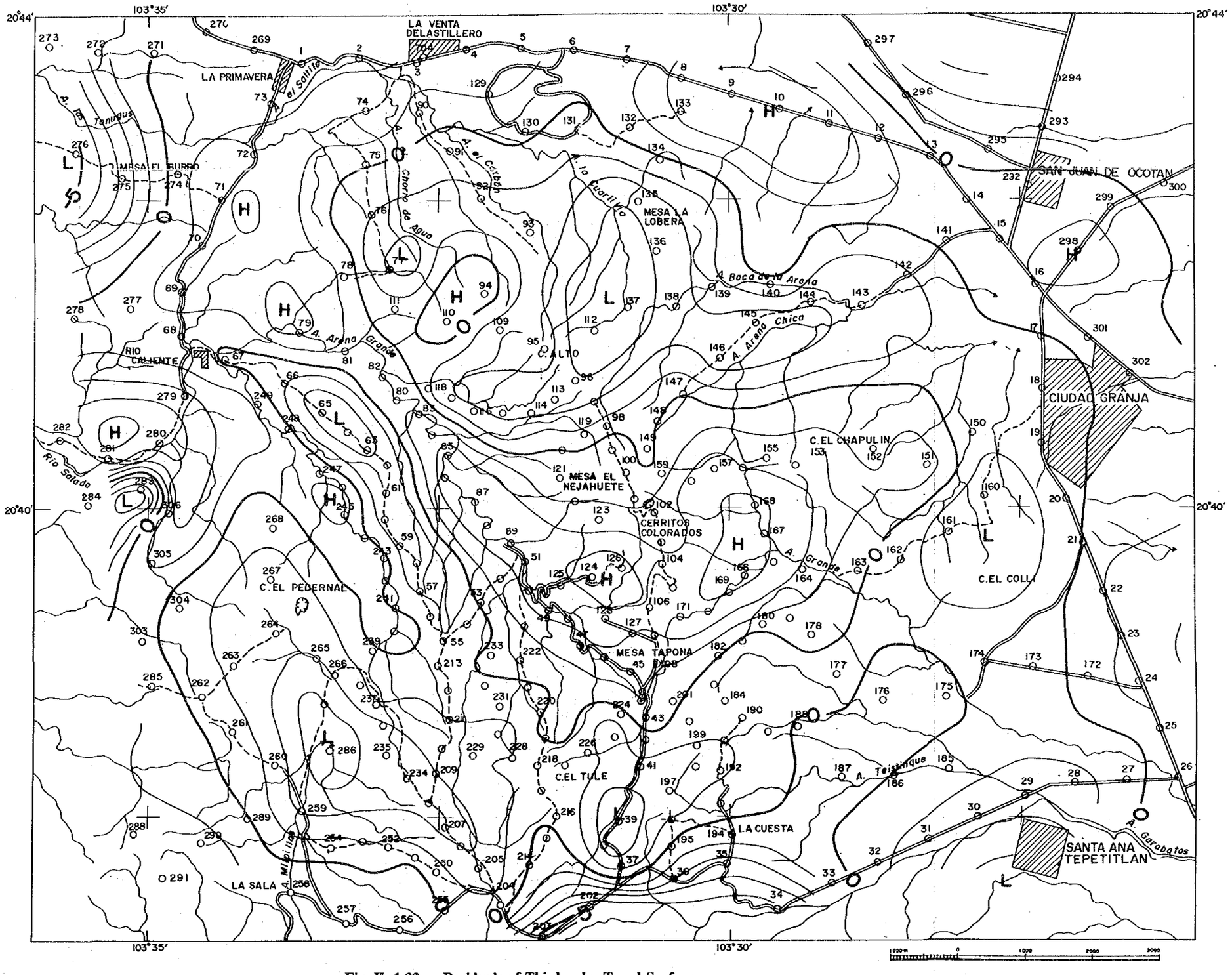

Fig. II. 1-32 Residuals of Third-order Trend Surface

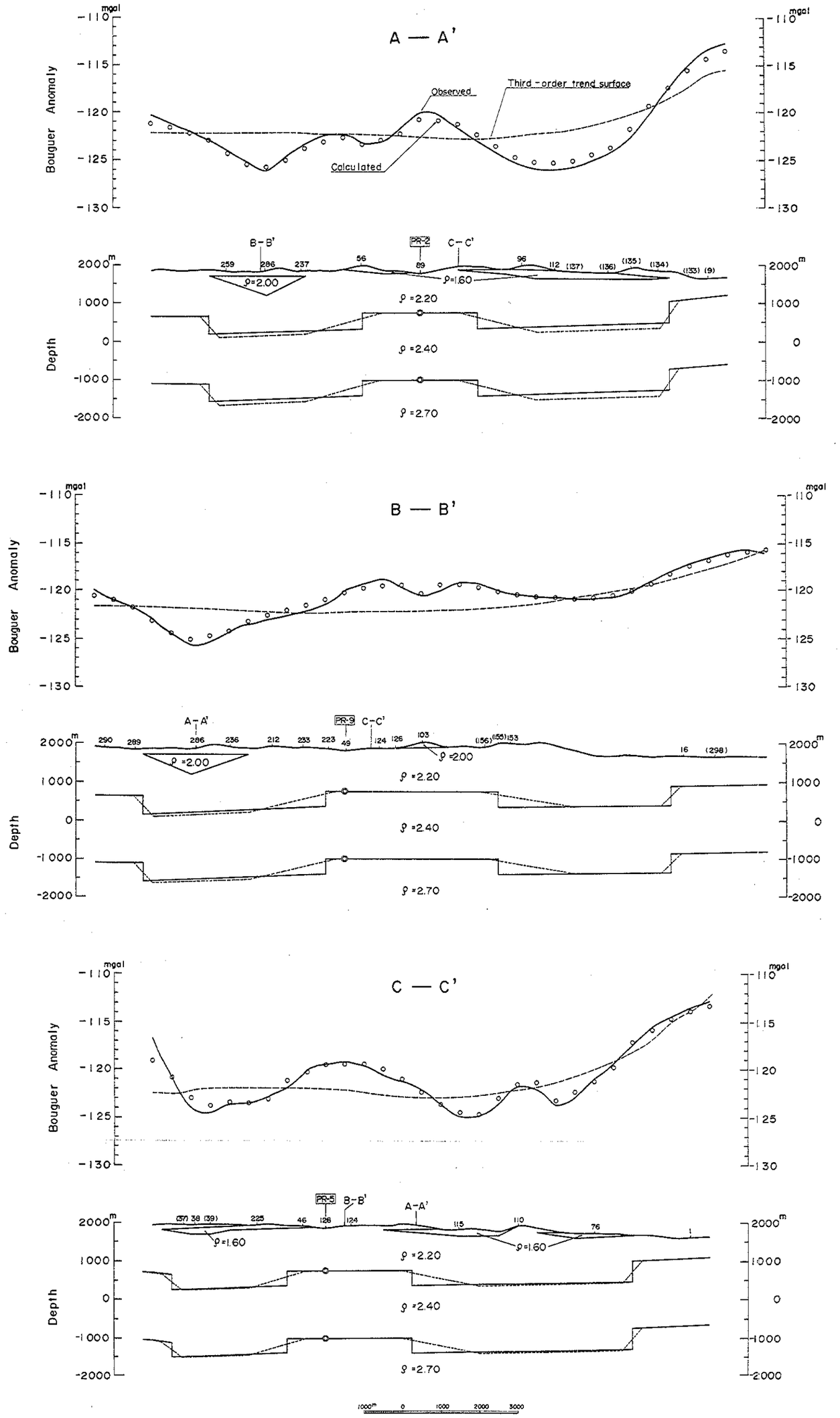

Fig. II. 1-33 Two-Dimentional Gravity Analysis, Lines A-A′ B-B′ and C-C′ are Shown in Fig. II. 1-27

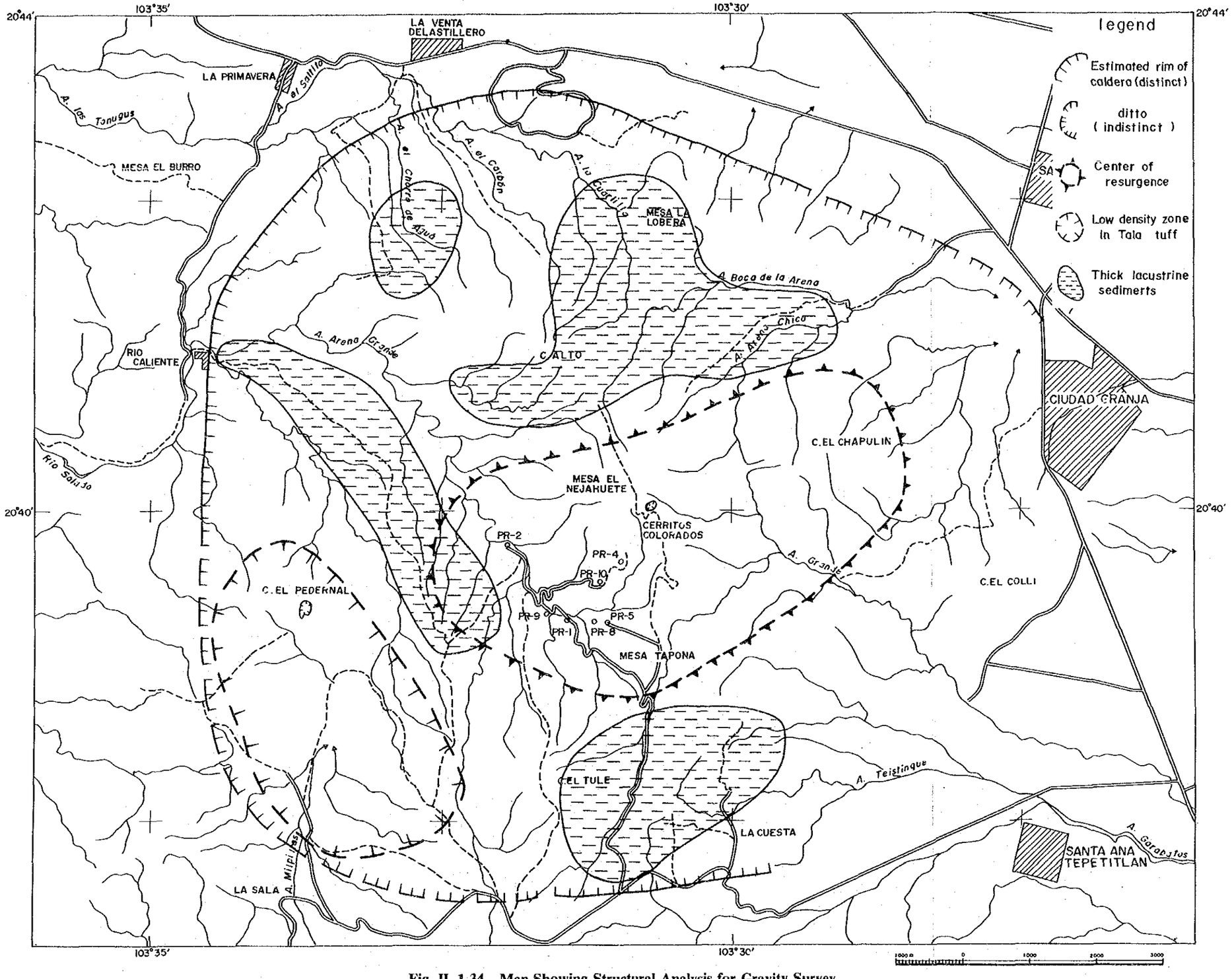

Fig. II. 1-34 Map Showing Structural Analysis for Gravity Survey

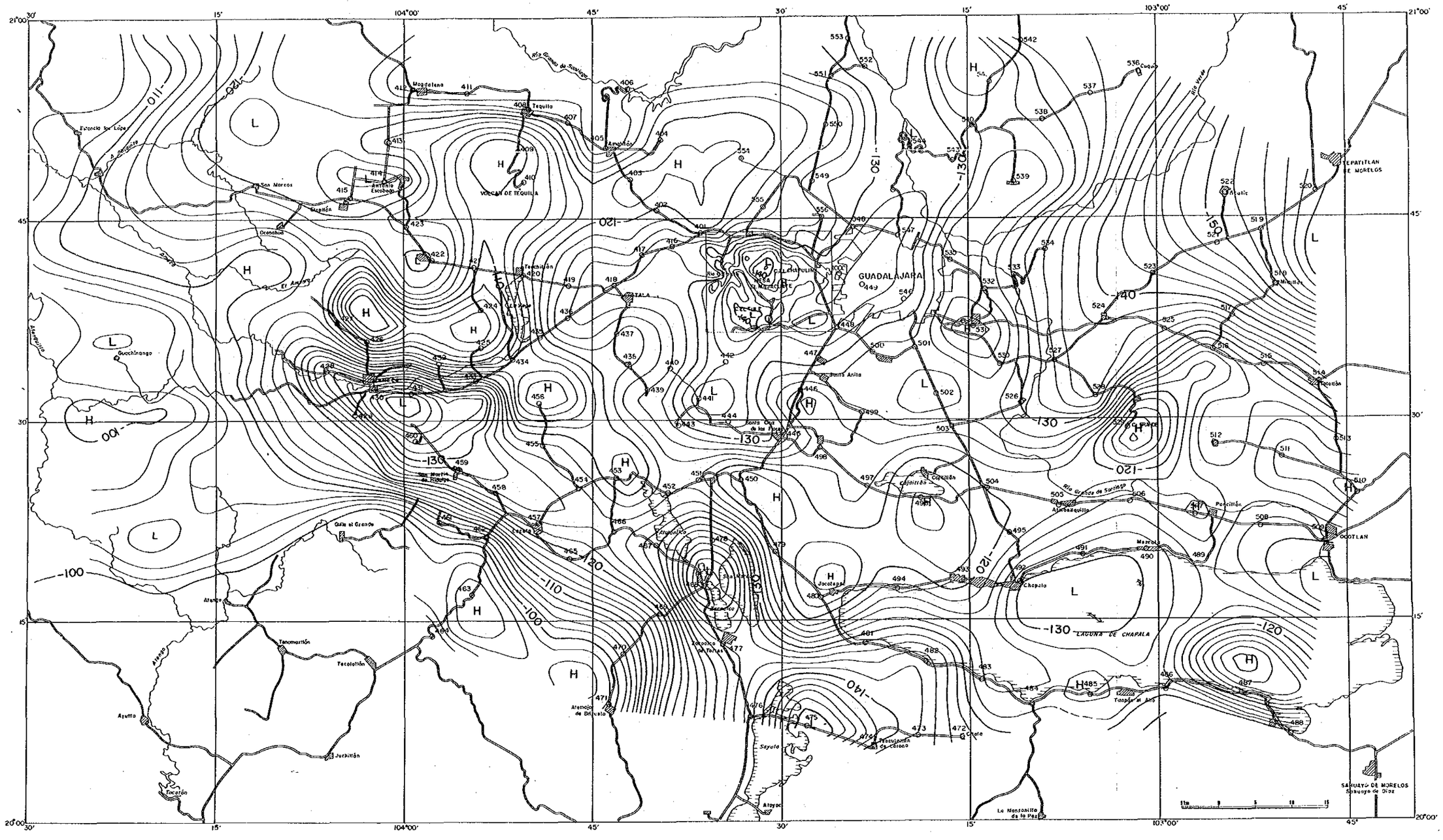

Fig. II. 1-35 Regional Bouguer Anomaly Map (ρ=2.20g/cm³)

1.4 Magnetotelluric survey

1.4.1 Summary of Magnetotelluric survey (MT survey)

The Remote-Reference Magentotelluric method was carried out as a deep electrical survey in order to obtain the information about the geothermal reservoir through the resistivity structure and to correlate with the deep-seated formation in the geothermal manifestation area.

The results are summarized as follows:

① The noise-free signals were recorded and the resistivity-depth curves by inversion analysis were clear in this MT survey. This is due to the fact that the resistivity structure consists of a one-dimensional horizontal three-layers (that is, high resistivity, low resistivity and high resistivity from the surface to the deeper formation). The one-dimensional structure is supported by the structure index analysis with a few exceptions.

② The main reservoir is characterized by the low resistivity with 5 ~ 20 Ω·m, judging from the horizontal resistivity distribution map drawn using the resistivity-depth curves after inversion. In particular, a lower resistivity anomaly due to up-flow can be identified to the south of PR-1 and PR-8 showing vertical extension.

③ The NW-SW trending resistivity structure is dominant as the depth increases. Therefore, the presence of geothermal fluids is mainly controlled by the NW-SE trend.

④ The upflow zone is made clear by a one-dimensional model profile, which is made by connecting the resistivity-thickness solution obtained from inversion, and a two-dimentional model profile. Moreover, it can be found that the wells offering excellent steam production were drilled in the low resistivity zone. Thus, the low resistivity zone at intermediate depths is localized as the fracture dominant geothermal reservoir.

1.4.2 Result of Magnetotelluric survey (MT survey)

(1) Field work procedure for MT survey

① Measuring station: Fifty four sounding stations were selected around the geothermal manifestation area as given in Fig. II.1-36. Among 54 stations, eight stations were tried resounding to verify the data quality. These sounding stations were arranged at intervals of about 300 m in and around the wells and of about 500 m in other area. Measurements in the area of steep topography were carried out by the remove of equipments.

② Field measurement: The Remote Reference Magnetotelluric method (i.e. simultaneous measuring at two points) was adopted to improve the data quality. Three components of magnetic field (Hx, Hy and Hz) and two components of electric field (Ex and Ey) naturally induced in the earth were measured in the MT method. Figs. II.1-37~38 show the field measurement procedure of these components.

③ Recording band width and duration: Recording was based upon three band widths of frequency, that is, high frequency (125Hz ~ 3Hz), middle frequency

(15Hz ~ 10 second) and low frequency (0.5Hz ~ 200 second) for each components. The recording duration and other parameters of MT survey is given in Table II.1-13.

④ Data acquisition system: The data acquisition system is composed mainly of signal conditionor, quartz clock, magnetic sensor, telluric sensor and field processor as shown in Fig. II.1-39. The apparatus for MT survey was movable by the power of men, and was worked by the batteries. The signals of each component in time are recorded in the field processor through sensors and signal conditionor. The field processor includes three CPUS, CRT of 5 inch and a hard disk drive of 5 M byte, resulting in the possibility of data processing in real time. The data acquisition and processing systems were operated by the keyboard connected to the field processor. The accuracy of quartz in clock was 10^{-9} second per second and 10^{-6} second per cycle.

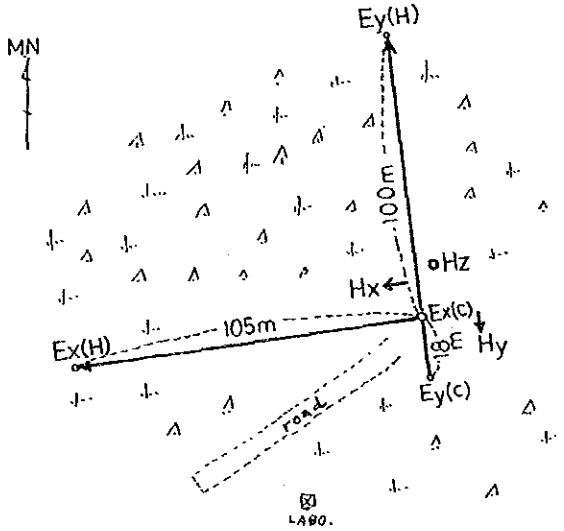

Fig. II. 1-37 Positioning of Sounding Station of No.27

Table II. 1-13 Recording Band Width, Parament and Duration of MT Survey

	Band width of frequency	Sampling channel rate	Length of each recording segment	Segment number for 1 file	Recording duration for 1 file	File number	Sampling number for FFT	Q value
HF	125Hz 3Hz	each 500Hz	512	64	about 1 min.	3 ~ 5	512	6
MF	15Hz 10 second	each 60Hz	512	64	about 9 min.	3 ~ 5	512	6
LF	0.5Hz 200 second	each 2Hz	512	30 ~ 40	130 ~ 170 min.	1	1024	4

(2) Data processing

The field processor can calculate apparent resistivity, impedence phase, impedence strike and tipper strike in real time during acquiring the MT signals (Fig. II.1-40). This calculation aims at the data improvement by quality control of the data.

The final data processing is as follows:

① Compilation of data in time
② First Fourier Transform
③ Single data processing and Remote Reference data processing
④ Calculation and indication of the following MT parameters:
  i) apparent resistivity (ρ_{XY}, ρ_{YX})
  ii) phase (Φ_{XY}, Φ_{YX})
  iii) impedance strike
  iv) tipper magnitude
  v) skew
⑤ Automatic elimination of low quality data by the coherency check which is the correlation of electric field with magnetic field.

An example of comparison the field processing in real time with the final data processing at station 07 is shown in Fig. II.1-41. Both the Single data processing and the Remote Reference data processing are used for the final data processing.

(3) Model inversion analysis and structure index

① Model inversion analysis: The MT data obtained in the field indicates the relation between apparent resistivity (ρ_a) and period (T). Model inversion analysis is required for the conversion to resistivity (ρ) in depth (thickness, h). At first, an one-dimensional model inversion analysis was carried out under the assumption of horizontal multi-layered resistivity structure in the subsurface to calculate the underground apparent resistivity. The analysis procedure is given in Fig. II.1-42. As shown in Fig. II.1-42, the important point of the analysis is to put various assumptive resistivities in depth against the apparent resistivity-period curves obtained from measurement, after that to find an adequate resistivity value.

Fig. II.1-43 shows an example of the inversion analysis at station 07. The resistivity-depth curves in bottom right of Fig. II-1-43 and Fig. II.1-44 are obtained from the inversion analysis after coherency check which is shown in bottom left of Fig. II.1-41. The curves are based on the final RRMT data processing.

All results of one-dimensional model inversion are appended in the last of this report.

② Selection of TE mode and TM mode: A problem of adaptability is present for such model inversion analysis when the subsurface structure does not exhibit horizontal multi-layer. If the subsurface has two- or three-dimensional structure, it must be taken into consideration of adaptability of the one-dimensional analysis. Two mode types can be generally considered in case of two-dimensional resistivity structure, because of the existence of two different apparent resistivities (ρ_{XY}, ρ_{YX}) as follows:

TE mode: the direction of electric field is parallel to the structure axis.

TM mode: the direction of magnetic field is parallel to the structure axis.

The magnetic field is changeable easily depending upon surrounding geological situations (rock magnetism, rock alteration etc.) and upon lateral influence. So that, the analysis by TM mode is not suitable for one-dimensional analysis. Accordingly, TE mode was selected out for the present analysis.

Angles of the tipper strike indicating the TE direction and of the impedance strike indicating the ρ_{XY} direction were checked for determining TE mode out of ρ_{XY} and ρ_{YX}. If the angle is smaller than $\pi/4$, ρ_{XY} is TE mode. If the angle is bigger than $\pi/4$, ρ_{YX} becomes TE mode.

③ Structure index

The tipper magnetude (T) and the skew (S) were used to judge the dimension of underground resistivity structure:

one-dimensional structure: $T \fallingdotseq 0$ and $S \fallingdotseq 0$

two-dimensional structure: $T \gg 0$ and $S \fallingdotseq 0$

three-dimensional structure: $T \gg 0$ and $S \gg 0$

Figs. II.1-45 and 46 show the distribution maps of tipper magnitude and skew respectivity. The surveyed area shows the one-dimensional structure as a whole, except for some two-dimensional structures by stations of 01 and 46. Three dimensional structure was not recognized in this area.

1.4.3 Resistivity structure by Magnetotelluric method

(1) Horizontal resistivity distribution

Apparent resistivity maps with TE mode were prepared on three periods (0.01 second, 1 second and 30 second) to determine apparent resistivity in horizontal profile. These characteristics are as follows:

① A period of 0.01 second — High apparent resistivity with more than $50\Omega\cdot m$ is observed all over the surveyed area. In particular, high apparent resistivities with more than $200\Omega\cdot m$ are recognized in the north (stations No. 14, 20, 29 and 54) and in the east (stations 41, 49 and 52) of this area.

② A period of 1 second — Low apparent resistivity of about $10\Omega\cdot m$ is distributed over the whole surveyed area, and the contrast in resistivity is not clear.

③ A period of 30 second — The connecting line with PR-2 and PR-5 separates resistivity value, namely comparatively high apparent resistivity is present in the northeast, while comparatively low apparent resistivity is present in the southwest of this area. The apparent resistivity has a tendency to trend NW-SE. A marked low apparent resistivity zone is found near the stations No. 10, 18 and 22 (near PR-1 and PR-8), showing a striking contrast in resistivity. Fig. II.1-47 shows a distribution drawing on a period of 30 second with TE mode which represents the characteristics of reservoir in this area.

Then, a resistivity-depth curve was drawn by appling the Bostic inversion to the initial apparent resistivity-period curve. A horizontal resistivity map was prepared by the resistivity-depth curve with TE mode. The map is obtained from extracting resistivity value on each

sounding station at optional depth. A total of 7 horizons (6 horizons with 500 m interval from 1,500 m to −1,000 m above sea level together with a −3,000 m horizon) was selected for preparing horizontal resistivity distribution. Among them, the following are representative characteristics of resistivity:

① 1,500 m above sea level (Fig. II.1-48) — High resistivity with more than 50Ω·m surrounds the geothermal manifestation area showing a contrast for low resistivity. Lower resistivity with less than 5Ω·m is observed locally. The resistivity value is considered to be affected by the degree of alteration and water saturation in rocks rather than rock facies, although various rock facies such as the Tala Tuff, lithic tuff and rhyolite are distributed in this level.

② 1,000 m above sea level (Fig. II.1-49) — Low resistivity of about 10Ω·m is found all over the surveyed area showing a obsure contrast in resistivity. This level belongs to the upper part of the Cordilleran Volcanics, so that low resistivity depends upon the density of fractures per unit area.

③ Seal level (Fig. II.1-50) — Low resistivity ranging from 5 to 20Ω·m is widely distributed over the whole area. A lower resistivity anomaly with less than 2 to 5Ω·m exists to the south of PR-1 and PR-8 near the station No. 18. The low resistivity zone over the whole area is ascribed to the presence of geothermal fluids, since this level belongs to the main geothermal reservoir.

④ 500 m below sea level (Fig. II.1-51) — The resistivity pattern of this level show the same pattern as sea level. A lower resistivity anomaly located to the south of PR-1 and PR-8 continues vertically from this level to 3,000 m below sea level. This fact emphasizes that the anomaly is consistent with the uplift zone confirmed by the geological survey and with the up-flow zone discovered by the fluid inclusion study and the downhole temperature measurements.

⑤ 3,000 m below sea level (Fig. II.1-52) — High resistivity with more than 50Ω·m is dominant all over the area with the exception of lower anomaly located to the south of PR-1 and PR-8. In particular, the eastern portion of this area are occupied by the high resistivity. The above facts suggest that the presence of fractures is restricted to comparatively small areas and no fracture (that is, the absence of geothermal fluids) exists in the high resistivity zone.

The following conclusions are reached from the above resistivity distribution:

i) The resistivity structure is not NE-SW trend but NW-SE trend.

ii) The above tendency is emphasized as the depth increases.

iii) The presence of geothermal fluids is not controlled by the NE-SW trending faults found in the surface, but controlled by the NW-SE trending fractures in the deep-seated formation.

(2) Vertical profile analysis

The relationships between apparent resistivity versus period and resistivity versus depth are shown in Figs. II.1-53~54 respectively. They are vertical profiles along survey line 3. Low apparent resistivity zone exhibits a wide-spread feature upward and sideward in Fig. II.1-53. On the contrary, low resistivity zone indicates a funnel-shaped feature and an existence of

up-flow in Fig. II.1-54 which is vertical profile applied the Bostic inversion.

A one-dimensional vertical profile can be made by connecting the resistivity-thickness solution obtained from inversion along the survey line. Profiles were prepared for nine survey lines. Line B and line 3, as a representation, have been used to make the model profiles shown in Figs. II.1-55 and 56. The figures show a typical three layer structure consisting of high resistivity layer, low resistivity layer and high resistivity layer from the surface to the deeper formation. The shallow high resistivity seems to reflect a dry formation of the Tala Tuff. The thought is supported by the fact that the geothermal fluids from PR-1 and PR-8 flash in the formation (i.e. water shortage in shallow formation).

In the intermediate horizon, low resistivity values are found uniformly for line 3, while different resistivity values are recognized for line B depending on the position of the line. By plotting the tracks of existing wells into Fig. II.1-55, it has been made clear that the wells offering excellent steam production are drilled in the low resistivity zone. Therefore, attention should be paid to this low resistivity zone in the intermediate horizon as a prospective geothermal reservoir with dominating fractures. A low resistivity anomaly is present at the deeper part of station No. 18 showing a different type from neighborhoods.
It appear to have a relation with the up-flow.

High resistivity zone occupies the stations 20, 21 and 40 in Fig. II.1-56, resulting in the limited extension of geothermal reservoir. It cannot refer to such consideration in Fig. II.1-55. The results of one-dimensional vertical profile reflect obviously the extent of geothermal reservoir.

Finally, a two-dimensional model analysis also has been tried for line B and 3. The result of this analysis shows similar resistivity distribution and structure compared with the one-dimensional profile. However, the horizontal multi layered structure and the contrast in resistivity are emphasized in the two-dimensional profile.

That is to say, the two-dimensional profile in Fig. II.1-57 shows a concentrated low resistivity anomaly with less than 5Ω·m near PR-1 and PR-8, and a continuously horozontal distribution of low resistivity layer with 5 to 50Ω·m. On the contrary, the one-dimensional profile in Fig. II.1-55 shows a locally divergent distribution of low resistivity layer in the intermediate depth.

On the other hand, the two-dimensional profile in Fig. II.1-58 indicates more narrow distribution of low resistivity with less than 5Ω·m in comparison with the one-dimensional profile in Fig. II.1-56. Moreover, the value of low resistivity anomaly in the vicinity of station No. 18 in Fig. II.1-58 is lower (less than 1Ω·m) than the value in Fig. II.1.56 showing vertical continuity from the shallow part to the deeper part.

High resistivity zone in the deeper formation has horizontal continuity in Fig. II.1-58 in spite of a scattered distribution in Fig. II.1-56.

(1) Setting of magnetometers

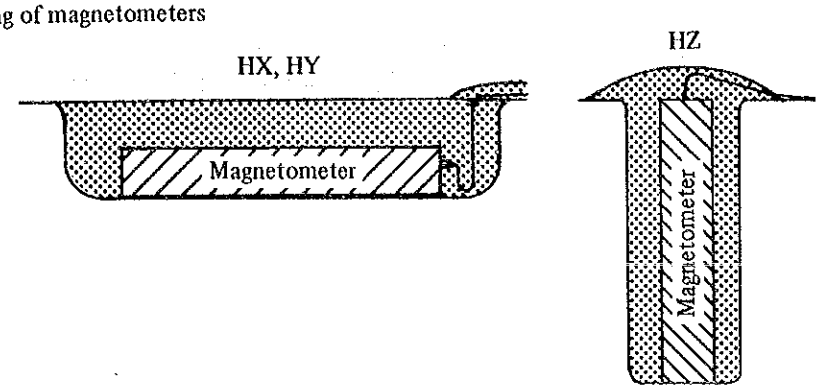

(2) Setting of electrode

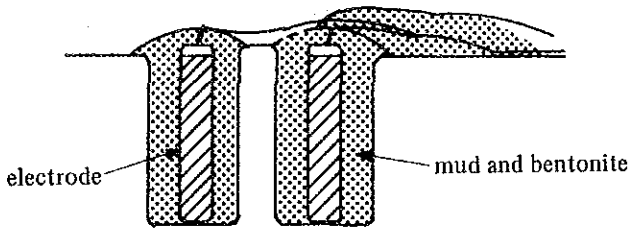

(3) Example of cable setting
(Example of good setting)

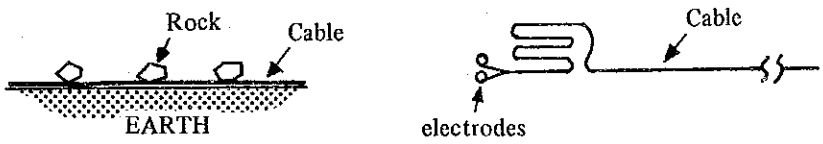

(Example of bad setting)

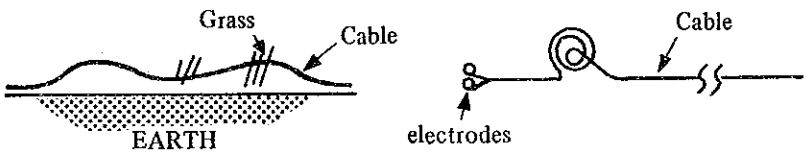

(1) Setting of magnetometers
3 magnetometers were buried in the earth completely.
(2) Setting of electrode
2 or 3 electrodes were buried in each hole (4 holes for 2 lines) with bentonite and mud.
(3) Setting of cables
Cables were setted on the earth not to move. And sometimes cables were buried in the earth.

Fig. II. 1-38 An Example of Setting of Magnetometers, Electrodes and Cables

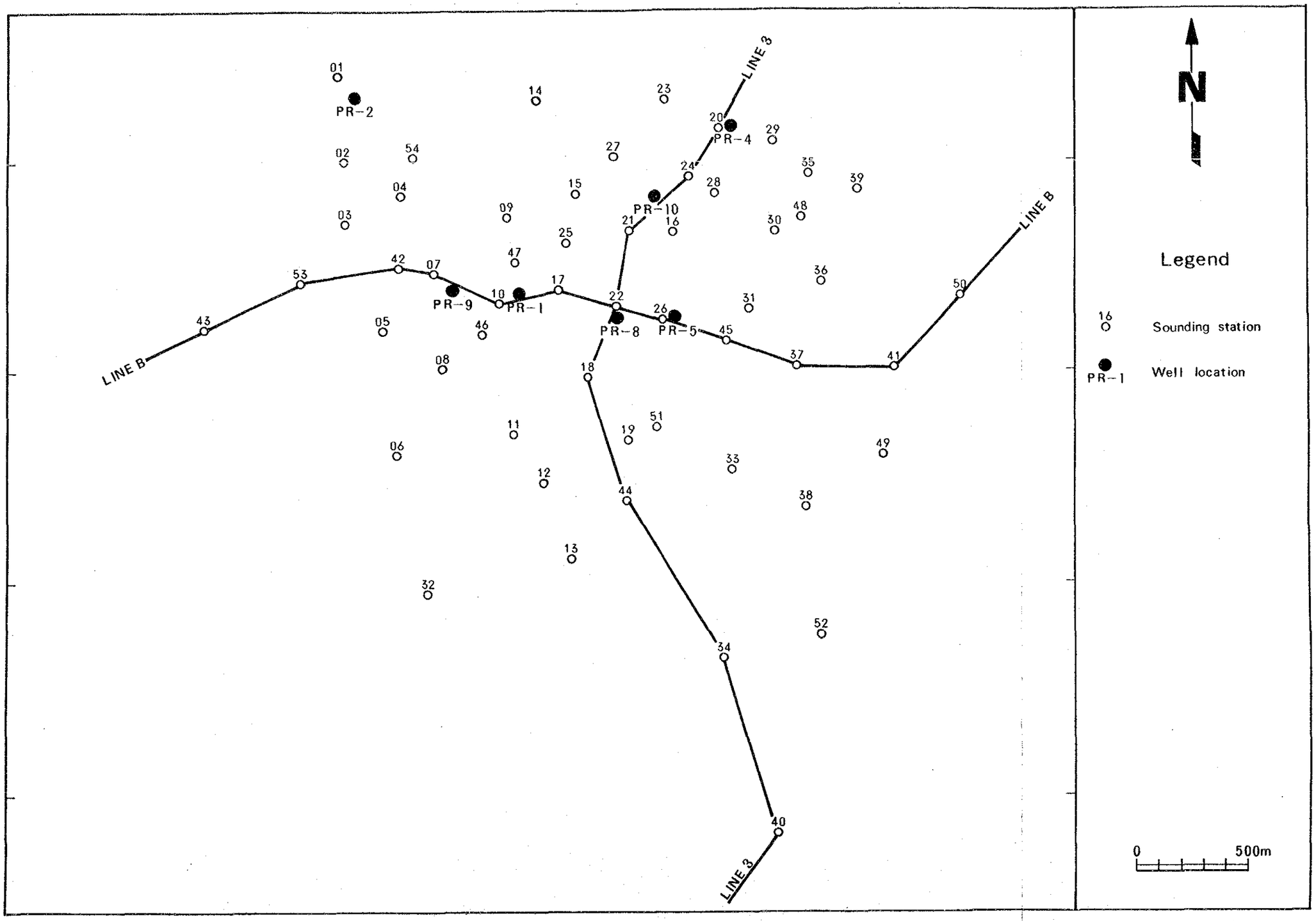

Fig. II. 1-36 Map of Location and Line for MT Survey

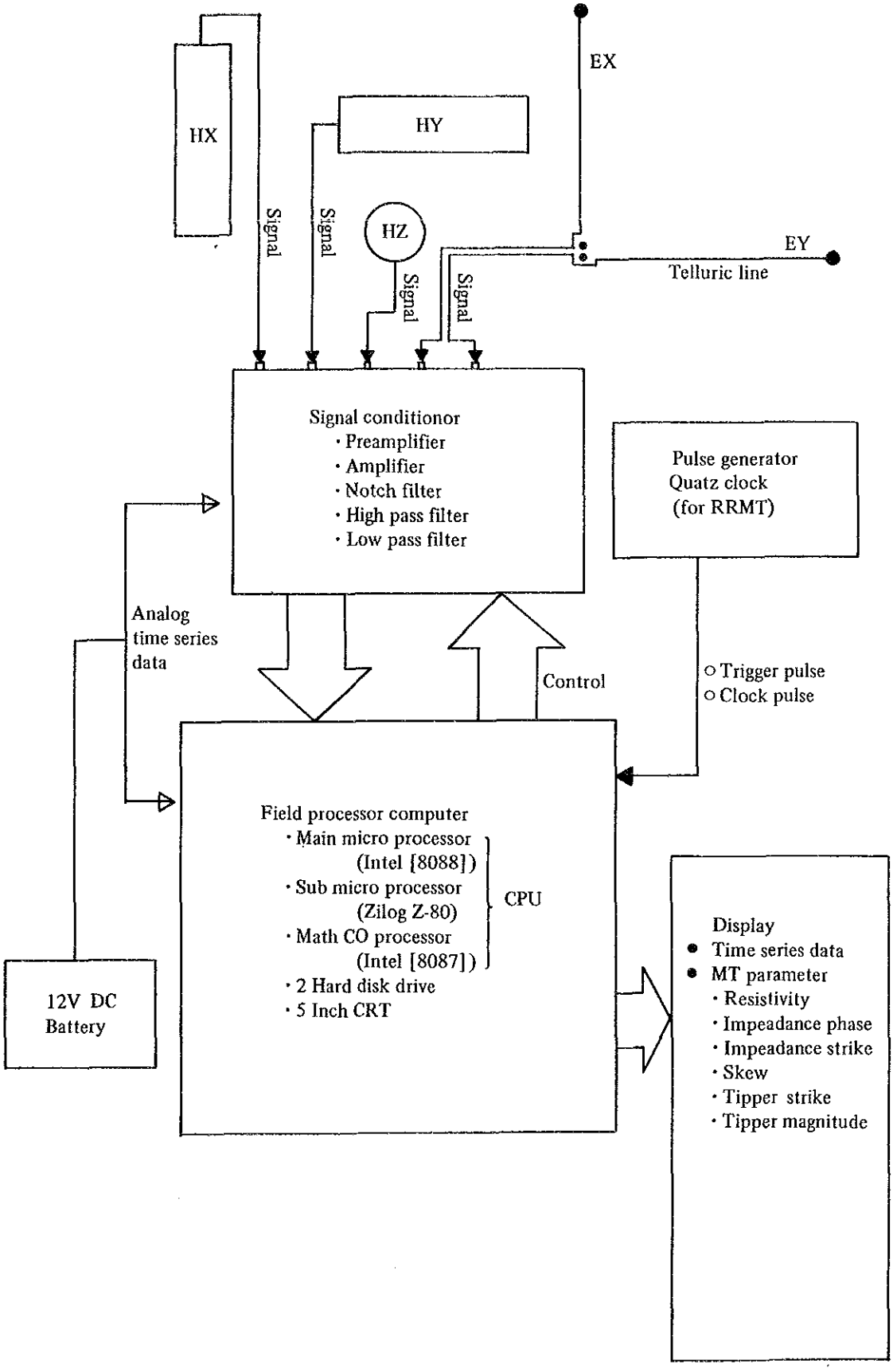

Fig. II. 1-39 Outline of MT Data Acquisition System

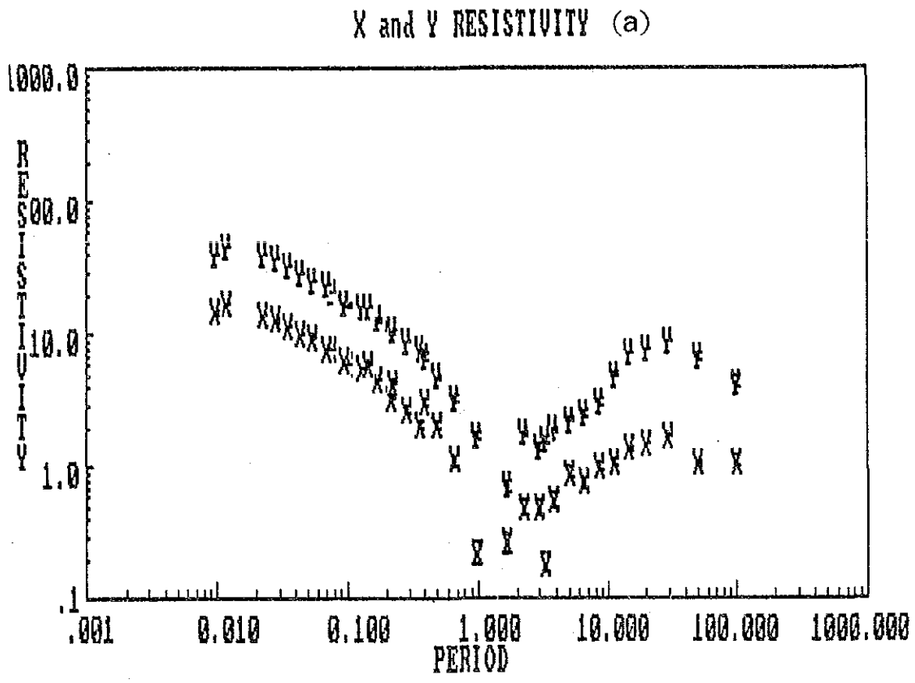

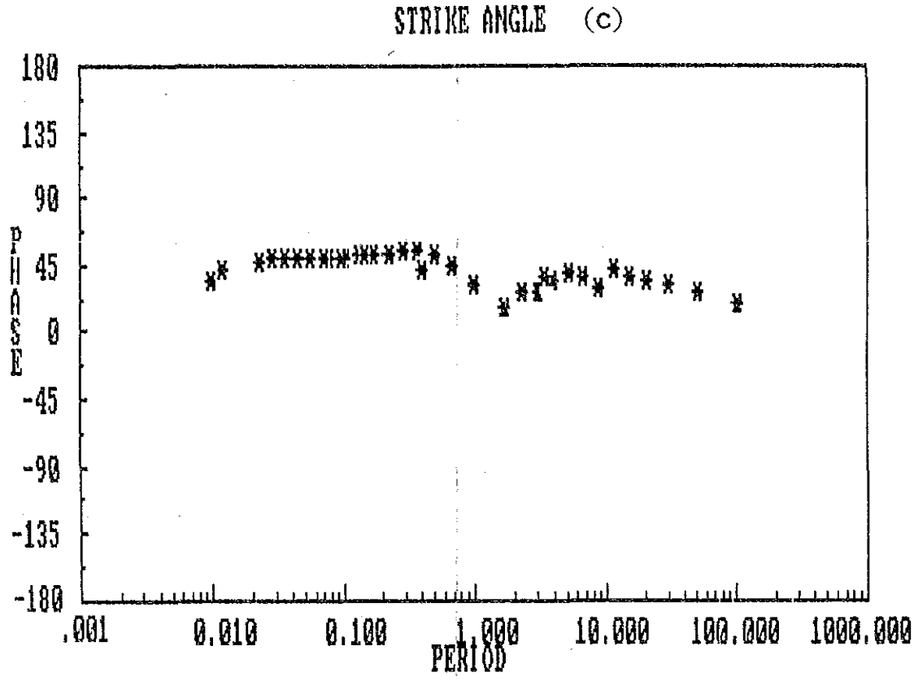

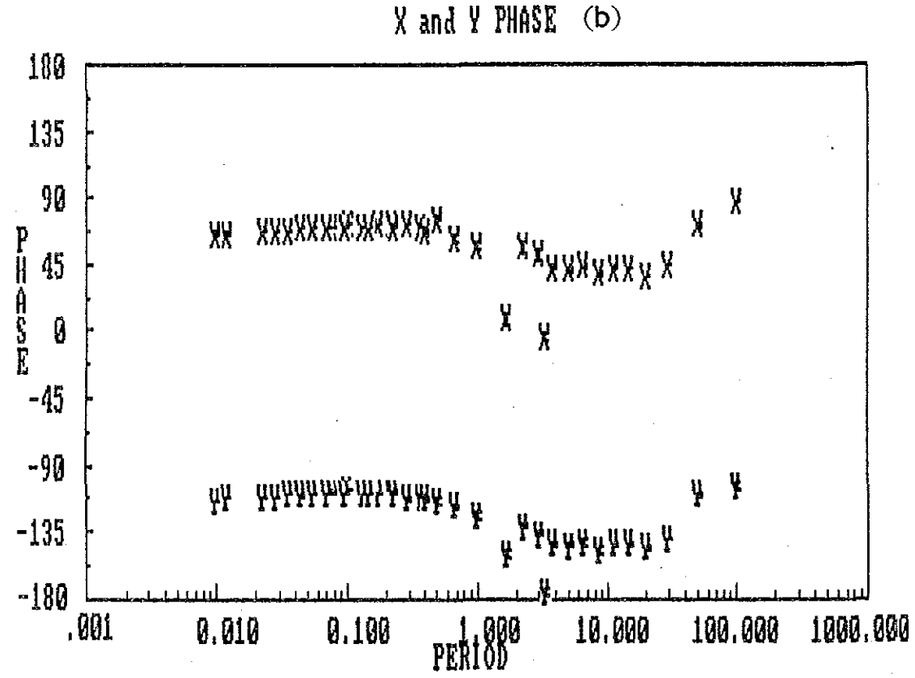

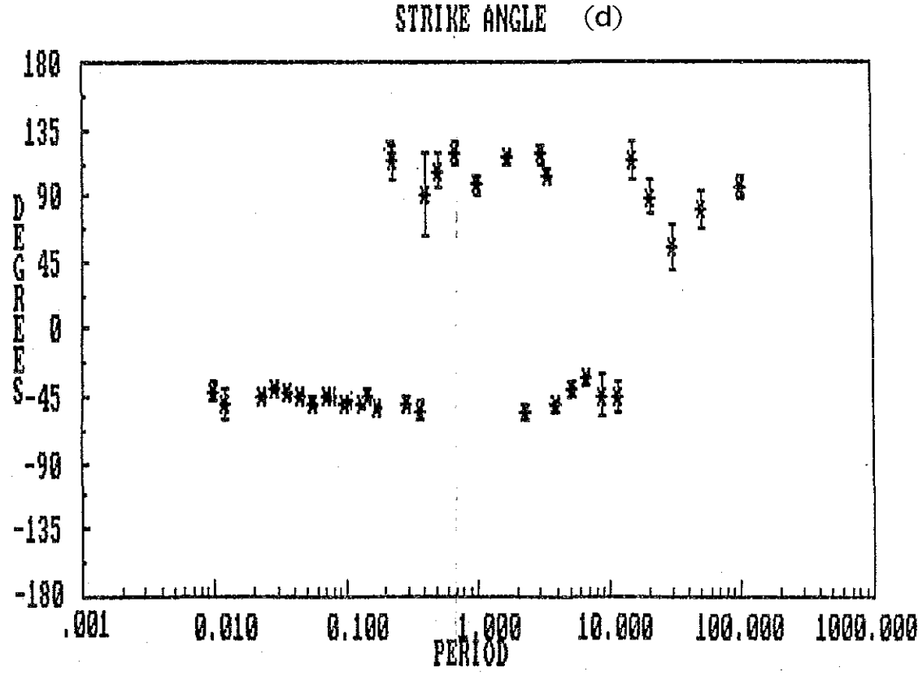

Fig. II. 1-40 Examples of Field Data Processing Result of Station 06

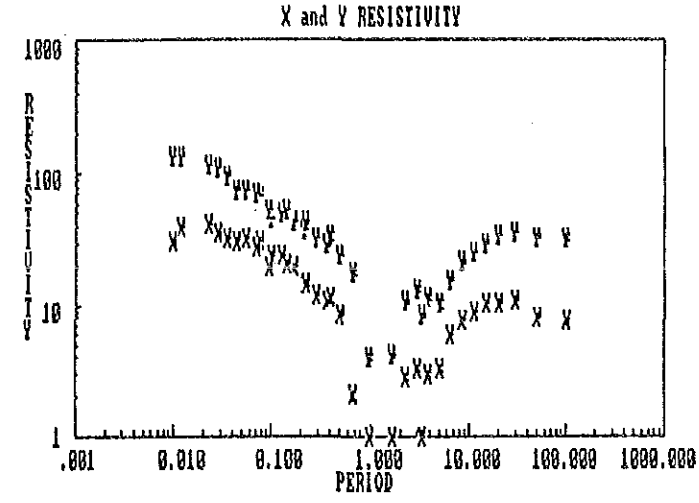

a) Single Data Processing Result using Field Processor (in Field)

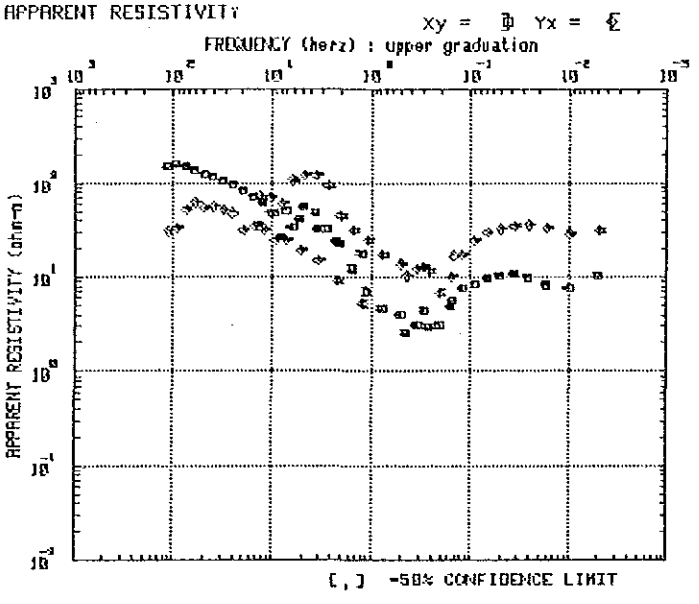

b) Single Data Processing Result after editting using Data Processing System

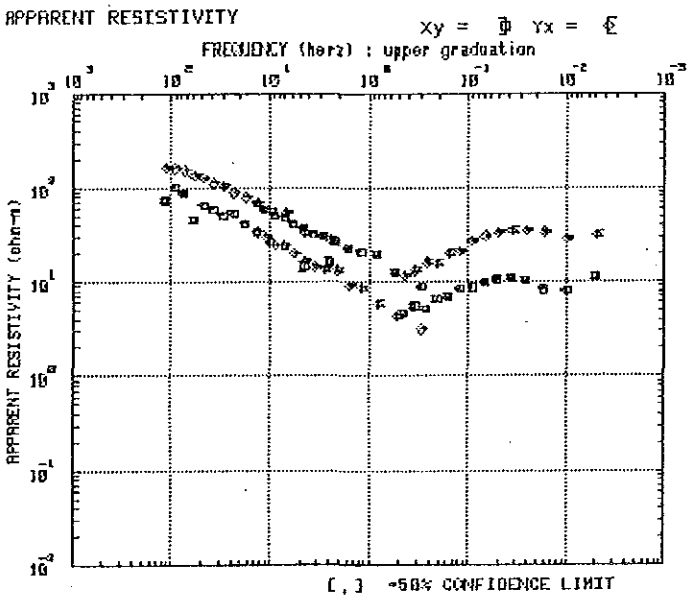

c) Final Remote Reference Data Processing Result using Data Processing System

Fig. II. 1-41 Comparison with Field Processor and Final Data Processing of Station 07

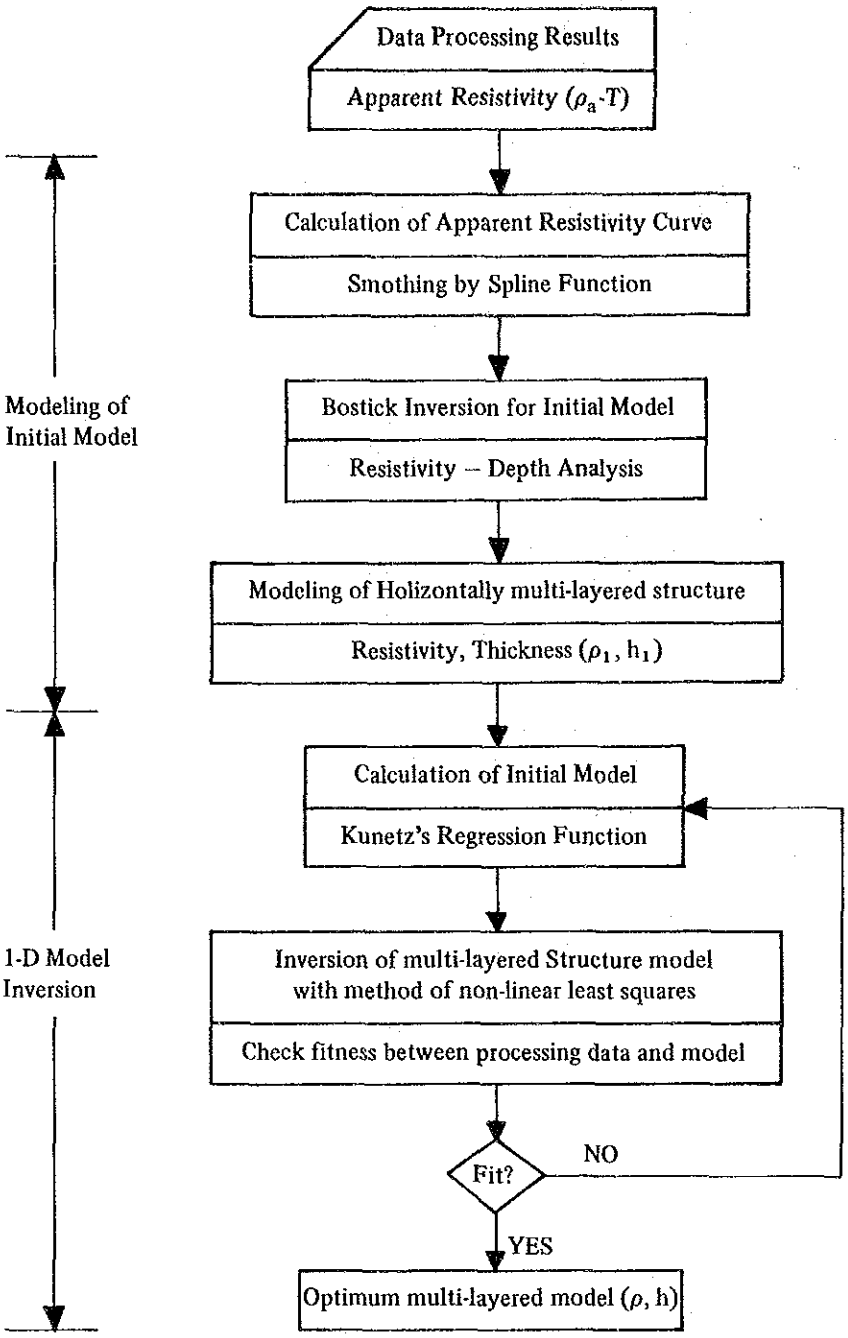

Fig. II. 1-42 Flowchart of 1-D Model Inversion

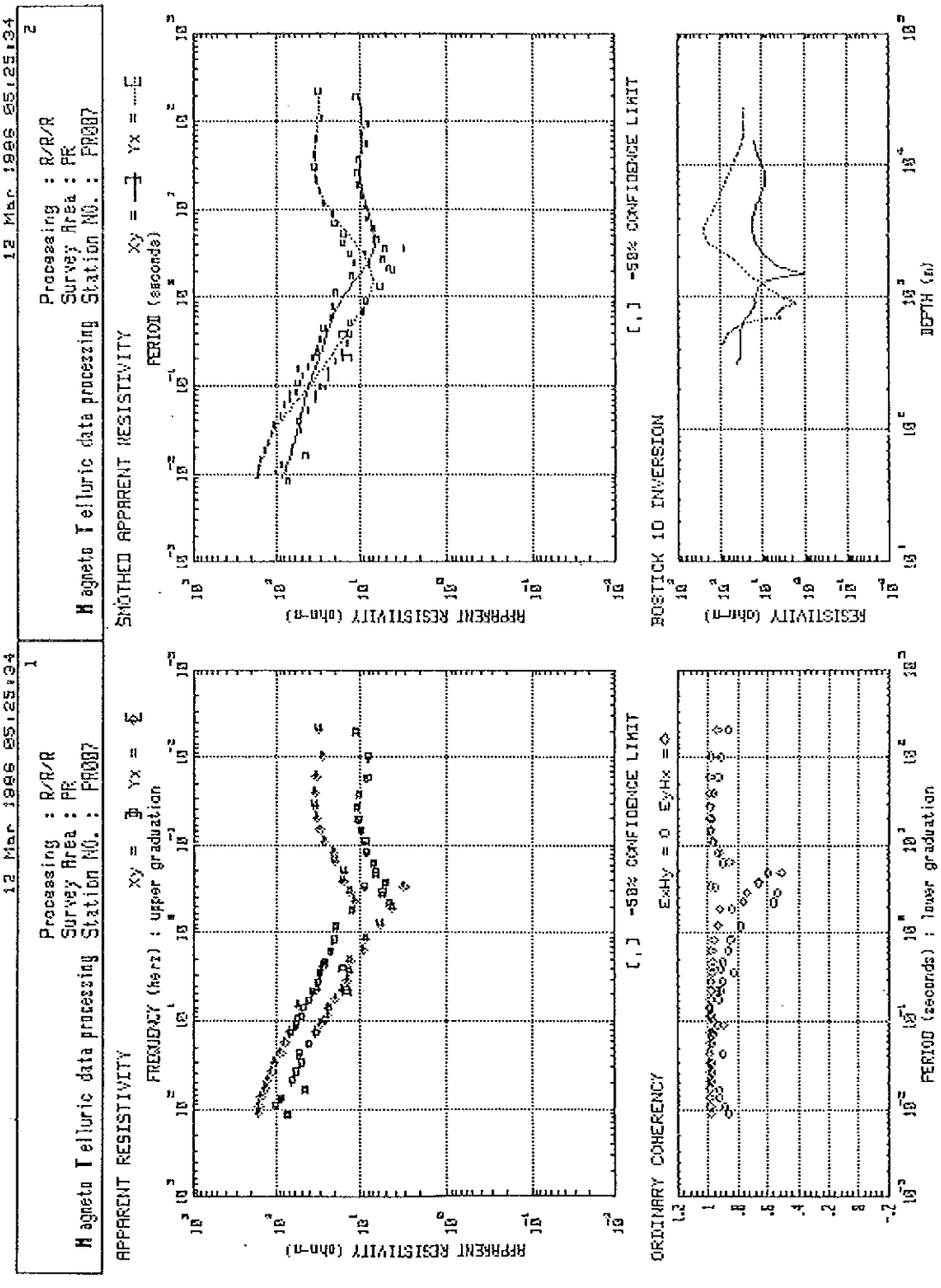

Fig. II. 1-43 Process of 1-D Model Inversion (Station 07)

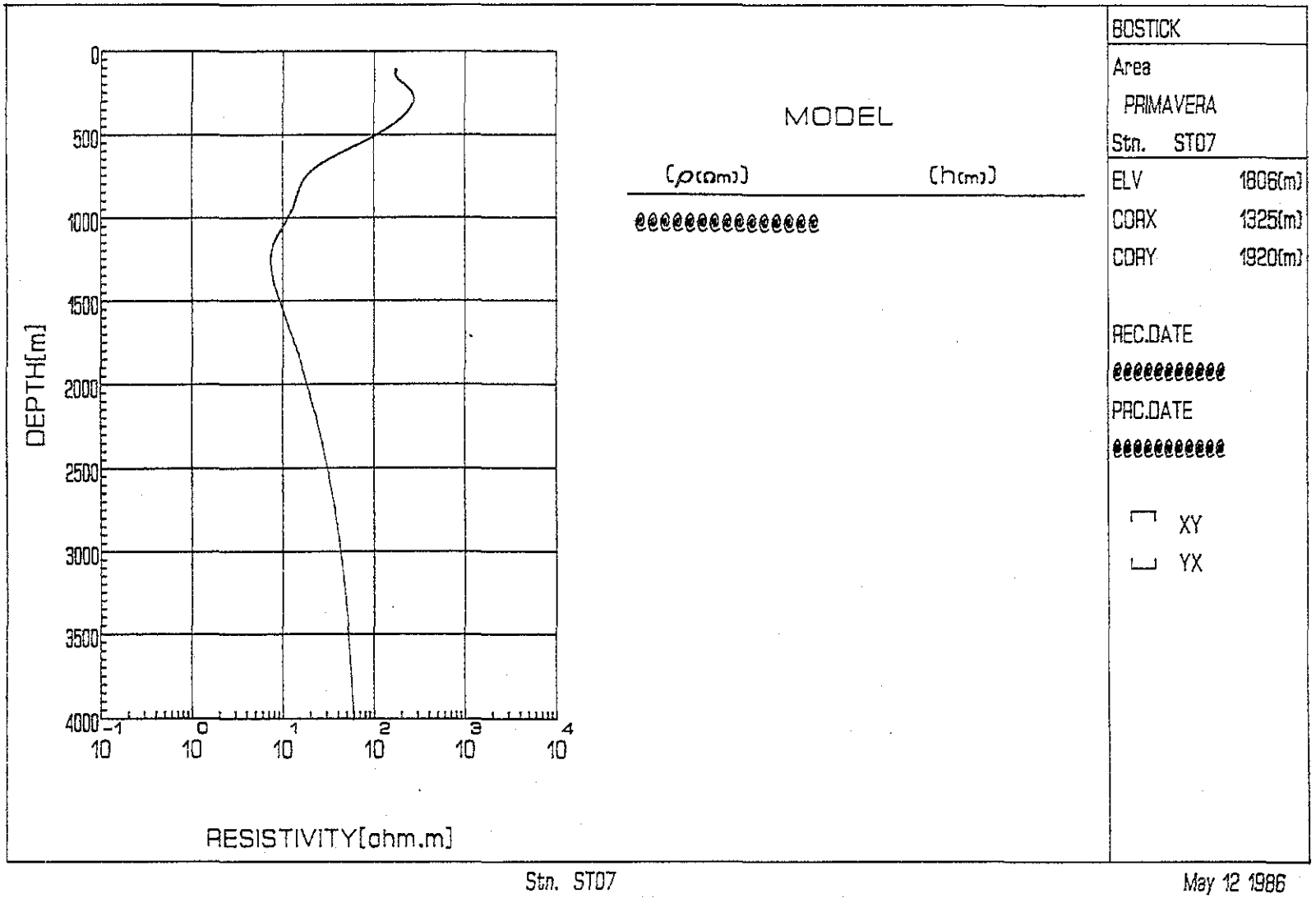

Fig. II. 1-44 An Example of Result of 1-D Model Inversion (Station 07)

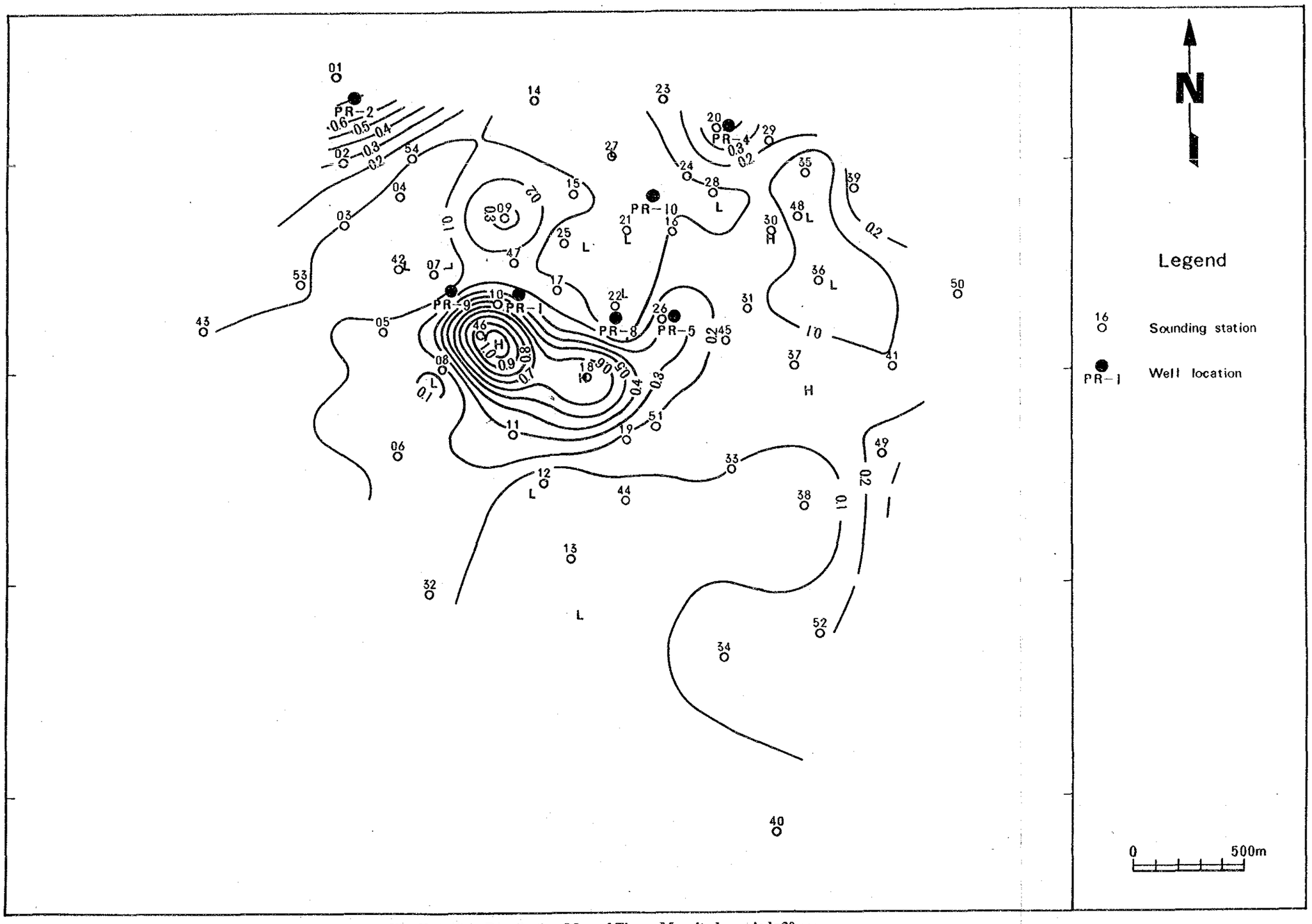

Fig. II. 1-45 Distribution Map of Tipper Magnitude, period=30 sec

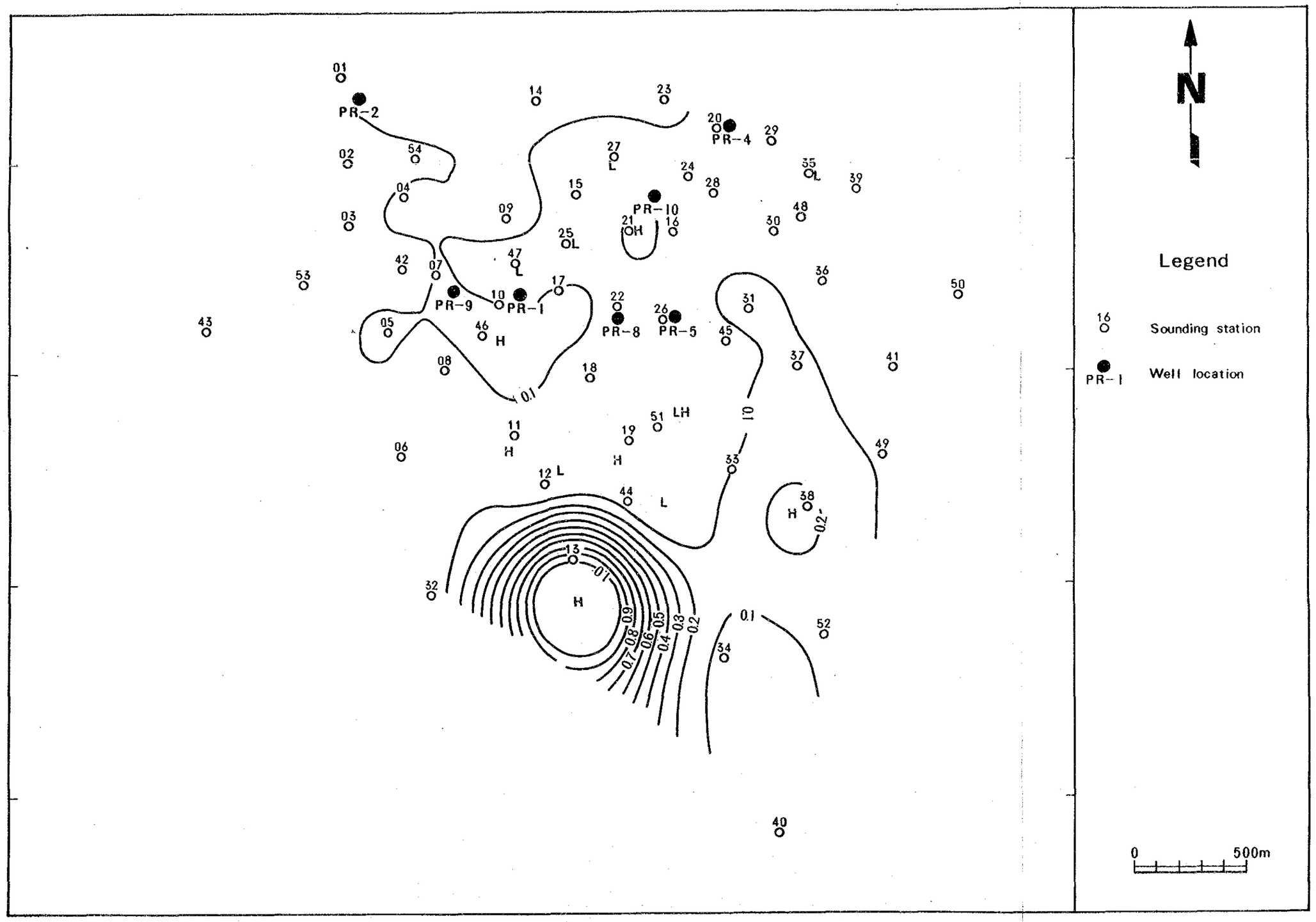

Fig. II. 1-46 Distribution Map of Skew, period=30 sec

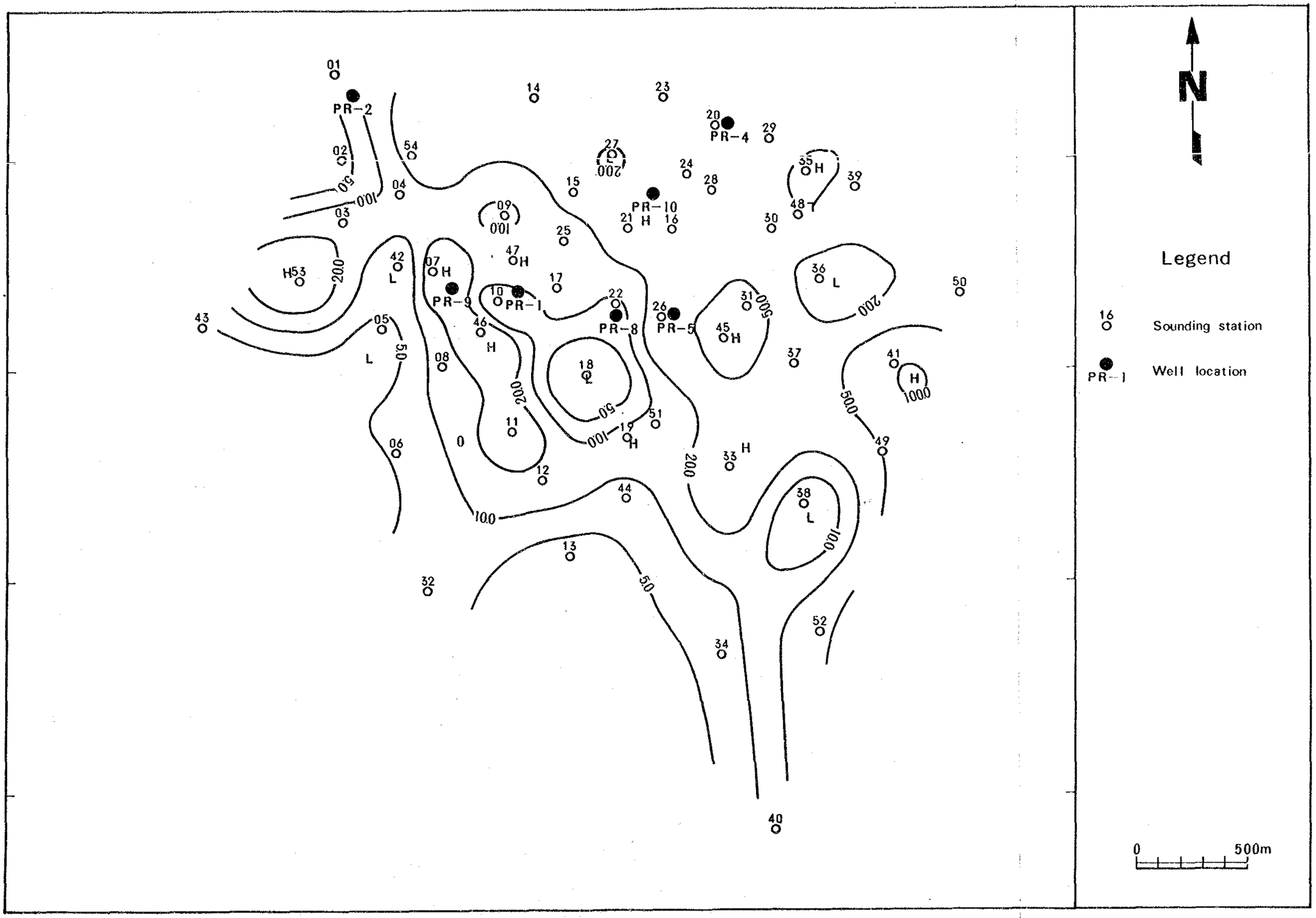

Fig. II. 1-47 Apparent Resistivity Map (TE mode), period=30 sec

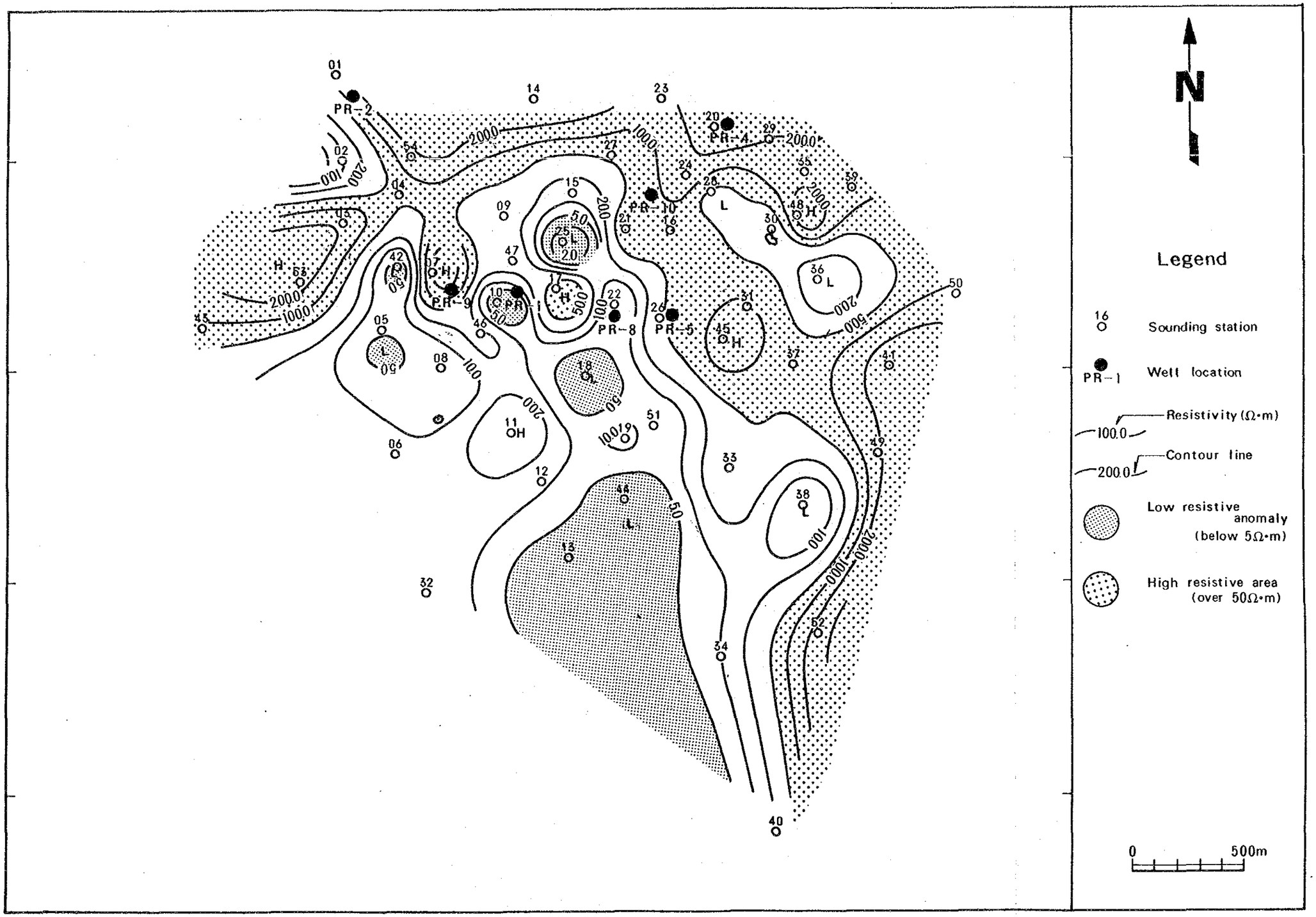

Fig. II. 1-48 Resistivity Map (TE mode; SL 1,500m)

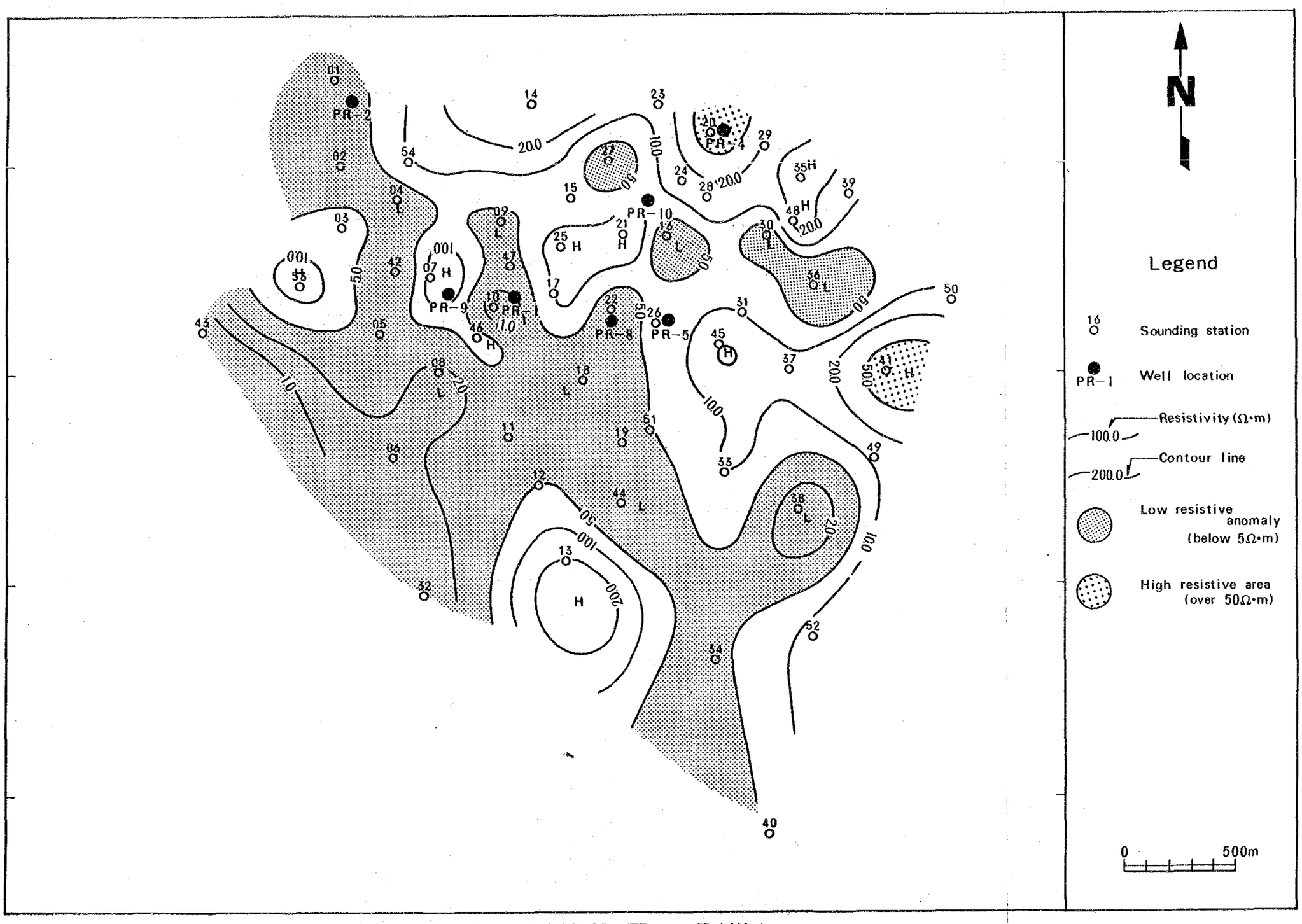

Fig. II. 1-49 Resistivity Map (TE mode; SL 1,000m)

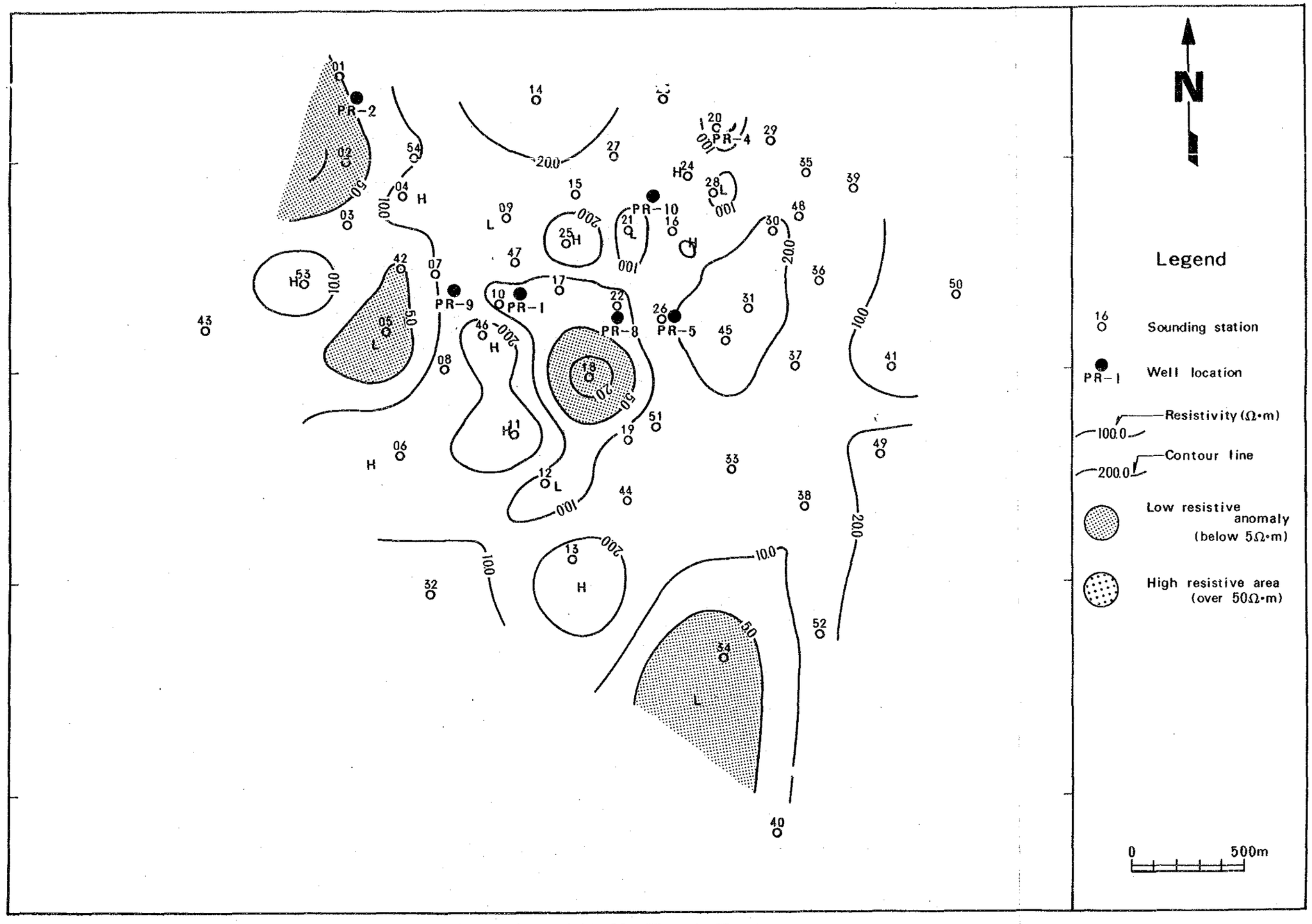

Fig. II. 1-50 Resistivity Map (TE mode; SL 0m)

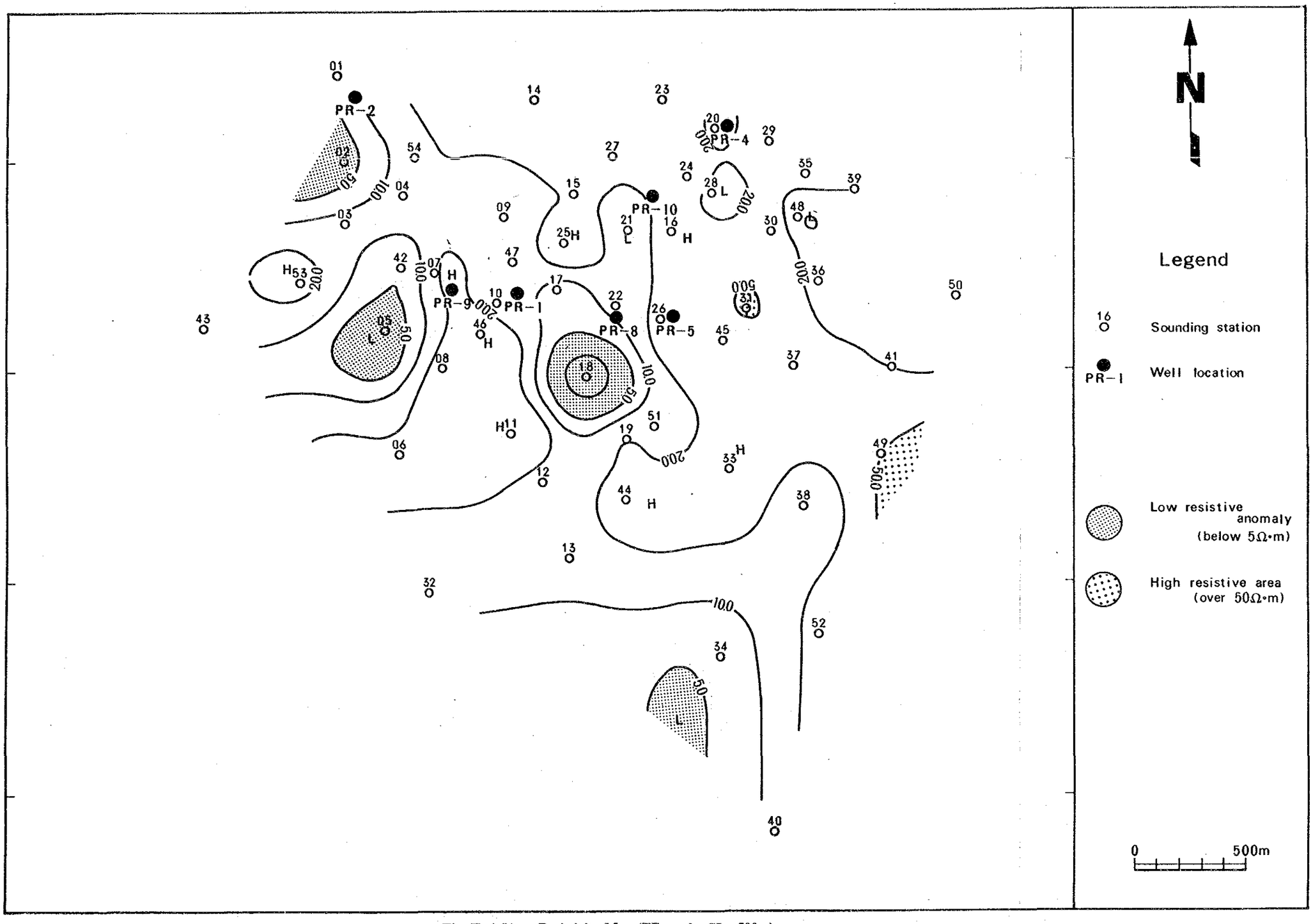

Fig. II. 1-51 Resistivity Map (TE mode; SL -500m)

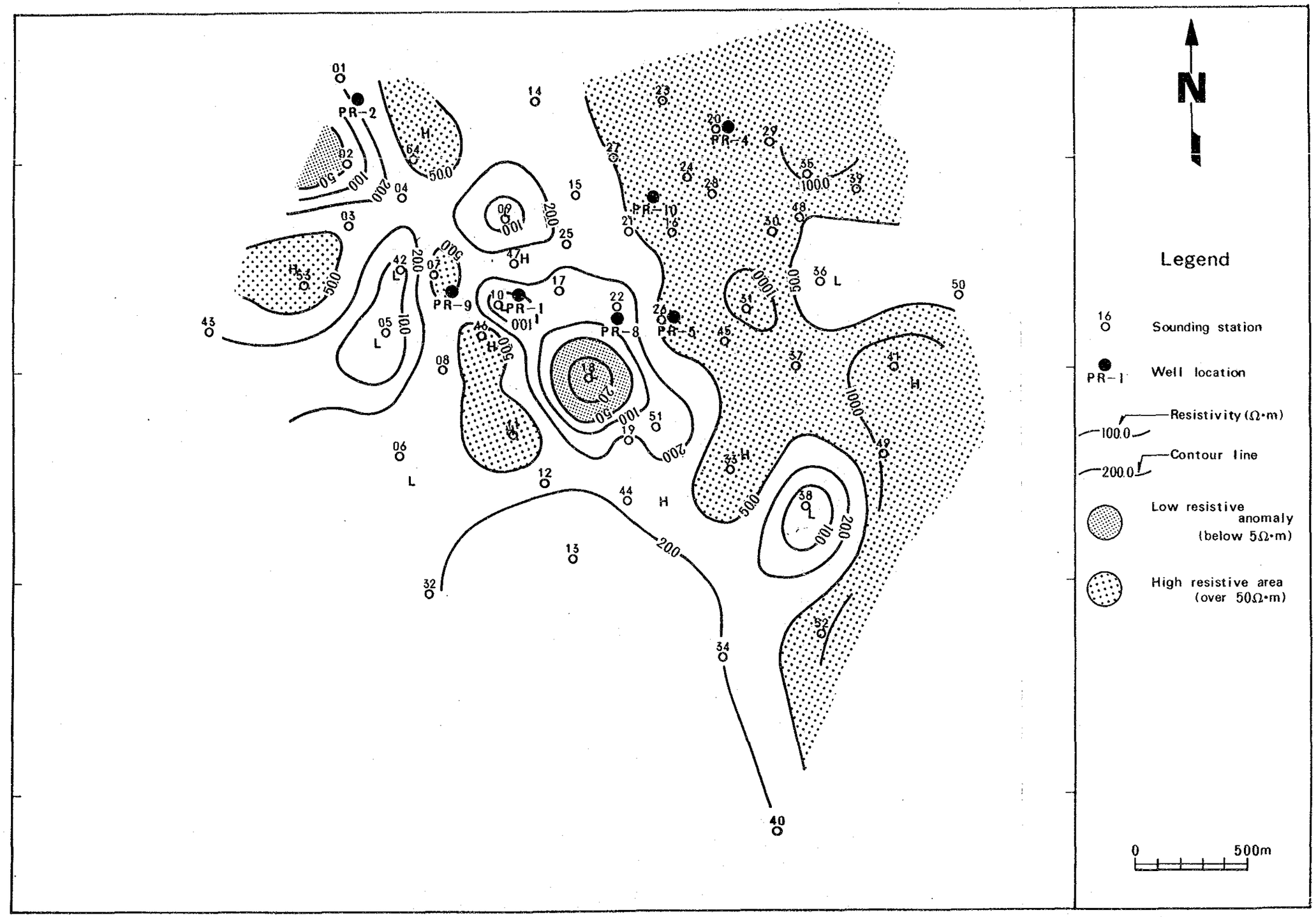

Fig. II. 1-52 Resistivity Map (TE mode; SL -3,000m)

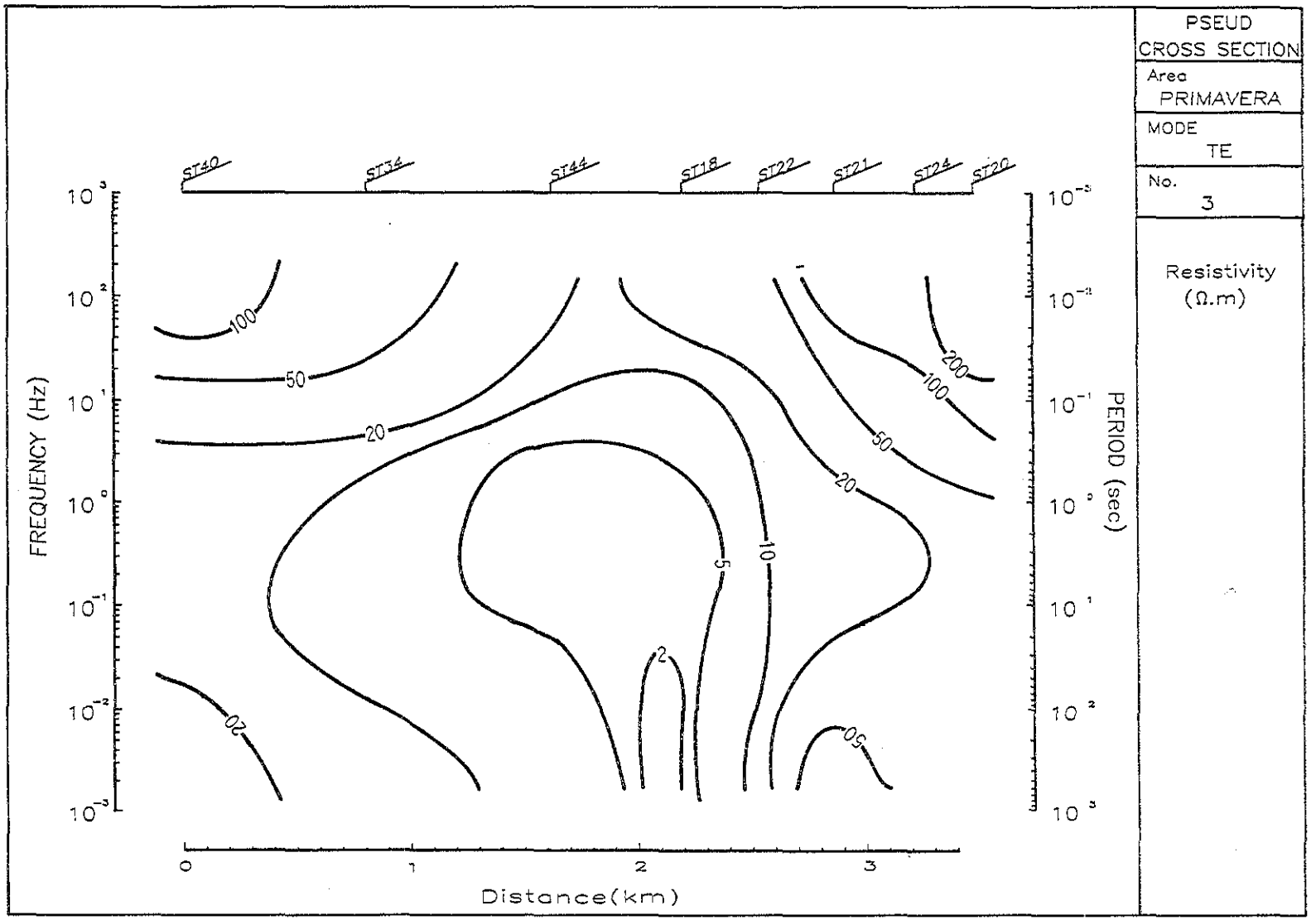

Fig. II. 1-53 Pseudo-Cross Section of Apparent Resistivity (TE mode), Line 3

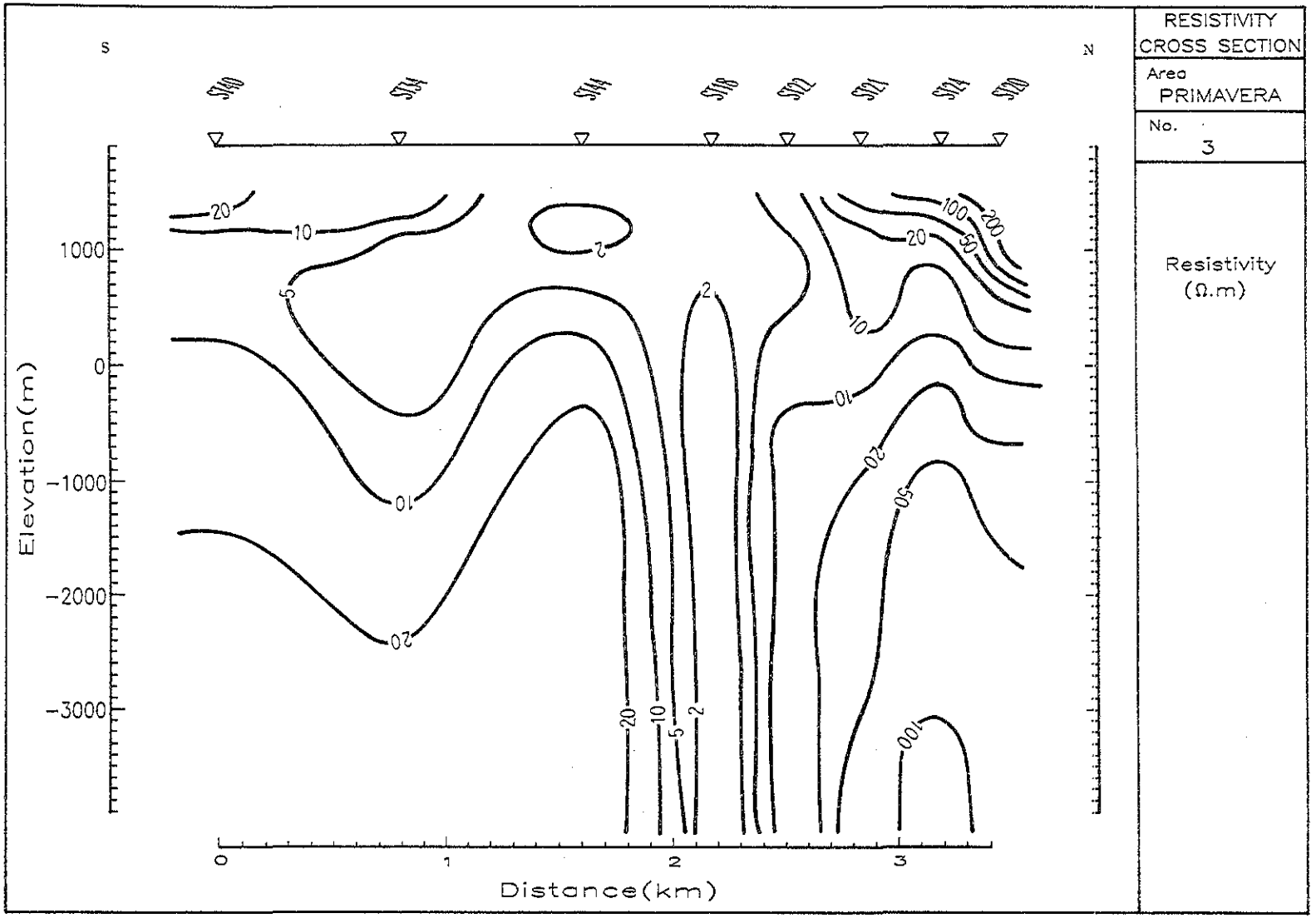

Fig. II. 1-54 Cross Section of Resistivity (TE mode), Line 3

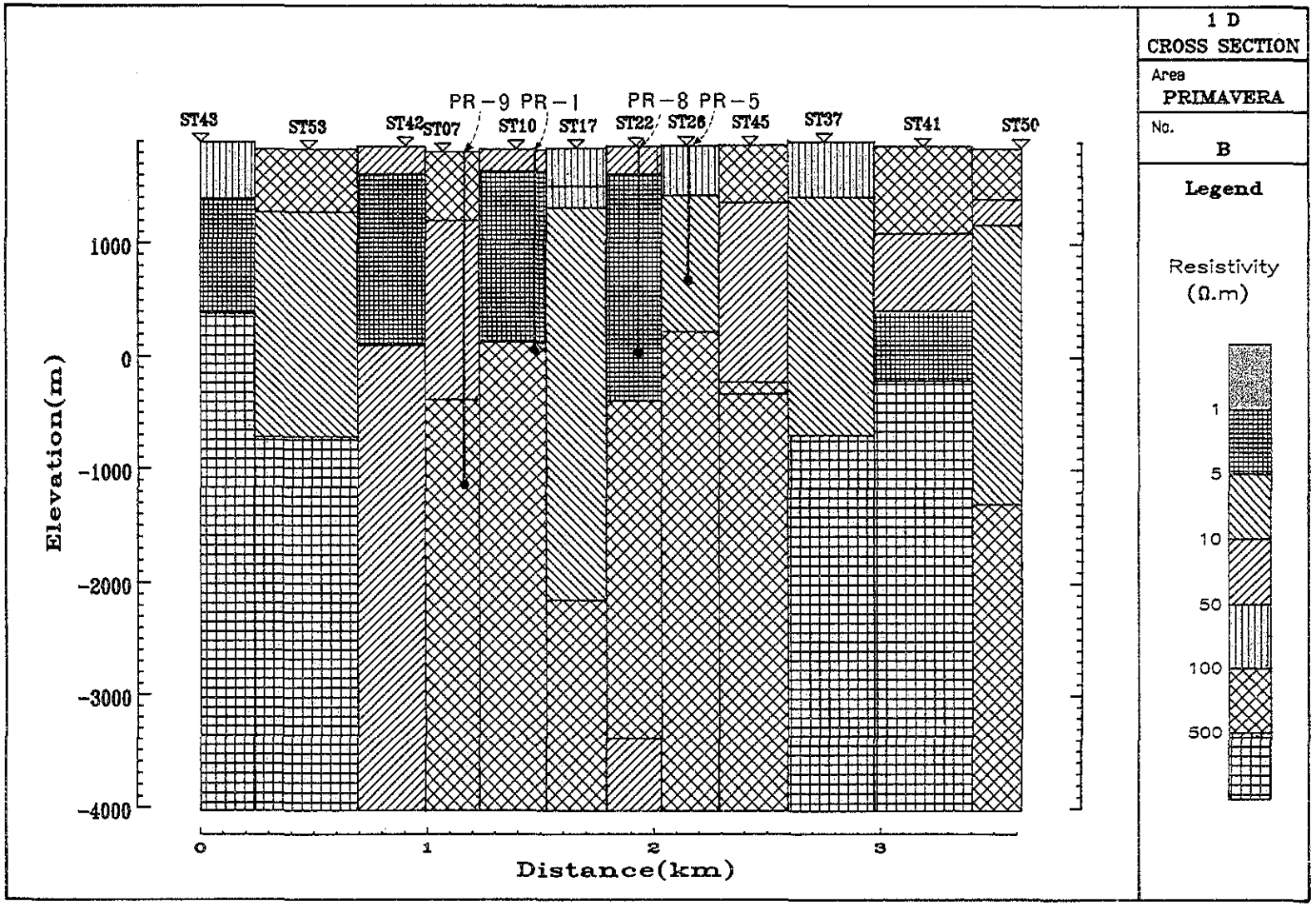

Fig. II. 1-55 1-D Model Cross Section, Line B

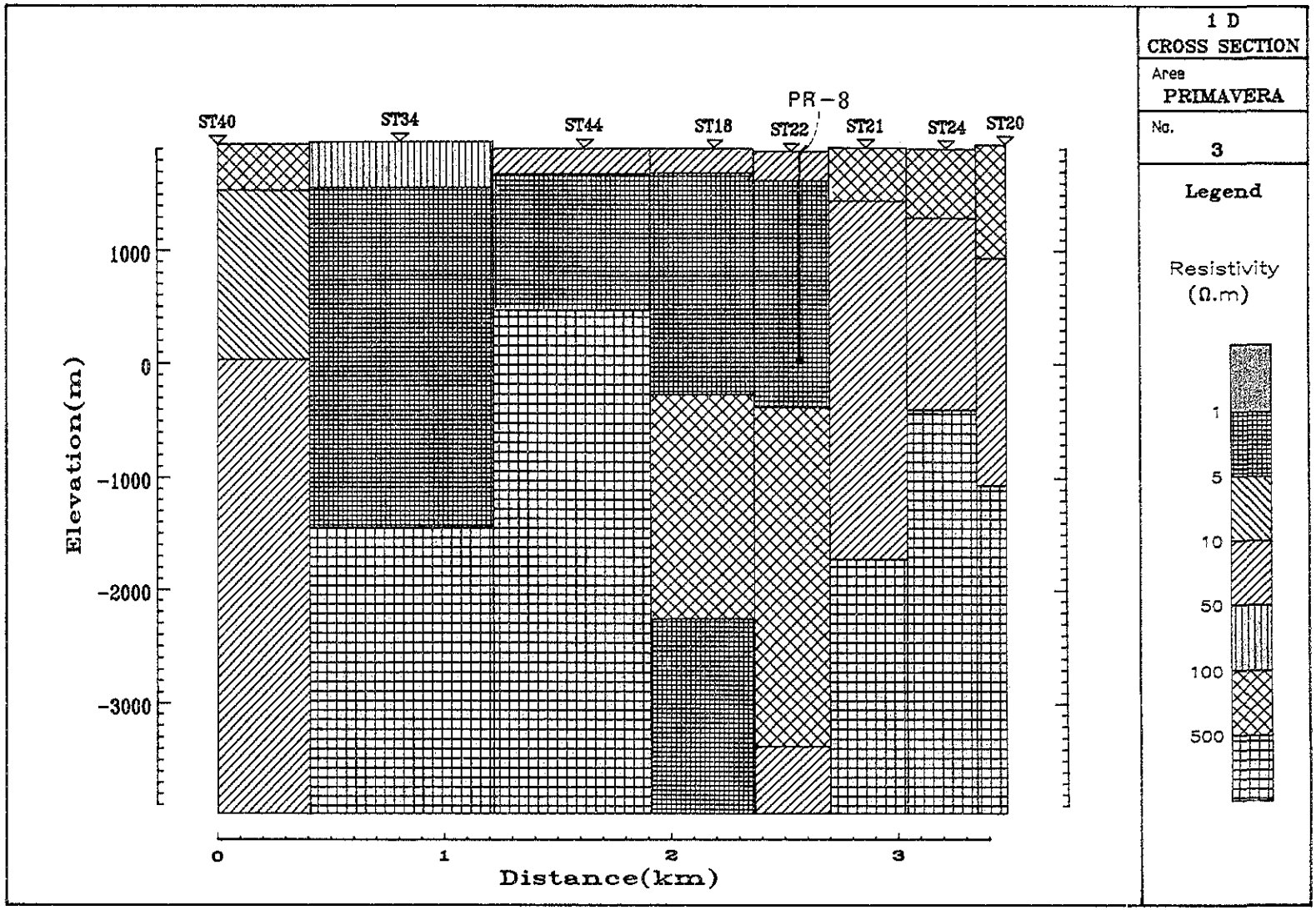

Fig. II. 1-56 1-D Model Cross Section, Line 3

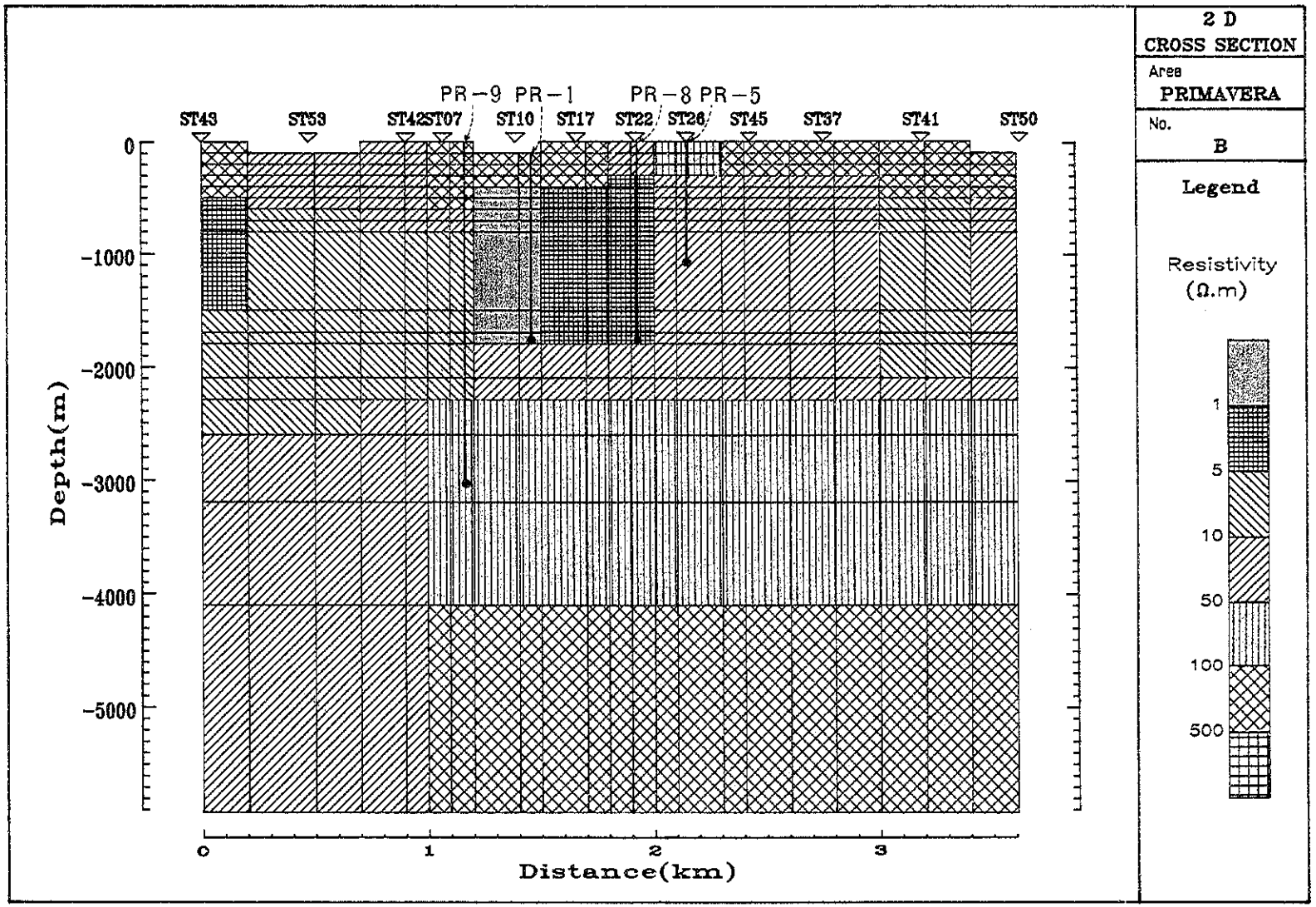

Fig. II. 1-57 2-D Model Cross Section, Line B

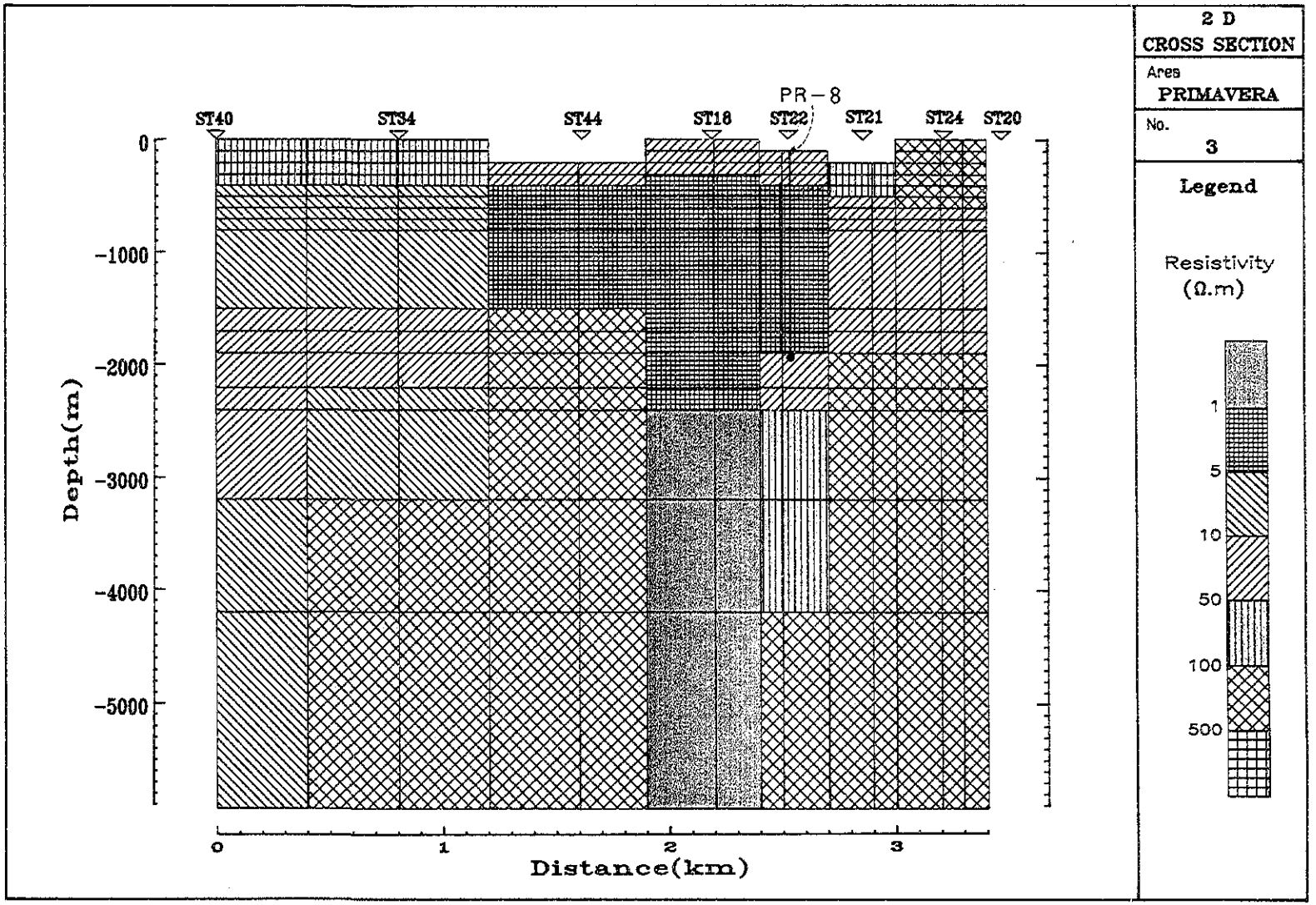

Fig. II. 1-58 2-D Model Cross Section, Line 3

1.5 Well tests

1.5.1 Summary of well tests

Downhole temperature and pressure under the dynamic state, namely the condition of producing fluids from the wells, were measured on wells PR-1 and PR-8 from which steam is blowing out. The purpose of measurement is to grasp the condition of the inside of the borehole and to calculate the formation permeability around the borehole. The results of measurements were as follows:

① The value of permeability-thickness (kh) around PR-1 is 7.6×10^{-13} which is calculated from the downhole pressure measurements under the changed producing conditions of two stages. The kh value is not as high as that of other geothermal area. However, fluid temperature researches a very high value of 299°C at 1,800 m in depth. From these facts, the geothermal fluids are flashing in the formation and are flowing under the condition of two-phase flash flow in PR-1.

② The value of kh around PR-8 is 2.1×10^{-13} which is calculated from the downhole pressure measurements under static and dynamic conditions. The value of downhole temperature is 231°C at 1,750 m in depth. The geothermal fluids emitted from PR-8 are also two-phase flash flows on the inside of borehole.

③ In PR-1, the change in pressure gradient is observed between 1,400 m and 1,450 m. Whereas, in PR-8, the downhole equipment could not go down beyond 1,750 m. The phenomena are probably ascribed to the anomalies on the inside of boreholes, for instance, the effect of pierced casing pipe and the collapse of formation.

1.5.2 Result of PR-1 test

(1) Method of measurement

The well test conducted on PR-1 was to measure downhole temperature and pressure under the producing condition in the borehole. Each flow rate was set by adjusting wellhead valve. Because the test must be done under pressurized condition of wellhead, the work of insertion and removal of equipment should be carried out through a lubricator (Fig. II.1-59).

The equipment used is Kuster type connected with stainless wire of 5 mm in diameter. The downhole values are recorded in a metallic plate of recording parts, and can be red out after retrieval of equipment from borelhole.

(2) Process of measurement

In case of PR-1, judging from the discharge condition on a value of 3 inch in diameter, both permeability and fluid temperature were expected to be very high. As a result, measurements were carried out under the changed producing condition of three stages as given in Table II.1-14, taking into consideration of insertion possibility of equipment. The first test was done under the flow adjustment by 3"ϕ orifice and full opening of 2nd valve. At that test, the fluid velocity in 4"½ casing became too high to insert the equipment because of voluminous flow rate and high quality. So that, measurement stopped at 1,150 m in depth.

The second test was a simultaneous measurement of temperature and pressure by using

2″ϕ orifice.

The third test was a pressure measurement with orifice of 2″½ in opening diameter.

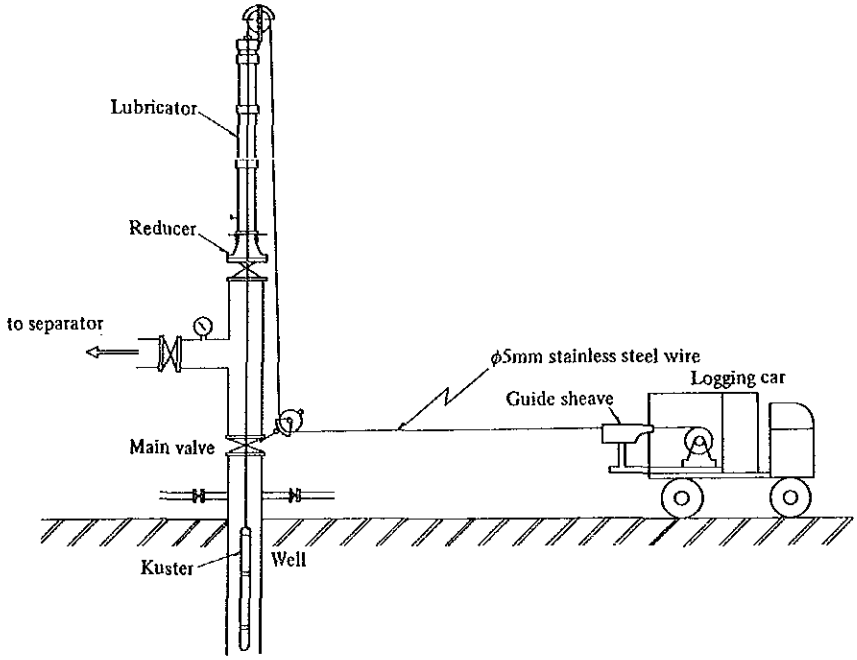

Fig. II. 1-59 Shematic Diagram of Well Test

Table II. 1-14 Conditions of the Well Test of PR-1

Measurement	Well head condition	Well head pressure	Flow rate	Quality at atmosphere
(1) temperature	3″ϕ orifice 2nd valve: full open	28 kg/cm²G	Gs = 53 t/h Gw= 51 G = 104 at atmosphere	0.31
(2) temperature pressure	2″ϕ orifice 2nd valve: full open	42 kg/cm²G	Gs = 43 t/h Gw= 40 G = 83 at line press.	0.25
(3) pressure	2½″ϕ orifice 2nd valve: full open	36 kg/cm²G	Gs = 50 t/h Gw= 40 G = 97 at line press.	0.27

(3) Result of measurement

Table II.1-15 and Fig. II.1-60 show downhole temperature and pressure in PR-1. Based on these results, the condition of the inside of PR-1 borehole is as follows:

① The relationship between temperature and pressure indicates a nearly saturated condition throughout the whole depth, forming two-phase flash flow entirely in the wellbore.

② The fluid temperature reaches a very high value of 299°C at 1,800m near the bottom. Since the formation temperature under a static condition reached 304 ~ 305°C at the same depth (measured by CFE), the fluids appear to flow into the wellbore after flashing in the formation surrounding the well.

③ The change of pressure gradient is observed between 1,400 m and 1,450 m. Concerning this phenomenon, two different interpretations arise.

The first interpretation is as follows:

i) The fluids are, after flashing in the formation, flow into both the annulus and the wellbore itself independently. The annulus exists between the wall of borehole (7″ϕ) and the pierced casing pipe.

ii) Then, they become one flow at a depth of about 1,400 m above which no pierced pipe exists any more.

Another thinking is based upon the presence of fracture at 1,440 m where lost circulation occurred during drilling. The fracture seems to be still open even though it was plugged by cement. So that, the fluids from the fracture at 1,440 m are joined with the fluids from below.

At the third measurement, the equipment moved smoothly down in the 4½″ casing pipe as far as 1,420 m. However, wire tension was loosened thereafter and further insertion was impossible even if the descent velocity was changed. Attemps were made by throttling the fully opened 2nd valve and increasing the descent velocity, resulting in success in passing this point. In addition, pierced casing pipes were installed below 1,440 m. The latter thinking seems to be acceptable from the above experiences.

④ The main feed point of fluid flow is situated at the bottom where lost circulation occurred during drilling, although distinct point was not confirmed by the well test. There must be a little water column near the bottom, judging from the contamination of the retrieved equipment.

(4) Calculation of the value of permeability-thickness

The value of permeability-thickness (kh) around PR-1 well is calculated from the result of downhole pressure measurements. As mentioned above, the fluids from PR-1 are likely to flash in the formation, namely they are under two-phase flash flow in the wellbore. However, the volume ratio of steam to water is sufficiently high in the formation. The pressure loss caused by flow in the formation is mainly related with the voluminal flow. As a result, an equation of gas-phase flow has been applied for approximative calculation of kh. Under the assumption of an adiabatic process at phase transformation, an equation of radial flow of gas-phase can be expressed by the following formula:

$$G = \frac{2\pi kh\,\gamma_w\,(P_e^{1+m} - P_w^{1+m})}{(1+m)\,\mu_w\,\ell_n\frac{r_e}{r_w}\cdot P_w^m} \qquad (1)$$

where,

G : Steam flow rate

k : Permeability

h : Effective thickness

γ_w: Specific weight of fluid

P_e : Reservoir pressure at inflow depth

P_w: Pressure in wellbore at inflow depth

μ_w: Fluid viscosity

r_e : Radius of influence area

r_w : Wellbore radius

m : Polytrope index (saturated steam = 1.135)

Because the measurements of PR-1 were carried out under the changed producing condition of two stages, an equation (1) can be expressed as follows:

$$kh = \frac{(1+m)\,\ell_n \frac{r_e}{r_w}}{2\pi\,(P_{w2}^{1+m} - P_{w1}^{1+m})} \cdot \left(\frac{G_1 \mu_{w1} P_{w1}^{m}}{\gamma_{w1}} - \frac{G_2 \mu_{w2} P_{w2}^{m}}{\gamma_{w2}} \right) \quad \text{(2)}$$

where, suffix 1 and 2 indicate the changed flow condition. G means the steam flow rate at feed point. G is applied under the assumption of iso-enthalpy transformation for the values of flow condition at wellhead or in-line. Table II.1-16 gives the terms and result of calculation. Since the value of kh around PR-1 well is less than 1 darcy·m, it cannot be regarded as better than the kh of other geohermal fields. However, the excellent steam production from PR-1 well might be attributed to the high fluid temperature in spite of such moderate permeability.

Table II. 1-16 List of Parameters used for Calculation and Result of Calculation of kh in case of PR-1

	1st step well head press. 42 kg/cm²G total flow rate 83 t/h	2nd step well head press. 36 kg/cm²G total flow rate 97 t/h
Pressure at feed point P_w kg/cm²G	92.5	84.8
Steam flow rate at feed point G t/h	20.4	26.5
Specific weight of fluid at feed point γ_w kg/m³	49.9	45.1
Viscosity coefficient of fluid at feed point μ_w kgs/m²	2.18×10^{-6}	2.15×10^{-6}
Kh (m³)	7.6×10^{-13}	

1.5.3 Result of PR-8 test

(1) Method of measurement

Method of measurement of PR-8 is all the same as that of PR-1.

(2) Process of measurement

Geothermal fluid from PR-8 was directly discharged into the atmosphere without separator. Accordingly, measurement was carried out only one flow condition as shown in Table II.1-17.

Table II. 1-17 Conditions of Well Test of PR-8

Measurement	Well head condition	Well head pressure	Flow rate	Quality at atmosphere
(1) dummy temperature	2nd valve: full open	7 kg/cm^2	Gs = 45 t/h Gw= 60 G = 105 at atmosphere	0.29
(2) temperature and pressure	idem.	idem.	idem.	idem.

(3) Result of measurement

Table II.1-18 and Fig. II.1-61 show the result of downhole measurement of PR-8. The condition of the inside of PR-8 borehole is as follows:

① Temperature and pressure at each depth are in a saturated relation from the wellhead up to 1,750 m beyond which the equipment could not go down. Therefore, the flow condition in the wellbore should be the two-phase flash flow being similar to PR-1.

② The fluid temperature is 231°C and the pressure is 30.7 kg/cm^{2}G at 1,750 m. In a static condition, the temperature is more than 270°C and the pressure is much higher than the above value, according to the CFE's measurement. This suggests that the fluids flows into the wellbore after flashing in the formation.

③ Because the downhole equipment could not go down beyond 1,750 m, a burried layer of about 100 m by collapse might be expected near the bottom in wellbore.

(4) Calculation of the value of permeability-thickness

Because measurement was carried out only one flow condition in PR-8 well, the equation (2) can not be used for the calculation of kh around PR-8. Therefore, by using the pressure value at a static condition, the equation (1) can be converted into as follows:

$$kh = \frac{(1+m)G\mu_w \ell_n \frac{r_e}{r_w}}{2\pi\gamma_w} \cdot \frac{P_w^m}{P_e^{1+m} - P_w^{1+m}} \qquad (3)$$

As shown in Table II.1-19, the permeability of PR-8 is lower than that of PR-1. The fact suggests two possibilities about low permeability of PR-8 as follows:

1) The permeability of fracture is originally poor.
2) Although the permeability is originally moderate, a burried layer of about 100 m plugs the main fracture about 1,790 m inducing lost circulation, and reduces the permeability of PR-8.

Table II. 1-15 Results of Measurement of PR-1

Date	7. Feb. 1986	8. Feb. 1986		10. Feb. 1986
Well depth	1,818 m			
Well head condition	3"ϕ orifice	2"ϕ orifice		2½"ϕ orifice
Well head pressure	28 kg/cm^{2}G	41.5 ~ 43 kg/cm^{2}G		36 kg/cm^{2}G
Depth (m)	Temperature (°C)	Temp.	Pressure (kg/cm^2)	Press.
20	228	249	42.2	34.1
100	231	251	44.0	35.0
200	233	253	45.7	36.0
300	235	255	47.3	37.0
400	237	257	48.9	38.1
500	239	259	50.4	39.1
600	241	261	52.1	40.2
700	243	263	54.2	42.1
800	245	266	56.3	44.2
900	249	268	58.4	46.3
1,000	252	270	60.7	48.4
1,100	254	273	62.9	50.4
1,160	257			
1,200		277	67.2	55.3
1,300		281	71.5	60.5
1,400		285	75.8	65.6
1,500		291	82.7	76.4
1,600		294	85.9	79.1
1,700		296	89.2	81.8
1,800		299	92.5	84.8
Number of Fig. II.1-60 and Table II.1-14	(1)	(2)		(3)

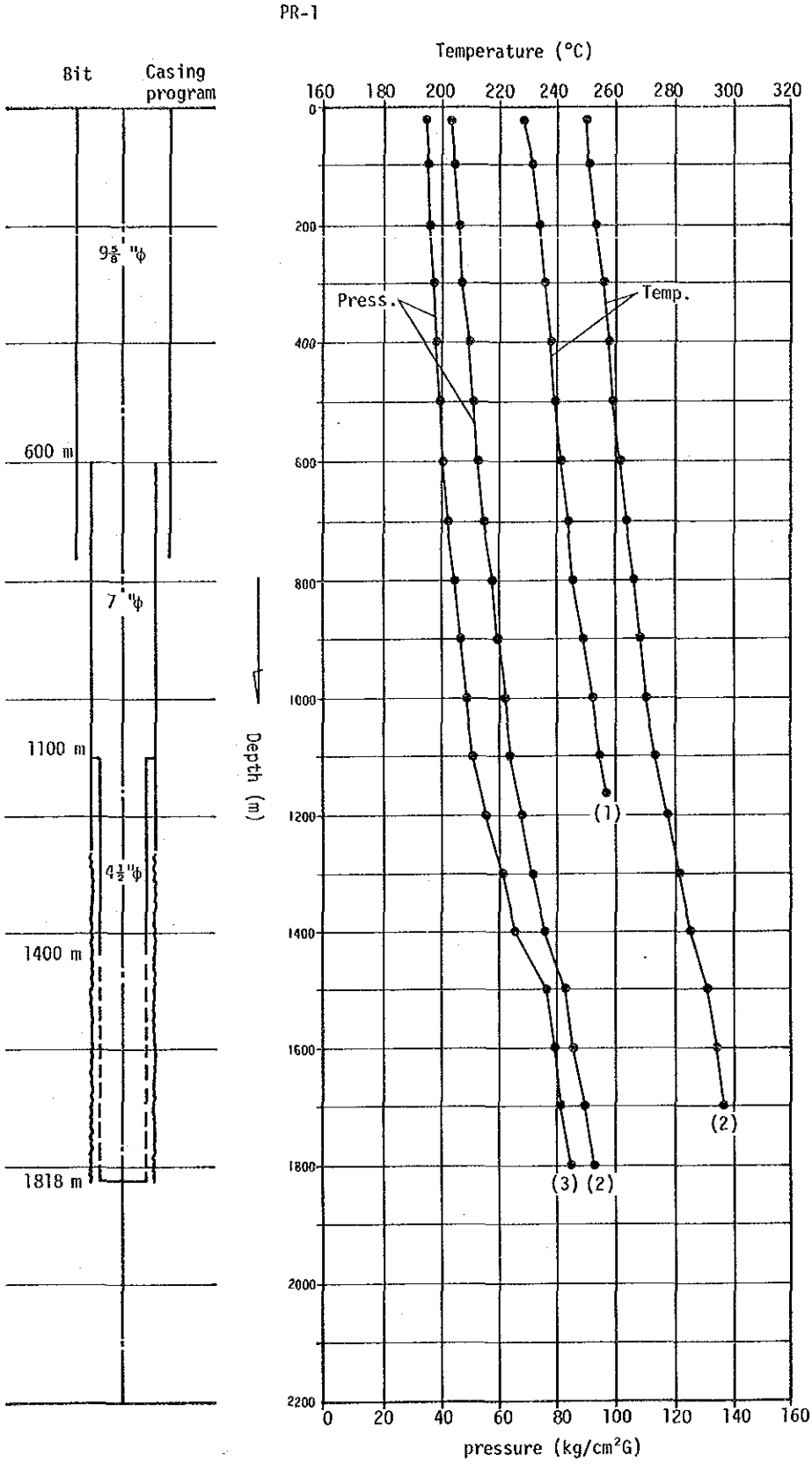

Fig. II. 1-60 Downhole Temperature and Pressure Curves of PR-1 in the Producing Condition

Table II. 1-18 Results of Measurement of PR—8

Date	30. Jan. 1986	31. Jan. 1986	
Well depth	1,861 m		
Well head condition	2nd valve: full open	2nd valve: full open	
Well head pressure	7.0 kg/cm^{2}G	7.0	
Depth (m)	Temperature (°C)	Temp.	Pressure (kg/cm^2)
20	167	166	7.1
100	171	170	7.9
200	174	173	8.4
300	177	176	9.4
400	180	179	10.1
500	183	182	10.8
600	185	185	11.5
700	188	188	12.4
800	191	191	13.3
900	194	194	14.2
1,000	198	197	15.3
1,100	201	200	16.5
1,200	205	204	17.8
1,300	208	208	19.2
1,400	212	211	20.8
1,500	219	218	23.8
1,600	224	224	26.8
1,700	229	228	29.2
1,750	231	231	30.7

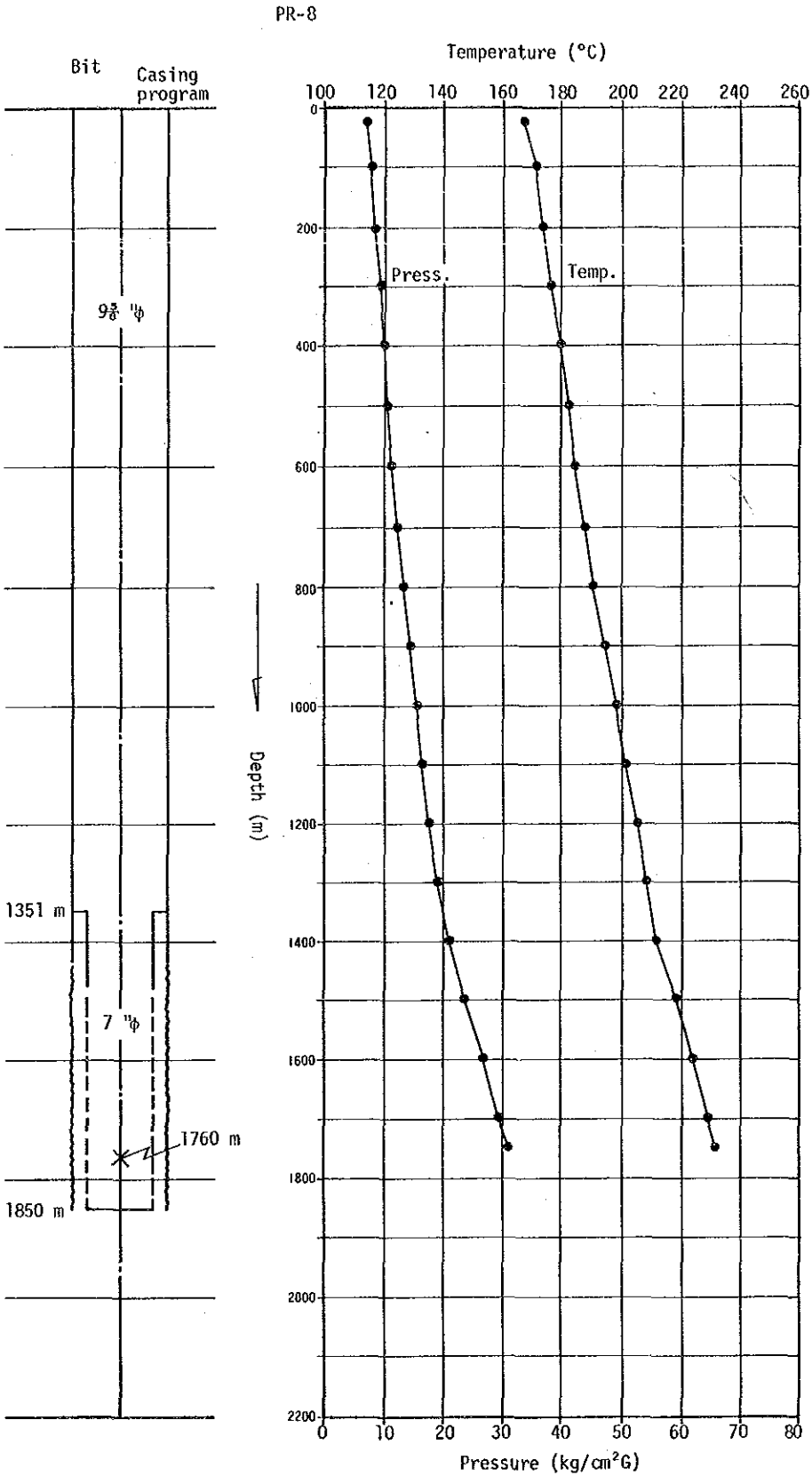

Fig. II. 1-61 Downhole Temperature and Pressure Curves of PR-8 in the Producing Condition

Table II. 1-19 List of Parameters used for Calculation and Result of Calculation of kh in case of PR-8

	Static test	Production test well head press. 7 kg/cm²G total flow rate 105 t/h
Pressure at feed point P_w kg/cm²G	123	30.7
Steam flow rate at feed point G t/h	–	21.5
Specific weight of fluid at feed point γ_w kg/m³	–	15.6
Viscosity coefficient of fluid at feed point μ_w kgs/m²	–	1.82×10^{-6}
Kh (m³)	2.1×10^{-13}	

2. Selection of Targets for PR-12 and PR-13 Wells by Exploration at First Stage

2.1 Integrated analysis on geothermal reservoir by exploration at first stage

2.1.1 Structure of geothermal reservoir

Taking main factors of reservoir into consideration, the structure of the geothermal reservoir in this area is as follows:

(1) Fractures

① The main reservoir in this area consists of an andesite dominated formation belonging to the lower part of the Cordilleran Volcanics which is found below about 1,000 m above 2,800 m in depth.

② Fracture survey reveals that NE-SW trending normal faults are dominated in the surface, and are cut by NW-SE trending strike-slip faults. The normal faults were formed by the uplift preceded by the Caldera collapse. On the basis of the restoration of paleostress field and the observation of tensional fracture, the center of the uplift is considered to be located near PR-1 and PR-8. The trends of surface rock alteration, high anomaly in soil mercury and high gravity anomaly are in accordance with those of the NE-SW trending faults.

③ An investigation was made on the measurement of remnant magnetization and on the restoration of stress field by observation of fractures in cores to determine whether the above mentioned fracture pattern could extend to the deeper part of the subsurface formation. Because the stress field above about 1,000 m in depth is harmonized with that of the surface, the fracture system observed in the surface can extend to the upper part of the Cordilleran Volcanics.

④ The surface survey in the geothermal manifestation area cannot reveal the fracture characteristics of the lower part of the Cordilleran Volcanics which is the main reservoir of this area. Resistivity structure in this part provided by the MT survey shows that the low resistivity zone has a NW-SE trend. The NW-SE trend is also found in the Bouguer anomaly by regional gravity survey and in the geological structure of the lower part of the Cordilleran Volcanics exposed surrounding the Sierra La Primavera Caldera. Therefore, the main feed points of PR-1 and PR-8 are inferred to be attributed to the NW-SE trending fractures.

⑤ As mentioned above, it could be concluded that the NE-SW trending fractures dominate above about 1,000 m in depth, while the NW-SE trending fractures exist in the subsurface deeper than 1,000 m in depth. Geothermal manifestations including fumaroles and rock alteration are distributed along the fractures having NE-SW direction. On the other hand, lost circulations during drilling of PR-1 and PR-8 were caused by encounters with the deep-seated fractures with a NW-SE direction. The NW-SE trending fractures consist mainly of high angle tensional fractures because of the direct influence of the uplift of the Caldera.

The NW-SE trending fractures observed in the surface are different in characteristics from those of the deep-seated formation. It has not been made clear whether both fractures are connected mutually.

(2) Temperature

① The up-flow zone of high temperature of about 300°C is recognized in the vicinity of PR-1 and PR-8, judging from the temperature profile obtained from the downhole temperature measurement and the minimum homogenization of fluid inclusion in cuttings. Therefore, geothermal fluids in this area are ascending from the deeper part of this vicinity.

The Na-K-Ca chemical thermometer, which is a suitable thermometer for this area, indicates about 300°C in PR-1 and about 280°C in PR-8.

② The well production tests of PR-1 and PR-8 make clear that both geothermal fluids are flashing in the formation around these wells and are flowing as two-phase flash condition in the boreholes. According to the measurement of downhole pressure in different conditions, the values of permeability-thickness around PR-1 and PR-8 are approximately 10^{-13} m^3, indicating moderate permeability. Excellent steam production from these wells in spite of having moderate permeability is ascribed to the high temperature.

③ Chemical analyses were made on the relationships of chlorite and enthalpy, chlorite and boron, gas ratios and isotopic components. The analyses suggest a mechanism that geothermal fluids with high temperature are ascending from the vicinity of PR-1 and are flowing to PR-5 through PR-8 toward PR-4, being affected by the ground water gradually along the NE-SW trending faults.

Hot water of PR-2 is considered to be derived from another separate reservoir.

④ From the fact mentioned above, it could be said that both the uplift zone and the up-flow zone are present near PR-1 and PR-8, forming a geothermal reservoir of the vertical fracture type. This was also supported by the result of the MT survey in which the low resistivity zone extends vertically to the deep-seated formation at southern part of PR-8 (i.e. sounding station 18).

2.1.2 Extent of geothermal reservoir

The geothermal reservoir in this area is characterized by a vertical fracture type having a NW-SE trend with an up-flow zone that nearly coincided with the uplift zone. Therefore, to estimate the extent of the geothermal reservoir, it was considered to be important to trace the extent of NW-SE trending fractures and to draw the map of subsurface temperature profile. The following information was needed to investigate the extent of geothermal reservoir:

① The result of the MT survey shows that the geothermal reservoir is included in the low resistivity zone in the second layer and that the lower resistivity zone with resistivity less than 5 Ω·m is contained in an area of 1.5 km along north-south and about 1 km along east-west, with the center being near PR-1 and PR-8.

② As a result of restoration of paleo-stress field by means of the surface and core surveys, an anticlinal axis in stress field reflected by the uplift has a NW-SE trend through the north of PR-1 (Fig. II,1-20). The axis is about 2 km long with its center being near PR-1.

③ Measurement of downhole temperature of PR-10 by CFE informs us of a maximum temperature of 144°C at 1,250 m in total depth about 600 m north of PR-8.

④ Chemical composition of hot water provided from PR-2 is different from that of other

wells and is derived from a separate reservoir.

Estimate of an areal extent of geothermal reservoir from ① to ④ is as follows:

Northern margin: near PR-10 (estimated from ① and ③)

Southern margin: about 1 km south of PR-8 (estimated from ①)

Eastern margin: about 1 km east of PR-1 (estimates from ②)

Western margin: near PR-2 (estimated from ② and ④)

When the four margins are limited by the above mentioned facts and the main direction of reservoir was considered to be NW-SE, the gross area of reservoir become about 3 km^2 which is estimated to be about 2 km in the NW-SE direction and about 1.5 km in the NE-SW direction (Fig. II.2-2). However, this estimate should be improved by the results of well drilling and reservoir simulation.

In any case, the reservoir in this area is characterized as the vertical fracture type whose center is locates near PR-1 and PR-8. Fractures in the reservoir extend in a NW-SE direction. If wells are drilled outside of this direction, they will not be able to encounter fractures and high temperature.

A conceptual geothermal reservoir model is drawn in Fig. II.2-1.

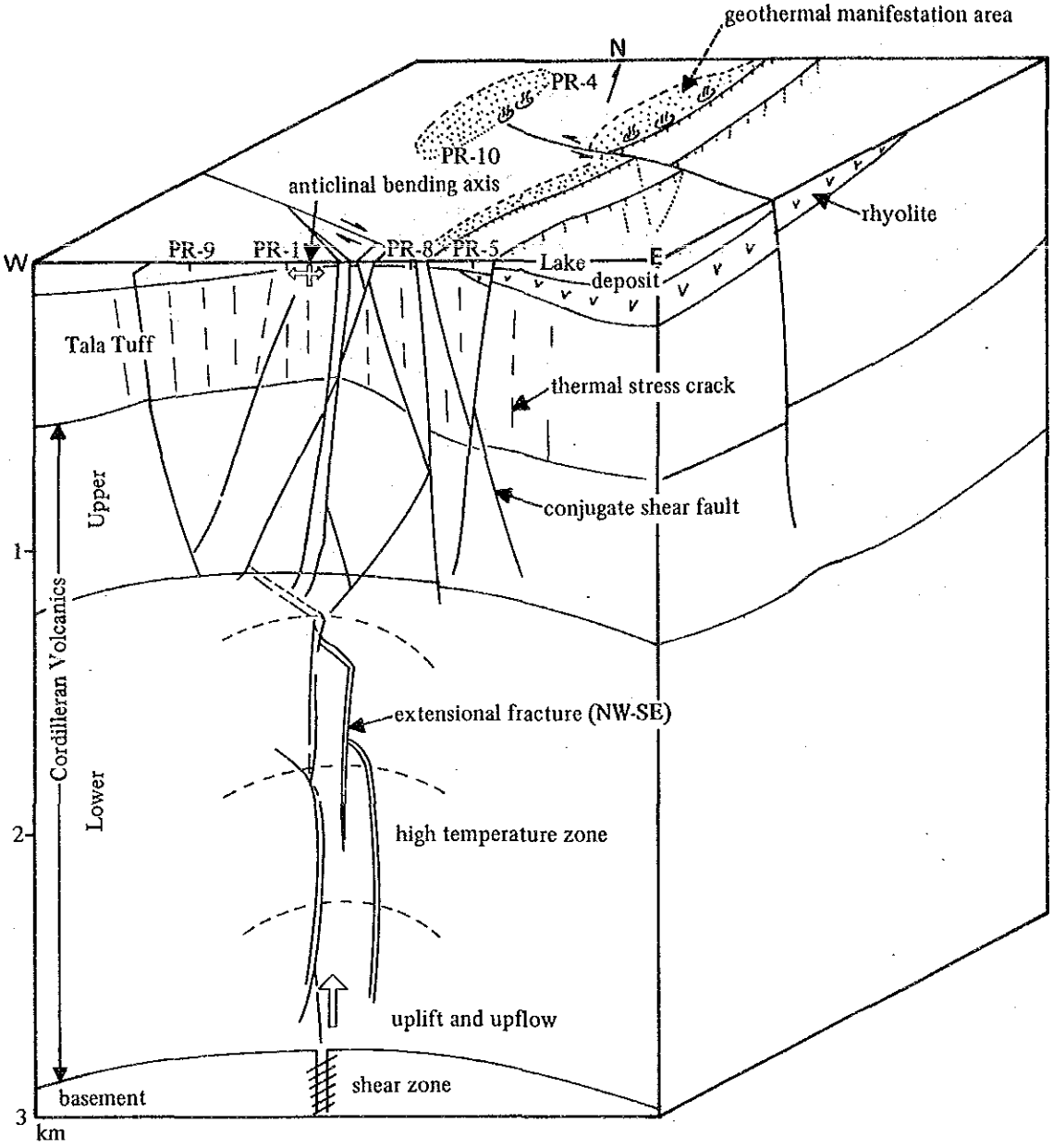

Fig. II. 2-1 Conceptual Geothermal Reservoir Model in the La Primavera

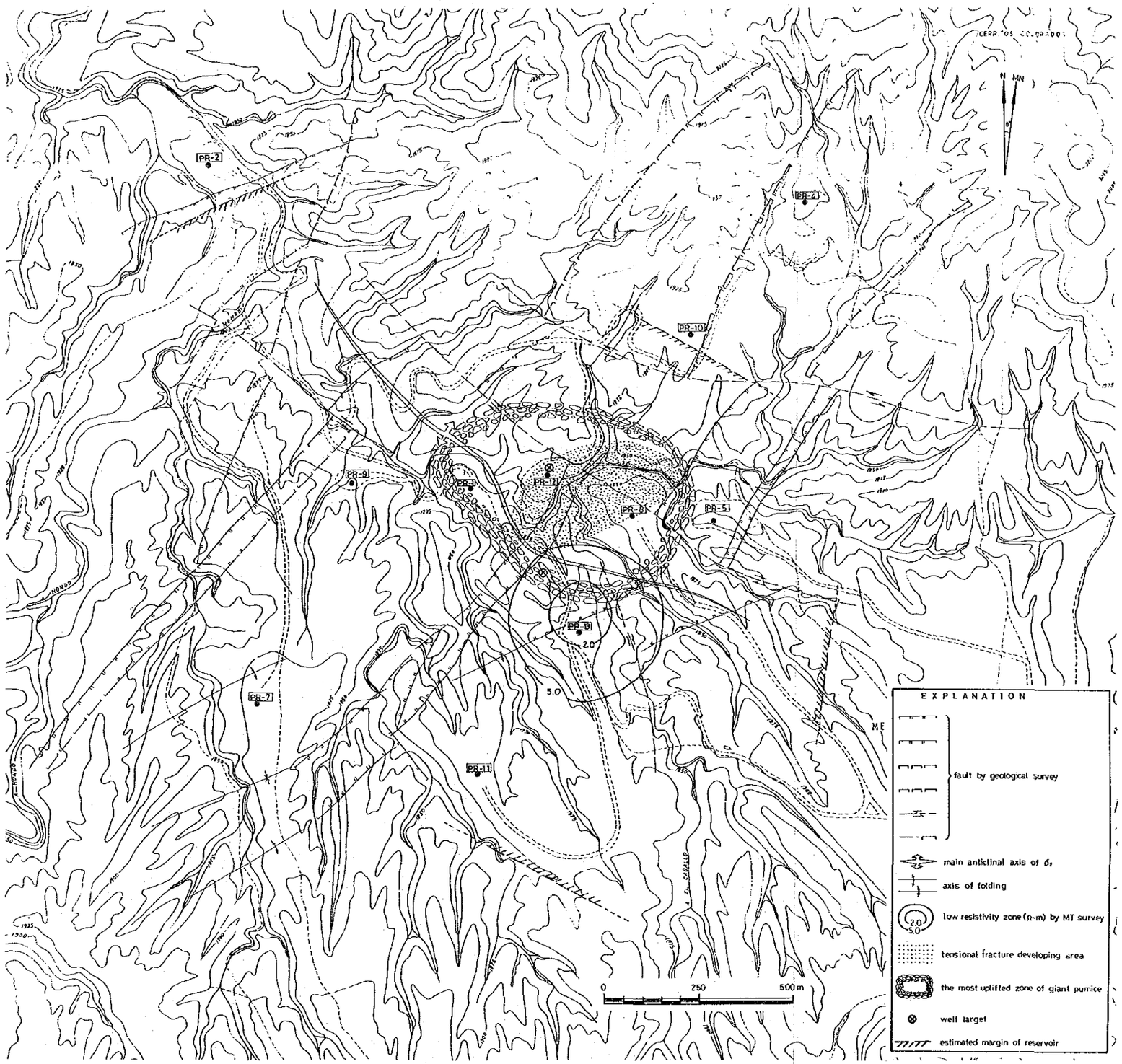

Fig. II. 2-2 Selection of Well Target of PR-12 and PR-13

2.2 Selection of targets for PR-12 and PR-13 wells

2.2.1 Proposal for the work plan of next stage

Geological, geochemical, gravimetric and electrical (MT method) surveys and well testing, in addition to review of the data on the exploration wells, have been carried out in 1985. From the results of a comprehensive analysis of the data, it became clear that the geothermal reservoir in La Primavera is controlled by the location of an uplifted zone which plays a role as an up-flow zone for geothermal fluids with high temperature.

According to the scope of work of the project, it was planned that three heat holes of 750 m in depth would be drilled by CFE in 1986. However, for the following reasons, it became change the work plan in 1986 to drill one exploration well of about 2,000 m in depth instead of drilling three heat holes.

① According to the investigation in 1985, the up-flow zone and the distribution of underground temperature are now clarified.

② Seven wells (600～3,000 m in depth) had already been drilled by CFE, and the thermal extension is already known.

③ Because of thick sedimentation of Tala Tuff above about 700 m in depth which caused frequent lost circulations, it would take a long time to drill through the formation.

Therefore it is more important for collecting useful data for evaluating the geothermal reservoir that a new deep well be drilled toward the up-flow zone rather than drilling heat holes.

Another exploration well would be drilled by JICA study team in 1987.

2.2.2 Purpose of drilling of exploration wells

At that time, only two exploration wells (PR-1 and PR-8) had been drilled through the up-flow zone in which fractures develop, but other exploration wells (PR-2, 5, 9 and 10) were located outside of the up-flow zone. In order to determine the optimum output of the planned power station by delineating geothermal reservoir, it was necessary to evaluate the potential of the up-flow zone. The purpose of drilling of exploration wells (2,000 m in depth) was to collect useful data of the up-flow zone and to estimate the geothermal reservoir. For this purpose, two targets were selected for exploration wells. One exploration well was as alternative to drilling three heat holes of 750 m in depth in 1986.

2.2.3 Reasons for selection of targets

Two targets, points A and B shown in Fig. II.2-2, were selected for exploration wells which would be drilled on and after 1986. Each target must be at a point necessary for determining the extent of developing area and the output of the planned geothermal power station by using the data of two exploration wells in addition to PR-1 and PR-8.

The reason that A and B points were selected is shown as follows:

Both points A and B

① Necessary points to detect the extent of geothermal reservoir

② Located of an up-flow zone

③ Located on possible deep seated fractures

Point A is

① Located on the horst estimated from the distribution of surface faults (Fig. II.2-2).

② Located on a tensional fracture concentrated zone obtained from tensional fracture distribution map on the surface (Fig. II.2-2).

Point B is

① Located on the low resistivity zone extending vertically near the station 18 found by MT method.

② Located on an anticlinical bending axis restored by the stress field (Fig. II.1-5).

③ Located on a maximum upheaval zone of giant pumice bed.

As to the selection of the targets for drilling of exploration wells, CFE has accepted the method of aiming at specific faults which are only recognized at the surface and has extended to the subsurface without physical consideration. This method is valid in the case of having a fault with large throw and a homogeneous formation from the surface to the deeper subsurface. However in Sierra La Primavera, the subsurface geology is different from the surface geology in the orientation of fractures and fracture characteristics. Moreover, the fracture behavior is easily changeable with high temperature and high pressure at the subsurface. Therefore, it was considered that it is better to select the targets by a comprehensive analysis of various survey with a consideration of deep seated fracture than to make a great point of surface geology only.

Point A is about 200 m distance away from PR-1 and about 250 m from PR-8, while point B is about 300 m distance away from PR-1 and about 270 m from PR-8. However, it was considered that it has no problem in scrambling of fluid among production wells because both A and B points are inside the up-flow zone where excellent geothermal fluids are provided from the deeper subsurface.

2.2.4 Plan of drilling of exploration wells

It was planned that point A would be drilled by CFE in 1986 and point B would be drilled by JICA in 1987. We called point A PR-12 and point B PR-13, showing well layout in Fig. II.2-3 and undertaking for wells in Tables II.2-1 and 2 respectively. After topographical survey, we decided the following wellhead positions:

PR-12: Because topographical flat plane is located to the south of point A within a little distance, we decided the center of flat plane to be wellhead PR-12.

PR-13: It becomes clear that point B is situated in a steep slope and has not enough space to construct a drilling rig. Therefore, the following methods are considered;

① vertical drilling at newly prepared drilling site

② side-tracking of PR-5 or PR-9 well

③ controlled directional drilling from the platform of PR-8 well.

Since the directional drilling was not acceptable in this area, ① was adopted as a final decision. Thus, the wellhead of PR-13 was determined in the center of flat place about 150 m southwest of point B. This place was only satisfied with the low resistivity zone among reasons for selection of target of point B.

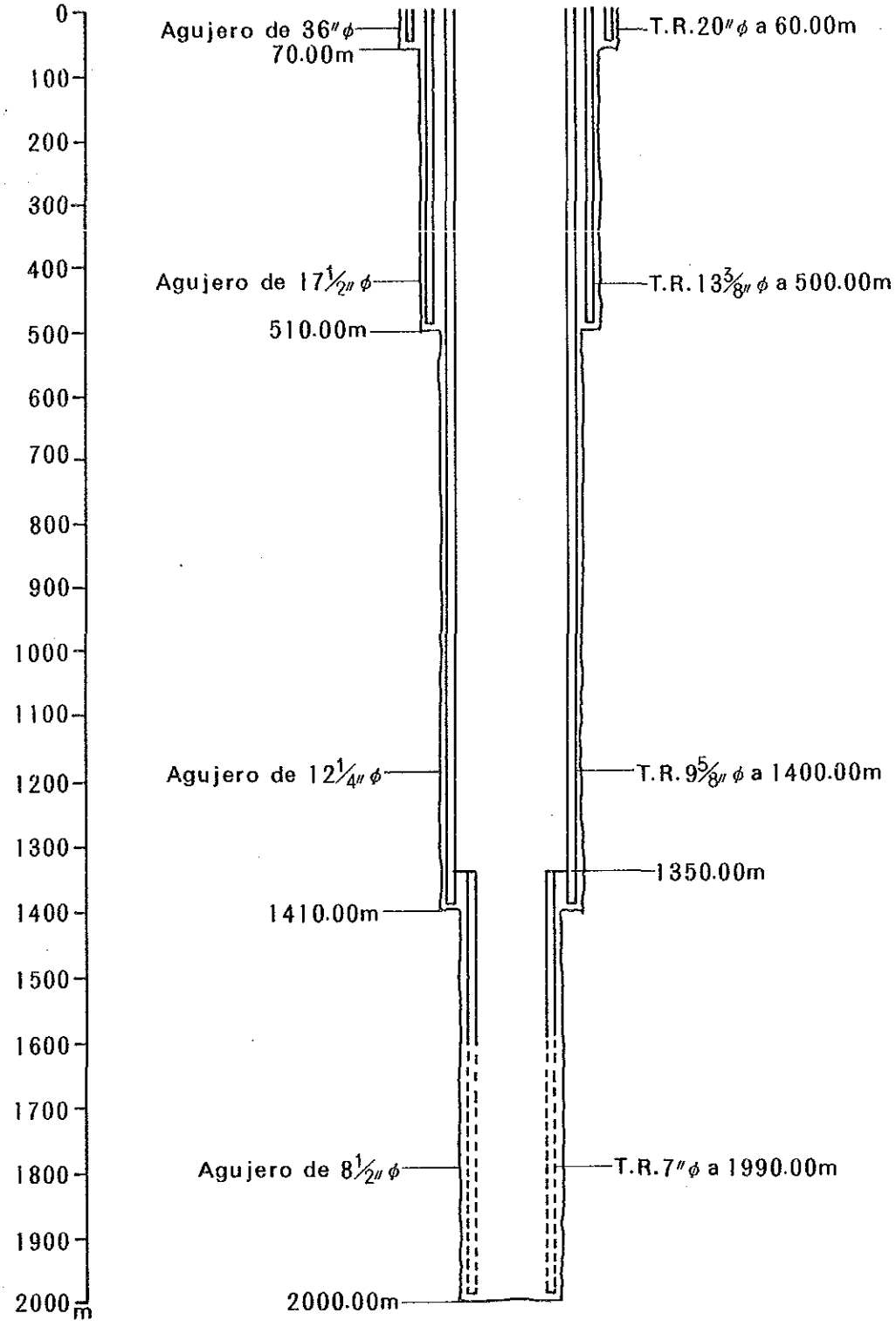

Fig. II. 2-3 Well Layout of PR-12 and PR-13

Table II. 2-1 Respective Undertaking for an Exploration Well PR-12

JICA	CFE
1. Determination of the well position and completion depth 2. Analysis of fluid inclusion, X-ray and Hg, As concentration of cuttings 3. Physical property and fracture analysis of cores 4. Chemical analysis and geophysical test of wellbore fluid which will carry out after the finish of PR-12 well.	1. Drilling works 2. Core sampling at 1,400, 1,700 and 2,000 m (each 1 ~ 3 m long of core) 3. General geological survey 4. Downhole temperature and pressure logging 5. Measurement of physical characteristics of geothermal fluid

Table II. 2-2 Respective Undertaking for an Exploration Well PR-13

JICA	CFE
1. Determination of the well position and completion depth 2. Supervision of the drilling work 3. Payment of the contract value 4. Analysis of cuttings and cores 5. Chemical analysis and geophysical test of wellbore fluid together with PR-11 6. Analysis and evaluation of the results	1. Drilling works 2. General geological survey 3. Downhole temperature and pressure logging 4. Measurement of physical characteristics of geothermal fluid

3. Exploration at second stage

3.1 Drilling work and survey of PR-12

3.1.1 Drilling work of PR-12

Drilling works were conducted by the CFE drilling team at the site between PR-1 and PR-8 selected by JICA. The drilling was started on the 13th September, 1986, and finally completed at a depth of 2,303 m on 17th January, 1987.

The casing program for PR-12 was as follows:

Bit:		Casing pipe:	
	40 inch, 0 — 12 m		30 inch, 0 — 12 m
	26 inch, 12 — 112.50 m		20 inch, 0 — 108 m
	17 1/2 inch, 112.50 — 460 m		13 3/8 inch, 0 — 455.92 m
	12 1/4 inch, 460 — 1,365 m		9 5/8 inch, 0 — 1,350.14 m
	8 1/2 inch, 1,365 — 2,303 m		

After finishing to drill the hole, 7″ slotted pipe were inserted at a depth between 1,293.58 m to 2,293 m.

Marked lost circulation occurred at a depth of shallower than 510 m. The lost circulation is ascribed to encounters with joint or tensional fracture in the Tala Tuff. The depths of total lost circulation are as follows:

30 m, 90 m, 138 m, 159 m, 160 m, 165 m, 191 m, 194 ~ 204 m, 210 ~ 214 m, 221 ~ 225 m, 269 m, 406 m, 424 m, 471 m, and 486 m

Lost circulation was not present in rocks from 510 m to 1,060 m in depth, consisting of rhyolite, lithic tuff and andesite. Partial lost circulations between 1,182 m to 1,364 m in depth were caused by enconters with the Los Muertos Fault in andesite layer. Additional lost circulations occurred continuously from 2,015 m to 2,293 m in depth except 2,061 to 2,154 m in depth, in particular at 2,156 m with a total loss of 35 kℓ/h.

After completion of hole drilling core was collected from 2,302.50 to 2,302.70 m in depth.

3.1.2 Core and cuttings survey of PR-12

Various geological characteristics were identified by using cores and cuttings taken from PR-12. Fig. II.3-1 shows the integrated result of drilling and survey of PR-12 including geology, logging, core and cuttings survey and lost circulation during drilling. Sixty-one cutting samples were collected from 1,070 m to 2,290 m in depth, and their result are shown below. The result of core measurement will be given in Chapter III 2.1.3.

(1) Chemical analysis of Hg and As in cuttings

Hg concentration generally has a very low value of less than 0.02 ppm, but has high values at depths of 1,070 ~ 1,250 m and 1,370 m. Hg concentration significantly affects the subsurface fractures. These high concentrations reflect probably small scale fractures occurred in lost circulations at depth of 1,182 ~ 1,364 m. Also peaks are observed at depths of 2,010 ~ 2,070 m, 2,210 ~ 2,230 m in Hg concentration and at a depth below 1,970 m in As concentrarion. These correspond to the fracture zones that are related to lost circulations at depth of 2,015 ~ 2,061 m

and below 2,154 m.

(2) X-ray diffraction analysis

Samples were taken from the cuttings to conduct X-ray diffraction analysis. Detected alteration minerals are montmorillonite, chlorite-montmorillonite mixed-layer mineral, chlorite, sericite, quartz, calcite, pyrite and laumontite.

Kimbara and Sumi (1975) clarified that montmorillonite disappears above 80 ~ 160°C, but sericite appears above 180 ~ 250°C. In the well, montmorillonite is widely distributed from 1,070 to 2,290 m in depth where the static borehole temperature (recovery time was 289 days and measured on the 11th November, 1987) ranges from 291 to 338°C. Also, laumontite, which is stable below 200 ~ 240°C, is distributed at a depth of 1,650 m where the static borehole temperature is 313°C. These suggest the geothermal reservoir has increased over about 130°C from the past alteration stage to present.

K-feldspar distributed at a depth of 1,870 ~ 1,930 m is derived from the phenocryst in rhyolite.

(3) Homogenization temperature of fluid inclusion

The homogenization temperature was measured in vein minerals from cutting samples. These are five samples of vein quartz from 670 m, 1,270 m, 1,670 m, 2,250 m in depth and one of vein anhydrite from 1,970 m in depth.

Homogenization temperatures are distributed in a narrow range of 2 ~ 8°C at three depths, 670 m, 1,270 m, 2,250 m. This shows that fluid inclusion formed simultaneously at the mineralization stage.

The minimum homogenization temperature has a tendency to increase abruptly from 182°C at a depth of 670 m to 284°C at a depth of 1,270 m, and to be about constant value of 284 ~ 300°C at the deeper parts.

3.1.3 Chemical analysis of wellbore fluids from PR-12

(1) Collecting and analytical methods

Sampling of wellbore fluids from PR-12 was carried out on the 28th, January in 1988. Steam and steam condensate are collected by using a small-sized separator that is connected with a sampling valve on steam line beyond a large separator. Hot water is collected from a sampling valve under two-phase line at the atmosphere condition. Fig. II. 3-2 shows the outline of sampling from PR-12.

The unstable components such as pH and H_2S are analyzed in field laboratory, while the rest is analyzed in Japan after the treatment of an annex of acid or alkali and a dilution by distilled water as to the changeable components in concentration.

(2) Result and discussion of chemical composition

The results of chemical and isotopic composition are listed in Table II.3-1. Total gaseous concentration in steam is 2.28 vol% under the condition of 5.3 kg/cm^{2}G at separator pressure. CO_2 gas reaches 98.5 vol% and CH_4 gas is rich in the rest of gas. These facts resemble the results of PR-1 and PR-8. The ratio of He/Ar is higher than that of PR-1 and PR-8, and the ratio of

$(He/Ar)/(N_2/Ar)$ is much higher than that of the Japanese geothermal fields.

Hot water from PR-12 is rich in Na and Cl, and is poor in SO_4 and Ca that show neutral. PR-12 well is located in the highest portion of Cl-enthalpy diagram.

The ratio of B/Cl is the same value as that of PR-1 and PR-8. This means chemically homogeneous characteristics of reservoir over a wide area and the same origin.

In the isotopic composition diagram, δD is -60.1‰ and $\delta^{18}O$ is -0.8‰. The δD value is higher than that of PR-1 and PR-8 in 1986, while the $\delta^{18}O$ value is intermediate between PR-1 and PR-8. The tritium concentration is 0.31 TR (1 TR = 10^{18} × T/H). This value is extremely lower than that of recent surface water (10 ~ 30 TR). This means few infiltration of the surface water to the reservoir.

Table II.3-2 indicates the chemical thermometers of PR-12. The estimated temperature ranges from 270°C to 330°C. The Na-K-Ca thermometer shows lower value than other thermometers. The SiO_2 thermometer is 308°C which exceeds the upper limit of applicable temperature. Downhole temperature measurement records 318°C at the condition of 96 hour's recovery time. Therefore, the Na-K thermometer is suitable for the reservoir temperature of PR-12, showing 320°C ~ 330°C.

The results of chemical composition suggest that the hot water of high temperature is ascending from the deeper part of PR-12 well.

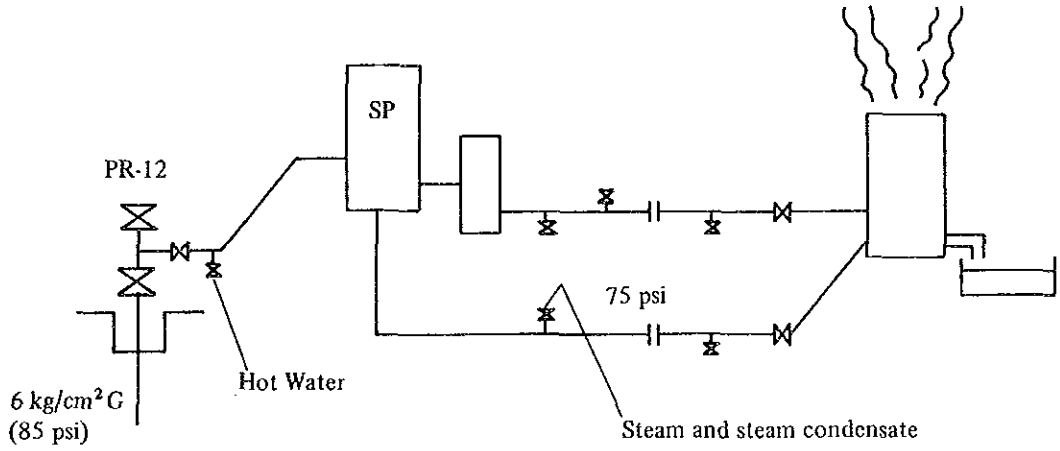

Fig. II. 3-2 Sampling Condition of PR-12

Table II. 3-2 Estimate of Reservoir Temperature of PR-12 and PR-13

Well	Geothermometer (°C)			
	Quartz-maximum steam loss	Na/K (Fournier)	Na/K (Truesdell)	Na-K-Ca
PR-12	308	322	330	270
PR-13	278	269	255	236

PR-12: 28/Jan./1988
PR-13: 12/Aug./1988

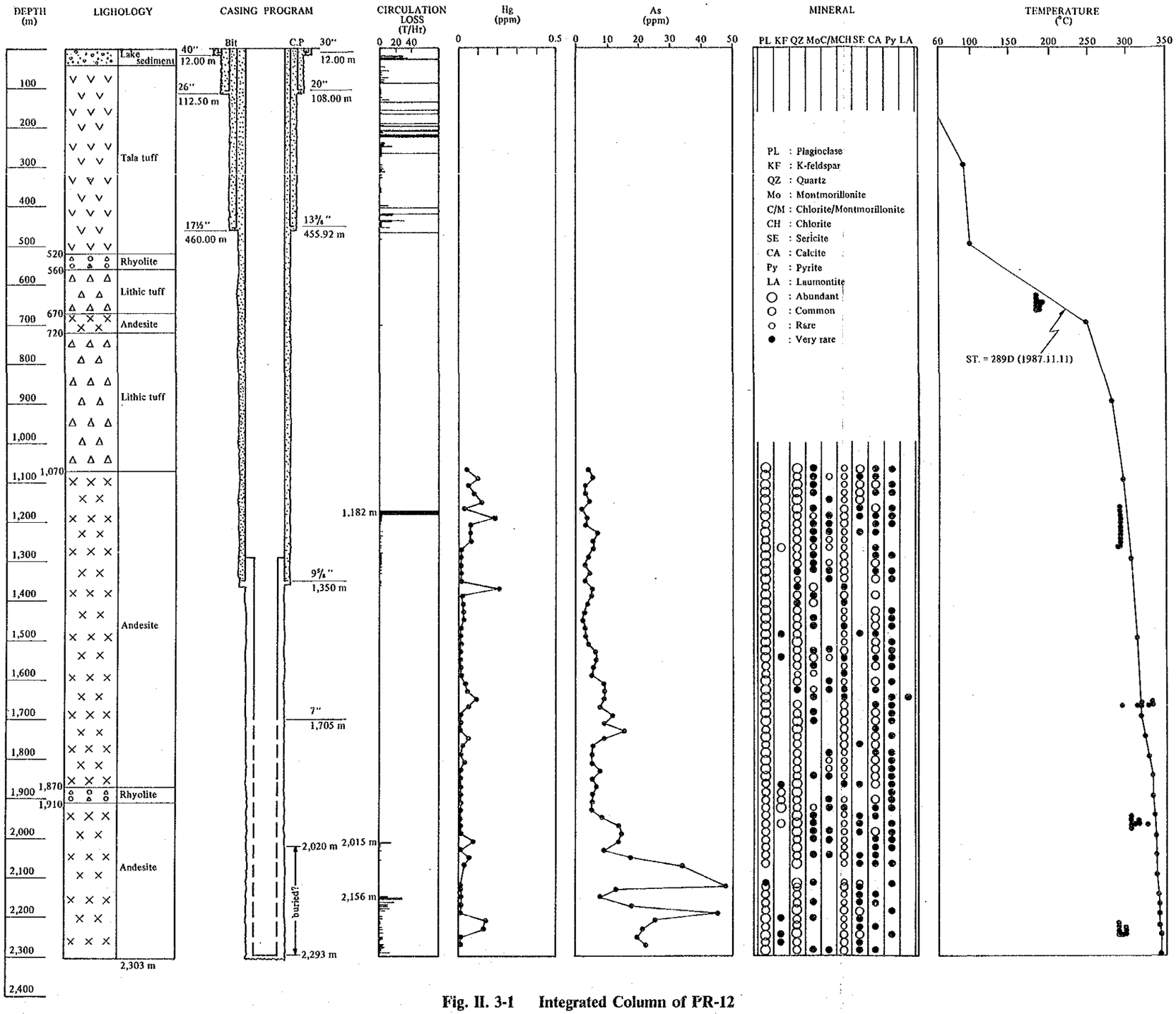

Fig. II. 3-1 Integrated Column of PR-12

Table II. 3-1 Chemical Composition of Well Discharge Sample from PR-12

(1) Gas composition of steam

		PR-12	PR-8	PR-1	PR-9	PR-11
Liquid-vapor (psi) separate pressure		75	105	*	*	Dry gas
Total gas in steam (vol. %)		2.28	2.39	0.24	0.12	100
Gas Composition	H_2S (vol. %)	1.0	0.4	1.6	4.4	0
	CO_2 (vol. %)	98.5	99.0	97.9	95.2	98.0
	H_2 (ppm)	895	81.0	515	101	2580
	N_2 (ppm)	1110	1450	2560	3560	2920
	CH_4 (ppm)	2960	4430	1870	276	14400
	He (ppm)	20.0	17.0	7.00	1.35	12.5
	Ar (ppm)	17.3	25.0	54.5	56.8	42.8

(2) Chemical composition of steam condensate

Component	Unit	PR-12
Electrical conductivity	μS/cm	185
pH	–	6.00
Cl	mg/ℓ	0.71
NH_4	mg/ℓ	24.5
As	mg/ℓ	0.004
Hg	mg/ℓ	0.0003

(3) Chemical composition of hot water

Component	Unit	PR-12
Electrical conductivity	μS/cm	4,470
Total dissolved solids	mg/ℓ	4,470
pH	–	7.32
Cl	mg/ℓ	1,280
SO_4	mg/ℓ	18.8
H_2CO_3	mg/ℓ	10
HCO_3	mg/ℓ	87
CO_3	mg/ℓ	<1
Na	mg/ℓ	740
K	mg/ℓ	203
Ca	mg/ℓ	4.85
Mg	mg/ℓ	0.06
Fe	mg/ℓ	0.17
Al	mg/ℓ	0.509
SiO_2	mg/ℓ	1,340
Li	mg/ℓ	9.37
B	mg/ℓ	200
F	mg/ℓ	2.6
NH_4	mg/ℓ	3.4
As	mg/ℓ	20.0
Hg	mg/ℓ	0.0003
D/H	‰ (SMOW)	-60.1
$^{18}O/^{16}O$	‰ (SMOW)	- 0.8
Tritium	TU	0.31

3.1.4 Well tests of PR-12

(1) Method and process of measurement

The well test conducted on PR-12 was to measure downhole temperature and pressure under the producing condition in borehole on each flow rate set by adjusting wellhead valve. Because the test must be done under pressurized condition of wellhead, the work of insertion and removal of equipment into and from wellbore should be carried out through a lubricator. A shematic diagram and instruments used for well test are shown in Fig. II.3-3 and Table II.3-3 respectively.

Measurements were carried out under three stages as given in Table II.3-4. The first test was done at 6.2 kg/cm^2 in wellhead pressure under the flow adjustment by 3″ϕ orifice and full opening of 2nd valve. The measurement stopped at a depth of 2,000 m, because the equipment could not go down beyond 2,020 m in depth in spite of 2,303 m in depth at the bottom of hole. The second test was the same wellhead condition as the first test, but the wellhead pressure showed 10.7 kg/cm^{2}G. The third test was a simultaneous measurement of temperature and pressure at 11.1 kg/cm^2 in wellhead pressure.

Because the well test of PR-12 was carried out just after the production, measurements was in unstable conditions such as the fluctuation of flow rate and the emission of sand.

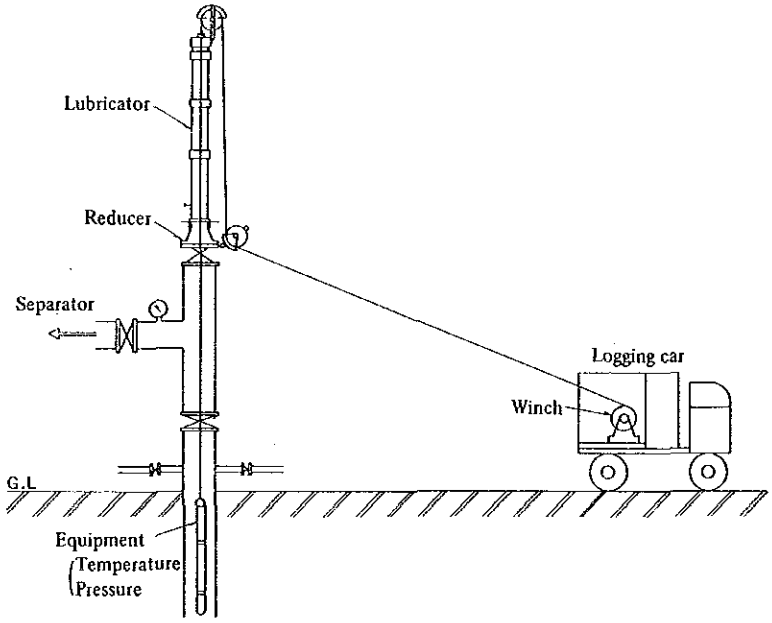

Fig. II. 3-3 Outline of Logging of PR-12

(2) Result of measurement

Table II.3-5 and Fig. II.3-4 show the results of downhole temperature and pressure. Based on these results, the condition inside of PR-12 hole is as follows:

① The relationship between temperature and pressure indicates a nearly saturated condition throughout the whole depth, forming thus two-phase flash flow entirely in the wellbore.

② The main feed point is situated near 2,000 m in depth, judging from the distributions of temperature and pressure.

Table II. 3-3 Instruments used for Well Test of PR-12 and PR-13

Description	Maker	Model	Specification
Temperature element	KUSTER (USA)	P/N 600-138KT	Temp. range: 50 ~ 350°C
Pressure element	KUSTER (USA)	P/N 10200-103KPG	Max. pressure: 250 kg/cm^2
Clock	KUSTER (USA)	P/N 1201-509KPG	6 Hrs (2 sets) Temp.: 175 ~ 350°C
Lubricator	SEKISAKU		Size: 2B x 5.51 m (total) Working pressure: 50 kg/cm^2
Wire rope	SHINKO		Material: SUS 304 Diameter of rope: 5 mm Const. of rope: 7 x 19 ss/o Spec. B.S.: 1,700 kg Length: 3,300 m
Drum	SEKISAKU		Max. line speed: ± 3,000 m/hr Drum spool size: 210 mmϕ x 500 mm Wire line capacity: 5mmϕ x 3,300 m Drive system: Roller chain drive (oil hydraulic)
Depth meter	SOKUKIKI		Digital display
Tension meter	NMB	CSD-801	Digital display

Table II. 3-4 Conditions of Well Test of PR-12

Stage	I	II	III
Date	30. Jan. 1988	31. Jan. 1988	2. Feb. 1988
Measurement	Temperature	Pressure	Temperature & pressure
Well head condition	3"ϕ orifice 2nd valve: full open	idem.	Regulated by 2nd valve
Well head pressure (kg/cm^{2}G)	6.2	10.7	11.1
Flow rate (t/h)	Gs ≒ 30 Gw ≒ 10 G ≒ 40 at atmosphere	Gs = 16.1 Gw = 20.4 G = 36.5 at separator (9.9 kg/cm^{2}G)	Gs = 18.9 Gw = 18.1 G = 37.0 at separator (10.3 kg/cm^{2}G)
Quality at separator		0.441	0.511

③ The fluid temperature reaches 200°C at a depth of 2,000 m, and the fluid pressure is 23.1 kg/cm²A at the same point. On the contrary, the formation temperature and pressure under a static condition is about 330°C and about 150 kg/cm²A at the same depth (measured by CFE). Therefore, the fluids flow into the wellbore after flashing in the formation surrounding the well.

④ A burried layer of about 300 m by collapse might be expected near the bottom, judging from the emission of sand and the wire tension.

(3) Calculation of the value of permeability-thickness

The value of permeability-thickness (kh) around PR-12 is calculated from the result of downhole pressure measurements. As mentioned above, the fluids from PR-12 is likely to flash in the formation. The volume ratio of steam to water is sufficiently high in the formation and the pressure loss caused by flow in the formation is mainly related with the voluminal flow. As a result, an equation of gas-phase flow has been applied for calculation of kh. We use the same formula as the kh calculation of PR-1 as expressed in (1) and (2) equations of Chapter II.1.5. Tables II.3-6 and II.3-7 show the parameters used for calculation and the result of calculation respectively. The value of kh is approximately 0.3 darcy·m. This is not so high as that of other wells because a burried layer reduces this value.

Table II. 3-6 List of Paramerters used for Calculation of kh in case of PR-12

Stage		II	III
Well head pressure	(kg/cm²G)	10.7	11.1
Total flow rate	(t/h)	36.5	32.2
Pressure at feed point	Pw (kg/cm² abs)	20.5	23.1
Steam flow rate at feed point	G (kg/s)	4.00	3.44
Specific weight of fluid at feed point	γw (kg/m³)	10.1	11.4
Viscosity coefficient of fluid of feed point	μw (kgs/m²)	1.64×10^{-6}	1.66×10^{-6}

Table II. 3-7 Results of Calculation of kh in case of PR-12

Well	kh (m³)
PR-12	2.7×10^{-13}

3.1.5 Comprehensive evaluation of PR-12

(1) Evaluation of fracture

Many lost circulations were observed at the Tala Tuff shallower than 520 m in depth. The static borehole temperature, measured 289 days after drilling, is very low, i.e., below 100°C.

These features suggest that Tala Tuff is a very permeable zone where the surface water easily infiltrates.

Production test by JICA on 30th, January ~ 2nd, February, 1988, shows that the initial single-phase fluids begin to separate into two phase boiling fluids near the feed point at 2,020 m where the lost circulation occurred. Judging from the transmissibility, i.e., 2.7×10^{-13} m^3, the permeability of the fracture at PR-12 is about equal to that at PR-8 and cannot be judged to be good.

Lost circulation and Hg, As concentration data indicates the existence of fracture at depth deeper than 2,020 m. Considering that about 280 m in depth of burried layer beyond 2,020 m in depth might be expected by the production test, we hope to remove the burried layer to obtain more steam.

An anticlinal axis is recognized at the deeper part of PR-12. The axis is determined by the shape of the upper boundary of rhyolite in the lower Cordilleran Volcanic's (see Horizon 3 in Fig. III.1-16). The axis means that the center of the uplift is located in this place. So that, fractures observed at a depth of 2,015 m and 2,156 m is ascribed to vertical fractures at an anticlinal axis.

Judging from the dip of fault, lost circulation at a depth of 1,182 m is due to the Los Muertos Fault.

(2) Evaluation of temperature

On the basis of the static borehole temperature measured 289 days after drilling, the reservoir temperature below 1,900 m is concluded to be very high temperature, over 330°C. The temperature increases abruptly from the surface to 1,200 m in depth, and then increases slowly to 1,700 m. But it increases abruptly by high gradient of 7.5°C/100 m from 1,700 m to 1,900 m in depth. From the profile, it is concluded that the reservoir boundary between the shallow and the deep reservoirs exists about 1,700 m, and that deep reservoir is high temperature. This hypothesis is supported by the abrupt increase of mud water at depth of 1,680 m ~ 1,720 m during drilling.

The homogenization temperature is 10 ~ 50°C lower than the static borehole temperature. As mentioned above, it was estimated that the reservoir temperature has increased over about 130°C from the past alteration stage up to the present.

Accordingly, these provide us with the following conclusions:

① Fluid inclusion had been trapped at quartz, anhydrite mineralization stage.

② Reservoir temperature has increased at the successive process: alteration stage, inclusion trapping stage, present.

(3) Comparison the reasons for selection of target with the result after drilling.

The reasons for selection of target were as follows:

① Necessary point to detect the extent of geothermal reservoir

② Located on an up-flow zone

③ Located on possible deep-seated fractures

④ Located on the horst estimated from the distribution of surface faults

⑤ Located on a tensional fracture concentrated zone

After the drilling of PR-12, the results for the above reasons are as follows:

① PR-12 is located within the geothermal reservoir because the well encounters good fractures and high temperature zone.

② The formation temperature by downhole measurement, fluid inclusion and chemical thermometer indicates more than 300°C.
In particular, judging from chemical analyses such as the ratio of He/Ar and the Cl-enthalpy, PR-12 is situated in the center of the up-flow.

③ Lost circulations occurred at a depth of 2,015 m and 2,156 m below 1,700 m. They ascribed to the deep-seated fractures because Hg and As concentrations in cuttings are high at that depth and static temperature curve shows so called convection.

④ Figs. III.1-10 and III.1-16 have been made clear that PR-12 is located on the most upheaval area, namely the center of the uplift.

⑤ PR-12 is located on the area existing vertical tensional fractures at an axis of anticline as shown in Figs. III.1-10 and III.1-18(b)

Therefore, the results give satisfaction to the reasons for selection of target.

(4) Well efficiency of PR-12

The efficiency of PR-12 should be estimated based on the measuring values of well tests as listed in Table II.3-4. The efficiency of PR-12 at the wellhead was calculated by the assumption of isentalpic changed fluids.

The result is shown as a relation between flow rate and wellhead pressure (Fig. II.3-5). Fig. II.3-5 shows that it can obtain the steam of 25 to 26 ton/hour under the condition of 7 kg/cm²G (8 ata) at the wellhead pressure. However, taking the following conditions into consideration, the efficiency of PR-12 is estimated at more than 30 ton/hour under the same wellhead pressure:

① Quality of stream increases as a production time elapses as known by Table II.3-4. This indicates that the measurement is carried out during temperature recovery.

② Fragments of burried rock are emitted from the well as the production continues, resulting in the increase of permeability and temperature.

③ PR-12 is located at the highest temperature zone in this area. That is to say, the formation temperature exceeds 330°C at the feed point, and the original hot water goes up from the deeper formation of PR-12.

In spite of such good condition, the fluid temperature is 220°C showing low temperature. This is ascribed to the reduced permeability by a burried layer in the wellbore.

If a burried layer would be taken way, the efficiency of PR-12 could be expected to increase in high degree of efficiency such as PR-1 and PR-9.

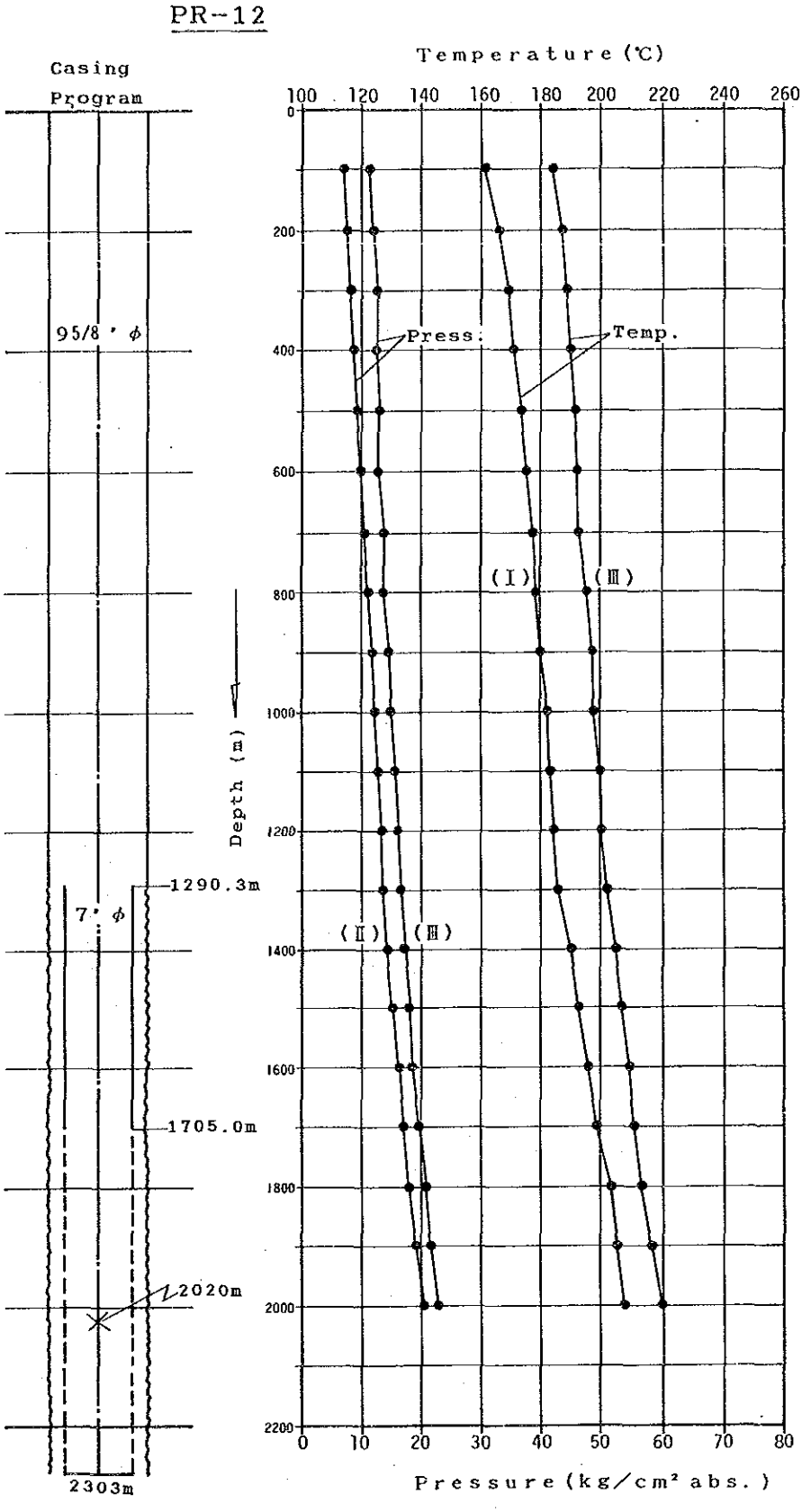

Fig. II. 3-4 Downhole Temperature and Pressure Curves of PR-12 in the Producing Condition

Table II. 3-5 Results of Measurement of PR-12

Stage	I	II	III	
Date	30. Jan. 1988	31. Jan. 1988	2. Feb. 1988	
Well head condition	3"ϕ orifice	3"ϕ orifice		
Well head pressure	6.2 kg/cm^{2}G	10.7 kg/cm^{2}G	11.1 kg/cm^{2}G	
Depth (m)	Temperature (°C)	Pressure (kg/cm^{2}abs)	Temp.	Press.
0	114		167	10.5
100	161	7.1	184	11.3
200	166	7.6	187	11.9
300	169	8.1	188	12.3
400	171	8.9	189	12.5
500	173	9.3	191	12.9
600	175	10.0	192	13.0
700	177	10.8	192	13.6
800	178	11.6	195	14.0
900	180	11.9	197	14.3
1,000	182	12.3	198	14.9
1,100	183	12.8	199	15.4
1,200	185	13.6	200	15.9
1,300	186	13.8	202	16.4
1,400	190	14.6	205	17.1
1,500	193	15.5	207	17.8
1,600	196	16.4	209	18.5
1,700	199	17.5	211	19.5
1,800	203	18.2	214	20.8
1,900	205	19.2	216	21.7
2,000	208	20.5	220	23.1

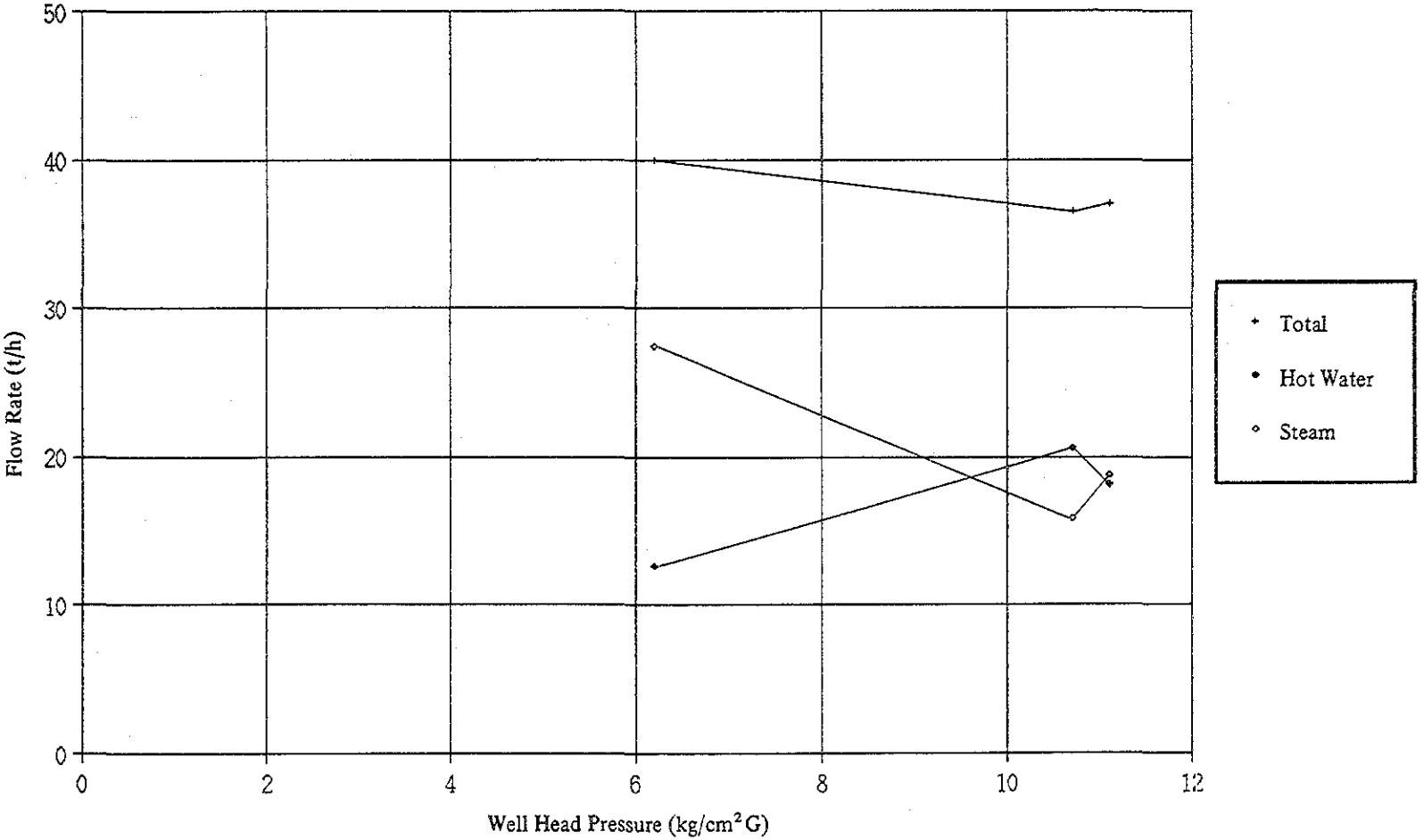

Fig. II. 3-5 Characteristics of Well head Pressure VS. Flow Rate of PR-12

3.2 Drilling of PR-13

3.2.1 Drilling plan

Well PR-13 was planned to be drilled in La Primavera geothermal field about 15 km northeast of Guadalajara city, state of Jalisco, Mexico (Fig. II.3-6). The projected depth of the well was 2,000 m with 8½" bit, and planned as a straight hole. Well design was to set 20" c.p. (casing pipe), 13⅜" c.p., and 9⅝" c.p. at the depths of 100 m, 600 m and 1,400 m from the surface respectively (Fig. II.3-7). Also 7" slotted pipe was planned to be set from 1,400 m to 2,000 m to protect against formation collapse. Casing strings were planned to be cemented from surface to the bottom. Two core samples were planned to be taken at depths of 1,500 m and 2,000 m, and also cutting samples are to be taken every 10 m. Temperature logs were planned before setting 9⅝" c.p. and 7" slotted liner, after pumping has been stopped 18 hours.

The well specifications are as follows:

Depth	:	2,000 m, straight		
Coring	:	1,500 m and 2,000 m		
Casing	:	20"	J-55 94 lb/ft	0 – 100 m
		13⅜"	K-55 54.5 lb/ft	0 – 600 m
		9⅝"	L-80 47 lb/ft	0 – 1,400 m
		7"	N-80 29 lb/ft	1,350 – 1,410 m
		7" (slotted pipe)		1,410 – 2,000 m
Logging	:	Before setting 9⅝" casing and 7" liner		

3.2.2 Summary of drilling activities

Perfensa's Drilling Rig No. 2 (IDECO MODEL H-1200) was moved to the location from on Oct. 5th 1987 and well was spuded on Oct. 6th, with 12¼" bit. The 12¼" hole was drilled to the depth of 112m and opened to 20" and then to 26". While drilling 12¼" hole to 112 m total lost circulation of drilling mud was encountered several times and 10 cement plugs were required to plug fractures. However fractures were not plugged completely, so open hole section at 20" and then 26" diameter from surface to 108 m were drilled with total lost circulation and no returns.

20" c.p. was run and cemented on Oct. 13th. Cement slurry (27,500 kg cement, 40% SiO_2, SG 1.85) was pumped but it did not return to the surface, so additional cement slurry, 17,200 kg cement total, was pumped into the annulus. After rigging up the blowout preventor (BOP) and flow line to the shale shaker, 12¼" hole was drilled from 112 m to 612 m. It took 18 days to reach 612 m, because of many lost circulation zones. Thirteen cement plugs, the 12th to 34th counting from the beginning, were set during those days. The hole was then opened from 12¼" to 17½". Seven cement plugs were set for the 17½" hole, but circulation was not obtained, so the hole opening operation from 12¼" to 17½" from 248 m to 416 m was drilled without circulation of mud to the surface. After the depth of 404 m, the first stuck pipe occured, but one oil spot did free the pipe. The 2nd stuck pipe occured at 416 m. About 30 days were required to free the pipe and to remove the fish. During those days, three oil spots, cleaning of the annulus with 13⅜" washover shoe and then with

17⅜" washover shoe operations were performed from just above the 17½" open hole, but the fish was not removed from hole. So finally, on Nov. 24th operations with 18$^{3}/_{16}$" hole-opener started from just below the 20" c.p. to the top of the fish (355.93 m) and then continued in the open hole with 18$^{3}/_{16}$" washover shoe to below the 17½" openhole at 417.20 m. The fish was finally out of hole on Dec. 6th. After the fish was out of hole, 15 cement plugs (43th to 57th) were set from the bottom of the 17½" hole to above the shoe of 20" c.p. to solve the lost circulation problems. The water level was measured each time before pumping the cement slurry and indicated fractures below 200 m caused a water level below 150 m and the ones above 200 m had levels at about 100 m. From the results of the cementing, it appeared that many fractures existed in the depth interval from 430 m to 100 m. Six days were spent for these cement plugs and another seven days were spent drilling out them. Circulation was only obtained during drilling out of cement to 190 m, below 190 m the cement plugs were drilled without circulation, down to a depth of 402 m. Another nine cement plugs (58th to 66th) were set, but did not plug the fractures completly and the hole opening from 12¼" to 17½" was done without circulation to 612 m.

After hole was conditioned, 13⅜" c.p. was set at 609.94 m and cemented using the two plug method, on Dec. 30th. A slurry volume about 60% excess of the annulus volume was pumped, but did not result in returns to the surface. So another 17 kℓ (kiloliters) cement slurry was pumped into the annulus from the surface in order to fill the annulus back to the surface.

After the wellhead equipment was changed out, the hole was drilled with a 12¼" bit from on Jan. 2nd with full circulation of the drilling fluid. An interval of 642 m was drilled in 5 days with only pertial lost circulation of drilling fluid. At 1,254 m the amount of lost circulation increased to 40 kℓ/h and 15 cement plugs (67th to 81th counting from the beginning) were set during 8 days.

On Jan. 16th the well was drilled to 1,415.40 m where 9⅝" c.p. was planned to be run and cemented. But while bottom hole assembly (BHA) was begun pulled out of the hole, stuck pipe occured at 711 m. While trying to free the drill pipe, the drill string was disconnected by accident and a 138.3 m length of BHA (including 12¼" bit, 5 joints stabilizers and 15 joints 8" drill collars) dropped down to the bottom of the hole. Three days were spent to retrieve all of the fish out of the hole. During those fishing operations, 2 oil spots were run. After the fishing job, the well was reamed and conditioned with mud, and then temperature logs were run 6, 10 and 14 hours after pumping was stopped. Maximum temperature recorded was 186.90°C at 1,406 m after 14 hours. Using those data it was calculated that the temperature would go up to 201°C at static conditions (without the influence of the mud circulation) at 1,406m.

After hole was washed to the bottom of casing point with the true gauge assembly, 9⅝" casing was run in the hole on Jan. 22nd. But mud circulation was not obtained at 937.24 m and all the casing was pulled out of the hole. Mud was circulated and conditioned with 2 kℓ/h lost circulation and gauging assembly was run again. The 9⅝" casing was rerun and cemented on Jan. 24th and 25th. The two stage cementing method was employed for the job. The casing was run to 1,407.24 m. A casing shoe, float collar and stage cementer were placed at the bottom, 2 joints above the shoe and at 775.84 m respectively. Also